1. Comparison of Volcanic Features of Elysium (Mars) and Tibesti (Earth)

2. Age of Martian Channels

3. Nature and Origin of Intercrater Plains on Mars

Thesis by

Michael Charles Malin

In Partial Fulfillment of the Requirement

for the Degree of

Doctor of Philosophy

California Institute of Technology

Pasadena, California

1976

(submitted June 24, 1975)

To the memory of my mother, Beatryce...

who sacrificed her dreams for mine;

who gave her life for mine.

ACKNOWLEDGMENTS

During the past four years, I have had the unique experience of working at the forefront of planetary exploration using spacecraft imagery. The opportunity to perform this research is the direct result of my association with Professor Bruce C. Murray, my research and thesis advisor. It gives me great pleasure to acknowledge the guidance, support, and intellectual stimulation which Professor Murray has given me throughout my years at Caltech.

Without the assistance, encouragement and good humor of two incredibly kind, generous, and gifted men, this thesis would never have been completed. Professor Robert P. Sharp has, over the past four years, unselfishly given his time and knowledge to guide my pursuit of that elusive essence of my chosen field -- credibility. It is a great honor and privilege to have been associated with him. Mr. G. Edward Danielson of the Jet Propulsion Laboratory, especially during the critical final stages of my research, moved virtual mountains to provide facilities not generally accessible. His generosity and wonderful sense of humor, combined with his talent for successfully accomplishing extremely difficult tasks, greatly eased the laborious birth of this thesis.

I would especially like to thank Mr. Don Lynn and Mr. James Soha of the Image Processing Laboratory (Jet Propulsion Laboratory) for their assistance and encouragement during the image processing required to produce many of the photographs used in illustrating this work. Mr. Jean Lorre and Mr. Arnold Schwartz extended my knowledge of image processing, and the improvements in image quality represented by the

processing scheme used for my thesis are the direct result of many useful discussions with these men.

Mrs. Enid Bell's rapid response in typing this work has removed from my mind one of the major causes of anxiety among Ph.D. candidates.

This research was supported in part by National Aeronautics and Space Administration (NASA) grants NGR 05-002-117 and NGR 05-002-305.

ABSTRACT

This thesis consists of three separate parts, each addressing a specific aspect of the surface morphology of Mars.

In Part 1, a comparison of large volcanic features is made using spacecraft imaging data. The Elysium volcanic province on Mars and the Tibesti volcanic province in Chad, Africa are studied using Mariner 9, Earth Resources Technology Satellite and Apollo photography. Elysium Mons on Mars and Emi Koussi on Earth show remarkable similarities in summit caldera and flank morphologies. Each has a large central caldera approximately 12 km in diameter and from 500 to 1000 m deep which contain numerous craters and large, irregular pits. Channel-like features which head at the calderas and taper downslope show evidence of collapse and possible lava erosion. Elysium Mons rises some 14 ± 1.5 km above its base and the summit is about 17 km above the 6.1 mbar mean martian pressure surface. Cratering data indicate most of the apparent cratering is endogenic in origin. The subdued, hummocky terrain on the flanks is distinctly different from the slopes of the younger Tharsis Ridge volcanoes, showing little if any sign of recent material flow.

The lack of aqueous erosional forms on Elysium Mons argues strongly against recent ($\sim 10^5$ to 10^6 year) pluvial episodes. The forms and associations of features throughout the Elysium region suggest central volcanism started earlier in Elysium than in Tharsis, and that the source of the Elysium volcanics is chemically evolved, with evidence of silicic magma. Finally, the data are consistent with the

view that the martian crust has been stable and essentially motionless for an extended period of martian geologic time.

Part 2 attempts to determine the age relationship between the large, sinuous channels on Mars and the terrains in which the channels are found. Crater counts, plain and mantle superposition, and geographic and geologic associations suggest that the channels are extremely old, are spatially and temporarily related to the ancient cratered terrain and are genetically related to the processes of fretting and chaos formation. There appears to be no evidence for recent channel activity.

Part 3 presents the results of an investigation of the morphologic characteristics of the plains which separate the craters in the heavily cratered regions of Mars. These intercrater plains appear to be composed of stratified consolidated and unconsolidated materials, probably loose debris blankets and volcanic flows. The topmost layer of the plains unit varies from location to location. An older, cratered surface may be partly exposed where the kilometers-thick plains unit is locally incised and eroded. The association of chaotic terrain, fretted terrain and major channels with the plains suggests that the volatile(s) presumed to be necessary to produce these erosional landforms may have been present among the plains materials. It is speculated that the unconsolidated material is impact-generated debris and eolian deposits, suggesting an early atmosphere conducive to material transport and possibly flowing liquids.

TABLE OF CONTENTS

Part 1. Comparison of Volcanic Features of Elysium (Mars) and Tibesti (Earth)

Introduction

In the past five years, the relatively youthful science of comparative planetology has taken several significant steps towards maturity. The Apollo flights to the moon, Mariner missions to Mars, Venus, and Mercury, and the Earth Resources Technology Satellite reconnaissance of our own planet Earth have provided, for the first time, data about each terrestrial planet which can be used in interplanetary comparisons. To date, the most stimulating of the remote sensing studies involve the Earth and Mars. The discovery of such diverse features as seen in the channeled, chaotic, troughed and layered terrains on Mars has greatly stimulated investigations of that planet (cf. 1-4). One of the most exciting discoveries was the evidence of large-scale volcanism (1-5).

Much attention has been focused on Olympus Mons and the other volcanoes of the Tharsis region, which represent the largest and most conspicuous examples of martian volcanism. Comparison with terrestrial volcanoes, especially those comprising the island of Hawaii, has been most fruitful (6).

In this paper, another martian volcanic province will be studied. The Elysium region has several structures which are not found elsewhere on Mars, as well as some which compare favorably with those in Tharsis. Comparison with terrestrial features will involve the Tibesti region of northern Chad, Africa, which displays a variety of volcanic forms similar to those of Elysium.

After establishing the regional setting of the volcanic fields,

two volcanoes, Emi Koussi on Earth and Elysium Mons on Mars, will be compared in more detail. A section containing plausible, but speculative, interpretations of the available data will conclude with suggestions concerning the evolution of the Martian surface environment.

Regional Setting

Tibesti (Earth)

A number of authors (7-9) have presented detailed descriptions and interpretations of the Tibesti region of northern Chad, Africa. In this section, only a brief review of a few of their results will be presented.

The Tibesti volcanic province occupies approximately one-third of a triangular upland region some 100,000 km^2 in area, approximately 1100 km south of the Mediterranean Sea and 2000 km west of the Red Sea (Fig. 1). The highest point is Emi Koussi at 3415 m; numerous areas are over 2000 m. The volcanic range is also triangular, with a right angle in the northeast, the long side roughly east-west (and pointing west) and the short side roughly north-south.

Most volcanoes in Tibesti exhibit two distinctive characteristics: wide, low-slope, shield-like profiles and large, central calderas. Unlike Hawaii, in some places the Tibesti shields appear to be formed of an ignimbritic mass covering older volcanics (Yirrigué in western Tibesti). The largest calderas are associated with these ignimbrites (Yirrigué, 15 km; Yéga, 20 km; Voon, 18 km) and are the result of collapse. The most common appearance of the other volcanoes is that of deeply dissected slopes surrounding large calderas. Tieroko (30-km

diameter, 8-km caldera) and Toon (30-km diameter, 10-km caldera) are representatives of this latter type, which has two distinct subclasses. One class (e.g., Toon) has roughly circular calderas, with erosional valleys cutting deeply into the volcanic flanks, and rhyolitic volcanism completely contained within the caldera. The second class (e.g., Tieroko) has a star-shaped central depression with radiating dikes guiding the dissection of the shield. The depression is not believed to be due to collapse.

Emi Koussi (19.7°N, 18.5°E, Fig. 2), situated at the extreme southern portion of the volcanic region, is distinctive among the Tibesti volcanoes because of its well-preserved form. This preservation may be the result of leeward protection from weather systems from the north by the east-west branch of the range of volcanic mountains. Emi Koussi ranges from 60 to 80 km across, with some 2000 m of volcanics resting on Paleozoic and Cretaceous sandstones which have been uplifted 1500 m. The original cone may have reached as much as 4000 m above sea level but is now only 3415 m, with a large (15 km), multiple-crater caldera some 500 m deep at the summit. Much of the volcanism occurred during the middle and late Tertiary, with only limited activity during the Holocene. Current activity is restricted to a few fumeroles near the southern base of the volcano. Most of the erosion occurred during the early Pleistocene.

The basement beneath the Tibesti volcanics is part of a vast Precambrian block, which has experienced uplifting for an extensive period. Where present, Paleozoic (Cambro-Ordovician) sandstones rest

unconformably on an eroded Precambrian surface and dip away from the uplifted massif. The Paleozoic is totally missing north of the east-west branch and immediately west of the lower portion of the north-south branch of the province. In these areas, Nubian sandstone of probable lower Cretaceous age lies directly on the Precambrian. Other evidence from regions in northern Chad suggests that the warping and uplifting which resulted in the erosional removal of much of the Paleozoic formations was post-Carboniferous and pre-Cretaceous (7-9). After the deposition of the Nubian sandstones, but prior to the Lutetian (lower Eocene), the massif was cut by NE and NNE-trending faults which follow the Precambrian trends. Subsequent uplift along a NNW-SSE axis was followed by the overall tilting of the entire block towards the NNE. Significant erosion then occurred, forming much of the topographic relief and establishing the drainage system still preserved throughout most of the area (7,8,10). This erosion has been placed roughly at the boundary between the Pleistocene and Pliocene.

The volcanism is believed to have started during the very early Tertiary (Paleocene?) with the extrusion of basalts and andesites in floods of probable fissural origin (lower or first black series). These are most clearly seen in central and northeast Tibesti, but are also present in the eastern portion of the province. This phase was followed (Miocene?) by the initial formation of large, central volcanoes (Koussi, Tieroko, Toon, Yéga, Oyoye, Voon, Timi, Sosso, and Toussidé) by the emission of a sequence of trachy-andesites, trachy-phonolites and some rhyolites (lower or first white series) and of essentially tholeiitic

basalts: labradorite-rich, olivine-poor porphyries with abundant magnetite and ilmenite (intermediate or second black series). The initial formation of two domes (Abéki and Dadoi) also occurred at this time. In the late Miocene, another white series accompanied the formation by collapse of the Yéga and Toon calderas and the partial collapse of some of the other volcanoes, and was followed by a final phase of plateau volcanism (basalts with some andesites -- upper black series) scattered throughout the north, central and east portions of the Tibesti. The Voon ignimbrite sheet postdates the erosion of the shields of Toon, Yéga and Oyoye, but is older than the massive valley incision which occurred at the beginning of the Pleistocene. The ignimbrites at Yirrigué and Koussi were apparently associated with the collapse formation of their calderas and were followed by a period of basaltic flows on the slopes of, and within the old valleys around, the calderas. This activity continued throughout the Quaternary (extending throughout the massif) and was accompanied in the west by the hybrid volcanism of Toussidé, Timi, and Mousgou (potassic trachyandesites preceding fluid doreites and andesites) and in the east by the formation of a second caldera at Koussi. The explosions which formed the craters Trau au natron and Era Kohor (the latter within the Koussi caldera), continued eruption of Toussidé, and the deposition of the sodium carbonates within the Trau au natron and Era Kohor, all occurred during the Recent Quaternary, and fumerolic activity is still present.

Regional Setting

Elysium (Mars)

The Elysium Plain is dominated by a group of three volcanoes located near 210° West longitude between 18° and 32° North latitude (Fig. 3). The region consists of a broad, elliptical dome (2400×1700 km, semi-major axis north-northeast), similar to the Tharsis Ridge, with a V-shaped summit (open to the east) rising approximately 4 km above the mean martian pressure surface (4). The three points of the "V" are occupied by one volcano each.

The northernmost, Hecates Tholus, is about 180 km in diameter. It is a flat-topped, dome-like volcano with relatively steep slopes that are convex in profile. A UVS altimetry scan which, fortuitously, traced across the dome shows its height to be about 6 km (12). The dome is in sharp and abrupt contact with the plain to the south and west. An embayment into the dome, flooded by plains material (but not to the level of the surrounding plain), appears in the northwest, and may have originated through erosion of the slope of the volcano, or through modification of a pre-existing depression immediately interior to the dome boundary (Fig. 4). The northern terminus is indistinct. The eastern edge is marked by a narrow, sinuous channel-like form some 60 km long, running roughly north-south. This in turn heads in the south into a short, stubby graben (45 km long, 7 km wide) which delineates the rest of the eastern boundary of the dome.

The surface of Hecates Tholus appears rough in both high and low resolution images. The surface shows numerous 3-10 km diameter craters,

but is deficient in larger craters which are prevalent on the surrounding plain. Surface lineations appear radial from a 12-km complex caldera which is offset to the southwest from the geometric center of the dome by some 30 km. The UVS data also suggest that the summit of the dome is offset to the southwest (12). Numerous channels are seen on the slopes, many formed by coalescing craters. A number of graben, concentric about the caldera, are also seen on the slopes of the dome. At high resolution, features reminiscent of the Olympus Mons flows are interspersed through a rough, knobby terrain (Fig. 4).

Albor Tholus, the southern member of the group, is about 130 km in diameter and 3 km in height (determined photogrammetrically). It has a complex central caldera, with the largest crater about 30 km in diameter. A small, 8-km crater is nested within and indents the northern rim of the larger crater. The periphery of Albor Tholus is marked by a circumferential graben to the south and west and by an escarpment in the north. The eastern margin of the volcano is indistinct. Concentric graben are seen to the west and south to a distance of at least 70 km.

The surface of Albor Tholus was photographed only at low resolution. It has the lowest density of 3-10 km craters of the Elysium volcanoes. There are faint lineaments radial to the caldera and some faint channel-like forms on the slopes.

The third volcano, Elysium Mons (Fig. 5), is 170 km in diameter and has a single central caldera about 12 km across. Elysium Mons is 14 ± 1.5 km high (as determined by photogrammetric techniques described

by Blasius (15)) and topographically asymmetric. The asymmetry is in the form of two distinct ridges which meet at the caldera, the shorter trending west and the longer southeast. The boundary between the volcano and surrounding plain is indistinct on all sides, although an apparent fault scarp may delineate the northeast portion of the perimeter.

In low-resolution images, the surface of Elysium Mons is roughly textured by what appears to be large hummocks with approximately 10-km spacing arranged in a crudely concentric pattern. Craters in the size range 3-10 km are more sparse than on Hecates Tholus, but more abundant than on Albor Tholus, and larger craters are totally absent. Concentric graben occur as far as 170 km from the base.

At high resolution, Elysium Mons appears significantly different from other martian volcanoes (Fig. 6). No flow features such as those on Olympus Mons can be distinguished; rather, the surface appears hummocky and extremely subdued. Long, shallow, linear depressions, with a distinct trend radial from the caldera, dominate the visual appearance of the summit region. Some of the depressions are steep-walled, channel-like forms, apparently the result of coalescing chains of craters. However, the majority of the depressions which give rise to the lineated appearance are areas between closely spaced, elongate, linear mounds of low relief, typically 1 km in length and 200-400 m across.

The Elysium Plain, which surrounds the three volcanoes, is moderately cratered, having abundant large (> 20 km) craters, and is believed

to be representative of the second oldest plains unit on Mars (4,13). A major tectonic trend (northwest-southeast, aligned with the semi-minor axis of the regional dome), appears to postdate this oldest unit. Similarly aligned are several large, closed, linear depressions, the volcanoes Elysium Mons and Albor Tholus, and the elongate form of Elysium Mons. Immediately north of Elysium Mons, and extending some 200 km, is a region of hummocky terrain of slight relief, showing numerous features suggestive of long, low ridges which trend north and north-northeast towards Hecates Tholus. The crater population on this plains unit is somewhat lower than on the surrounding surface. The graben concentric to Elysium Mons cut both plains units.

The age relationships between the volcanoes and their surroundings are not easily determined. In the very few cases where high resolution photography is available, evidence for plains both younger and older than the volcanoes is found within the same frame. In most areas, no superposition relationships could be discerned. It is inferred that plains materials were probably emplaced both before and after the massive central volcanoes were formed.

Crater statistics are equally ambiguous. The large number of smaller craters (< 10 km) on the volcanoes would indicate great age (as old as the Amenthes upland) if formed by impact. However, many of the craters are clearly of endogenic origin (e.g., coalescing chains of craters) and the cumulative size-frequency distribution of the singly-occurring craters is similar to the distribution for craters of obvious volcanic origin, suggesting many of the smaller craters were probably

not formed by impact (Fig. 7). This appears to be the case for craters smaller than about 1 km in diameter. On the other hand, the craters between 3 and 10 km do not follow the same statistical trend as the smaller craters. In fact, they seem to follow the trend of the craters on the surrounding plains, but have a normalized density greater than that on the plains. If the volcanoes are much older than the plains, one must then explain the paucity of larger craters (> 20 km) on the volcanic flanks. If the excess craters are not of impact origin, then a second population of large volcanic craters would seem suggested. At present, no way has been devised to distinguish between the alternatives. Since Hecates Tholus has nearly twice as many 3-10 km craters as Albor Tholus, this may indicate the northern dome was formed somewhat earlier than the southern volcano (if the mechanism of crater formation was in any way a time-dependent function). Alternatively, it may indicate substantially different forms of volcanism. Finally, all of the Elysium volcanoes display more cratering than the oldest Tharsis plains (Fig. 7), and than the Tharsis volcanoes (K. Blasius, personal communication, 1974). This suggests that the Elysium volcanoes may be older than the volcanoes of Tharsis.

Comparisons of Emi Koussi and Elysium Mons

Comparisons of Emi Koussi and Elysium Mons can be made in two areas -- the summit calderas and on the flanks of the volcanoes (Fig. 8). In discussing the calderas, both the large-scale features of the craters and the structures on their floors will be compared.

Caldera Features

The Elysium Mons caldera is approximately 14 km in diameter, with a rim height in the northwest of about 1 km but rimless in the south and southeast. The south rim may have been removed by upwelling and overflow of material from within the caldera, through burial by ash deposits, or by explosion. The caldera rim is marked by two concentric escarpments, separated by about 200 m, with the outermost scarp at least 100 m higher than the innermost. Although some features on the interscarp bench are suggestive of those on the caldera floor, it cannot be definitely established that the bench represents the remnant of a previous caldera which has undergone a second collapse. An equally likely origin is differential faulting and terracing accompanying a single episode of collapse of the caldera. The Emi Koussi caldera is very similar to the Elysium Mons caldera on Mars. The crater is about 12-15 km across and consists of two, nested calderas with a maximum depth of about 500 m (9). The collapse of the inner caldera occurred some time after the formation of the outer caldera. The rim of the Elysium Mons caldera is essentially smoothly curving, but that of Emi Koussi is occasionally indented and irregular. This difference is apparently related to the erosional environment, since the terrestrial caldera's irregularities are associated with channels and mass movements precipitated by aqueous erosion.

The floor of the Elysium Mons caldera contains numerous large, coalesced depressions bounded by escarpments of subtle relief. At least four levels and perhaps as many as six, are present, although

the boundaries are near the limit of resolution and cannot be drawn without some uncertainty. The floor is also pocked by at least 21 craters larger than 200 m. Size and resolution limitations prevent unique categorization of these craters as endogenic or exogenic. However, some craters appear rimless and shallow (a morphology typically endogenic, e.g., maars, or collapse craters), others appear to be bowl-shaped and to have raised rims (characteristic of impact craters), and a very few appear to have slightly raised and extended rims and shallow interiors (possibly the martian equivalent to terrestrial cinder cones (14)). Emi Koussi also has numerous craters on its caldera's floor. The largest, Era Kohor, is 3 km across and 350 m deep. It is accompanied by at least 2 and possibly more craters, and all are probably of phreatic origin (9). Crater morphologies are remarkably similar to some of those on Mars. Numerous basalt flows and cinder cones are visible on the floor of Emi Koussi caldera, but none are identifiable in Mariner photos of Elysium Mons. This may reflect, however, insufficient spatial and spectral resolution of the Mariner 9 data rather than the actual absence of these features on Mars.

Flank Features

The most distinctive, and probably most coincidental, features of similarity on the two volcanoes are the channel-like forms which emanate from the calderas. In both cases, a larger channel breaches only the outer caldera wall, while a second, smaller channel transects both walls. In addition, both larger channels head in roughly circular depressions. The smaller channels are somewhat more sinuous. All channels taper

downslope. The terrestrial examples connect to the regional hydrological drainage system; the martian examples become a discontinuous series of elliptical depressions and eventually disappear. The Elysium Mons channels trend north, the same direction as the tectonic trend reflected in the ridged plains and in the position of Hecates Tholus, relative to Elysium Mons. The channels on Emi Koussi follow the local and regional tectonic trend, and have been flooded by fluid basalts from within the calderas. Their origin is believed a combination of tectonic fracturing and collapse of the volcanic flank associated with the caldera collapse and subsequent volcanism, and possibly by collapse of lava tubes or lava erosion as basalts flowed from the caldera through the channels and downslope. It seems plausible that the channels on both planets reflect similar origins.

Other channel-like features mark both volcanoes. The lower flanks of Emi Koussi are deeply dissected, evidence of a major erosional period during the late Tertiary-early Quaternary. Numerous small channels reflect Pleistocene erosion (as many as five episodes are noted elsewhere in Tibesti), and some erosion is still taking place, at reduced rates. Only a few channels occur on Elysium Mons and are invariably formed by chains of coalesced depressions. Greeley (6) has interpreted these as partially collapsed lava tubes, which is entirely consistent with the available data. There appears to be no evidence of erosional channels of aqueous origin on Elysium Mons.

The slopes of Elysium Mons are heavily cratered. The largest crater seen in high resolution is about 5 km in diameter and located

just south of the Elysium Mons caldera (Fig. 6). It is essentially bowl-shaped, but has a small, flat floor. Low-sun shadow analysis places its depth at about 500 m. It is believed to be of impact origin. However, as noted earlier, many other craters are probably of endogenic origin. This is especially true for craters which occur in chains distinct from those mentioned above. These chains are formed primarily of circular craters and extend east from the caldera. Greeley (6) proposed that these features represented pit craters aligned over rift zones. The fact that the topography of Elysium Mons indicates a structural trend in that direction supports the hypothesis of rift zones. The larger, NW-SE ridge may also overlie a rift zone.

Emi Koussi has a few craters on its slopes, all of endogenic origin. The most likely explanation for these craters is phreatic eruption during the late Quaternary.

The greatest distinction between Emi Koussi and Elysium Mons can be made on the basis of overall flank morphology. The terrestrial volcano has numerous flows and cinder cones marking its slopes. These are discernible in both ERTS and Apollo photography at all wavelengths and sun angles for which imaging data was available (although flows were more visible in IR photos, and cones in the film and low sun frames). Emi Koussi has a form typical of a broad shield composed of numerous flows.

Elysium Mons, on the other hand, has a surface comprised of many subtle, irregular mounds of low relief, giving the slopes a hummocky appearance. The largest mounds seen are about 5 km across, but most

are significantly smaller. Flows as seen on Olympus Mons and the other Tharsis volcanoes are not visible, although many of the mounds appear to have short, stubby appendages which point downslope. The observed radial pattern of features resolves to elongate hummocks and narrow valleys, some of which are simply the depression between two primary ridges, others of which appear to be unassociated with positive relief features. Some of the mounds have subdued craters at their summits; most do not. The entire surface appears subdued, with little detail at high resolution. The slopes of Elysium Mons ($\sim$ 10-12°) are significantly steeper than those of Emi Koussi ($\sim$ 2-3°) and Olympus Mons ($\sim$ 2-5°; 15,16).

Conclusions and Speculations

Without ground-truth from the surface of Mars, any comparison between the origin and evolution of terrestrial and martian volcanoes is necessarily speculative. The following interpretations are presented as plausible possibilities, not as unique explanations. The following discussion will center on the nature and origin of the Elysium volcanics and on the implications of surface features for past environmental conditions on Mars.

Evidence of Magmatic Source Evolution

The Elysium volcanic province contains a wide variety of forms which are similar to those seen in Tibesti. Fissure eruption is likely the source of the plains units (both cratered and ridged plains) on Mars and of the plateaus in Tibesti on the Earth. Central volcanism is present in both regions in the form of large, shield-like constructs and domes. Hecates Tholus has the classic form of a volcanic dome

formed on a slope, although it is extremely large by terrestrial standards. The presence at its summit of knobby structures enhances the similarity to terrestrial volcanoes with highly viscous extrusions.

Elysium Mons is most likely a composite volcano. This conclusion is reached through consideration of three observations. First, the highly subdued appearance of the flanks of the volcano suggests the presence of a blanketing material which conforms to, rather than obscures, the irregular mounds (probably flows of viscous lava). This blanket has a lower albedo than the blankets which cover much of Mars poleward of 40° latitude, and may be comprised of pyroclastic materials. Second, the presence of numerous craters (other than those associated with rifts) suggests explosive ejection of magmatic material, likely to produce ash deposits. Finally, the steepness of the average slope ($\sim 12°$), nearly twice that of any other martian volcano yet determined, indicates the presence of materials other than fluid lavas. Whether comprised of viscous lavas, viscous and fluid lavas, or viscous and fluid lavas with ash deposits, Elysium Mons is not simply a shield of the Tharsis type.

Tectonics of Elysium Volcanic Province

In both Elysium and Tibesti, volcanism is associated with the doming of pre-existing materials. It is localized within a relatively small area and follows the tectonic trends established during the uplift. Differences in the 3-10 km diameter crater density on the three Elysium volcanoes may indicate either a slight age difference or a difference in the type of volcanism, with Hecates Tholus the oldest and/or most evolved and Albor Tholus the youngest/least evolved. It is tempting

to cite the observed trend as evidence for motion of the magma source. However, since Hecates Tholus shows no sign of earlier, less silicic volcanism, the observed trend would seem to indicate that the magmatic source region became less silicic as it evolved towards the south. This seems to contradict the terrestrial sequence of magmatic evolution where magmas from a single source become more silicic with time. Although multiple magmatic sources is a possible alternative, the local grouping of the Elysium volcanoes and the single, broad dome on which they are built suggest a common origin. With the ambiguous cratering relationships, it is possible to reduce or even reverse the observed "age" trend, and the lack of any other evidence for the migration of the volcanic center with time suggests that the source of magma may have been essentially stationary with respect to the surface. In addition, the general topography of Mars (11) shows the Elysium uplift to be bordered by two regional lows to the east and west. The implications of basin and swell topography in Africa have been examined (17,18,19) and related to mantle plume or "hot spot" activity beneath a stationary crustal plate. The absence of crustal rifting (often found in areas interpreted as uplifts above plumes) in Tibesti is attributed to melting and incorporation of crustal materials above the plume. The implication is that the martian crust has been essentially stationary with respect to the Elysium magma source, and that the absence of tectonic rifting is similarly the result of crustal melting (which may also be responsible for the evolution of the magma source). Crater densities indicate that the Elysium volcanic region is older

than the Tharsis volcanic region, reducing the velocity of any hypothetical crustal motion if Elysium has been active in any sense recently. This interpretation supports previous speculations that the martian crust has not undergone plate tectonic motion (5).

The age of the Elysium volcanoes is not only crucial to the above discussion but also to one concerning environmental change. In this case, however, it is not the total age but the age of the present surface which is important. As has been pointed out previously, cratering statistics are ambiguous. However, by comparing the trends on the Tharsis volcanoes (K. Blasius, personal communication, 1974) with those on Elysium Mons, it can be shown that Elysium Mons has a significantly greater proportion of raised-rimmed, bowl-shaped craters (diameters between 200 and 1000 m), probably of impact origin. The presence of many very subdued circular depressions on Elysium Mons may indicate a previous surface, since blanketed and re-cratered. Because the present crater population is essentially fresh in appearance, it is concluded that erosional and/or blanketing activity has been minimal for some period of time greater than the present oldest surfaces of the Tharsis volcanoes.

Constraints on Martian Environmental Changes

As can be seen by examining the satellite photography (Fig. 9), the major morphologic difference between Emi Koussi and Elysium Mons appears to be the presence of aqueous erosion on Earth. Emi Koussi and the entire Tibesti region record and preserve evidence of an erosional period which occurred almost two million years ago (although subsequent erosion is also responsible for some of the features seen).

Elysium Mons shows no trace of this type of erosion, nor do either of the other two volcanoes. Either martian volcanic materials do not record aqueous erosion as well as terrestrial volcanic materials, or aqueous erosion has not occurred since the last activity in Elysium. It seems unlikely that the rock types are so different as to erode on one planet and not on the other. If the surfaces of the Elysium volcanoes are as old as the relative cratering data suggests, then the last time Mars could have had an Earth-like erosional environment (if it ever had such an environment) must have been an extremely long time ago (perhaps as much as 10^9 years).

Sagan and others (20) have proposed that the surface of Mars is periodically subjected to high atmospheric pressure environments (approaching 1 bar) owing to runaway advective planetary heating. Significant amounts of water are necessarily included in such high pressure atmospheres (to promote planetary heating), and the advective model is geared towards producing an environment conducive to abundant running water. To initiate this condition, an increase in polar insolation of approximately 15% is required. Ward (21) has shown that astronomical perturbations which can change the polar insolation by over 100% occur on a 10^5 year time scale, so runaway advection (if it occurs at all) must have occurred during the last hundred thousand years. The absence of aqueous erosional features on ancient volcanic surfaces which should record such activity, greatly limits the amount of water and other volatiles that could have been released to the atmosphere. Murray and Malin (22) and Ward and others (23) have

proposed that the maximum possible atmospheric pressure is limited by the amount of volatiles stored at the poles (around 50 mbar). The evidence on Elysium Mons is consistent with this or slightly higher pressures but not with the environment proposed by Sagan.

APPENDIX

The photographic data used in this study come from three main sources: ERTS, Apollo, and Mariner imaging experiments (Table 1, Fig. 9). Additional data include individual ultraviolet spectrometer elevation profiles on Mars (10), a synthesis of martian topography derived from Earth-based radar and Mariner 9 radio occultation, ultraviolet spectrometer and infrared interferometer spectrometer data; and geologic maps of the Tibesti region and field reports on that area (5,7). This material is discussed in detail by the authors cited.

The ERTS data come from two on-board imaging devices, the multispectral scanner (MSS) and the return beam vidicon (RBV). The MSS consists of six photomultipliers in each of three bandpasses (green = .5 to .6μm, red = .6 to .7μm, IR1 = .7 to .8μm) and six photodiodes in one band-pass (IR2 = .80 to 1.1 μm), arranged in a 4 × 6 array with the short direction crossing the spacecraft's groundtrack. A flip-flop mirror moves the image across the array, acquiring data in swaths of six lines. On the forward sweep, the sensors image the terrestrial scene, while on the back-trace, the sensors are exposed to a lamp through a rotating neutral density filter to produce a wedge-shaped signal for calibration. The analog signal is encoded into six bits. The swath frequency is 13.62 Hz and the dwell time per picture element is 9.95 μsec. The frame height is arbitrarily cut at 447 swaths (= 2682 lines of 3755 samples each) to correspond roughly to the RBV field of view. The system has

essentially square resolution elements, with a modulation transfer function (MTF) of 0.29 and 0.31 across and along the groundtrack, respectively, when tested with a 69-meter equivalent bar chart. This corresponds to a resolution of approximately 137 m per line pair, and the total frame is roughly 185 km square. The RBV consists of three individual vidicons imaging identical scenes through 125 mm lenses simultaneously, through three filters (green=.475-.575, red=.580-.685, near IR=.69-.85μm). Each frame consists of 17×10^6 picture elements (4125 elements square). The data is transmitted to Earth and recorded analog. It can later be encoded into 8 bits for special processing. Two pixels have a projected surface resolution of $\sim$ 92 m. The frame is about 185 km on a side. Frame time for the RBV is 25 seconds.

ERTS-A is in a 918.596 km circular orbit ($e \simeq 0.0006$) inclined 99°, with a period of 103.16 minutes. Data are acquired only on the descending node (spacecraft motion from NE to SW), and are either transmitted in real time or recorded on-board for later transmission.

The Mariner 9 data also come from two imaging devices. These are identical vidicons imaging through 50 mm (wide angle/low resolution = A camera) and 500 mm (narrow angle/high resolution = B camera) lenses. Each frame is 832 samples wide by 700 lines high. Each picture element is encoded in 9 bits. Frame time is 42 seconds, alternating between cameras. At 1800 km altitude, the two pixel resolution of camera A is $\sim$ 1 km and of camera B, 100 m. Low-resolution frames were taken through a minus ultraviolet filter (broad-band centered roughly around 0.55 μm); high-resolution frames

through a linearly polarized orange filter (centered near 0.58 μm).

Mariner 9 is in an elliptical orbit (e ~ .62173) with a semi-major axis of 12,636 km, a periapsis altitude of 1387 km, inclined 64.37°, and has a period of 11.98 hours (Goldstone synchronous). Imaging data was tape-recorded and played back at 16 kbps to the Goldstone 210-foot antenna.

The Apollo data used in this investigation consists of a single Apollo 7 photograph taken with a hand-held Hasselblad 70 mm camera through a standard 80 mm lens on Kodak 121C color positive film. The spacecraft altitude at the time of exposure was approximately 213 km. The field of view of this slightly oblique photograph is 120 km by 150 km.

The original quality of the imaging data is hard to assess, since the materials used here are some generations removed from the originals. Additionally, differences in conditions during photography (e.g., illumination angle), ground reconstruction (i.e., picture element spacing), and spectral responsivity of sensors make it difficult to compare images, although some first-order interpretation is possible. Thus, the Apollo film photograph has by far the best resolution and displays the most physical detail because of the optimum illumination (low sun = large shadows) and the fine grain of the film. The Mariner 9 photos appear more detailed than the ERTS frames because of low sun angles and small picture element size (relative to spacing; i.e., reduced pixel overlap). Both MSS and RBV data appear less sharp than the Mariner 9 data, because the ERTS ground reconstruction equipment

made pixels larger than the inter-element spacing, causing a smoothing of the data. The ERTS MSS data are more detailed in the infrared, owing to the greater discernibility of certain rock types and the lower atmospheric interference at those wavelengths. The RBV frames are poor, probably the result of the electronic problems which eventually forced the premature shutdown of this experiment.

REFERENCES

1. H. Masursky, R. Batson, M. Carr, J. McCauley, D. Milton, L. Soderblom, R. Wildey, D. Wilhelms, B. Smith, T. Kirby, J. Robinson, C. Leovy, G. Briggs, T. Duxbury, C. Acton, Jr., B. Murray, J. Cutts, R. Leighton, R. Sharp, S. Smith, C. Sagan, J. Veverka, M. Noland, J. Lederberg, E. Levinthal, J. Pollack, J. Moore, W. Hartmann, E. Shipley, G. deVaucouleurs, and M. Davies, Television reconnaissance of Mars and its satellites, Science 175, 395 (1972).

2. J. McCauley, M. Carr, J. Cutts, W. Hartmann, H. Masursky, D. Milton, R. Sharp, and D. Wilhelms, Preliminary Mariner 9 report on the geology of Mars, Icarus 17, 289 (1972).

3. H. Masursky, An overview of geologic results from Mariner 9, Jour. Geophys. Res. 78, 4009 (1973).

4. M. Carr, H. Masursky, and R. Sanders, A generalized geologic map of Mars, Jour. Geophys. Res. 78, 4031 (1973).

5. M. Carr, Volcanism on Mars, Jour. Geophys. Res. 78, 4049 (1973).

6. R. Greeley, Mariner 9 photographs of small volcanic structures on Mars, Geology 1, 175 (1973).

7. P. M. Vincent, The evolution of the Tibesti volcanic province, eastern Sahara, in African Magmatism and Tectonics, T. N. Clifford and I. G. Glass (eds.), (Hafner Publishing Co., Darien, Conn.), pp. 301-319 (1970).

8. P. M. Vincent, Les volcans tertiaires et quaternaires du Tibesti occidental et central (Sahara du Tchad), Mem. Bur. Rech. geol. min. 23 (1963).

9. B. Geze, H. Hudeley, P. M. Vincent, and P. Wacrenier, Les volcans du Tibesti (Sahara du Tchad), Bull. volcan. 22, 135 (1959).

10. H. Hagedorn, Untersuchen über Relieftypen arider Raume an Beispielen aus dem Tibesti-Gebirge und seiner Umgebung, Zeit. für Geomorph., Supp· 11, 1 (1971).

11. E. J. Christensen, Martian topography derived from occultation, radar, spectral, and optical measurements (in press, Jour. Geophys. Res., 1975).

12. C. W. Hord, K. E. Simmons, and L. K. McLaughlin, Pressure-altitude measurements on Mars -- An atlas of Mars local topography, Laboratory for Atmospheric and Space Physics, University of Colorado, Boulder (1974).

13. L. A. Soderblom, R. A. West, B. M. Herman, T. J. Kreidler, and C. D. Condit, Martian planetwide crater distributions: Implications for geologic history and surface processes, Icarus 22, 239 (1974).

14. T. R. McGetchin, M. Settle, and B. A. Chouet, Cinder cone growth modeled after Northeast Crater, Mount Etna, Sicily, Jour. Geophys. Res. 79, 3257 (1974).

15. K. Blasius, A study of martian topography by analytic photogrammetry, Jour. Geophys. Res. 78, 4411 (1973).

16. S. S. C. Wu, F. J. Shafer, G. M. Nakata, R. Jorday, and K. R. Blasius, Photogrammetric evaluation of Mariner 9 photography, Jour. Geophys. Res. 78, 4405 (1973).

17. K. Burke and J. T. Wilson, Is the African plate stationary? Nature 239, 387 (1972).

18. J. T. Wilson, Mantle plumes and plate motions, Tectonophysics 19, 149 (173).

19. K. Burke and A. J. Whiteman, Uplift, rifting and the breakup of Africa, in Implications of Continental Drift to the Earth Sciences, D. H. Tarling and S. K. Runcorn (eds.) (Academic Press, London and New York), vol. 2, capt. 7.2, pp. 735-755 (1973).

20. C. Sagan, O. Toon and P. Gierasch, Climatic change on Mars, Science 181, 1045 (1973).

21. W. R. Ward, Climatic variations on Mars: I. Astronomical theory of insolation, Jour. Geophys. Res. 79, 3375 (1974).

22. B. C. Murray and M. C. Malin, Polar volatiles on Mars: Theory vs. observation, Science 182, 437 (1973).

23. W. R. Ward, B. C. Murray, and M. C. Malin, Climatic variations on Mars: II. Evolution of carbon dioxide atmosphere and polar caps, Jour. Geophys. Res. 79, 3387 (1974).

TABLE I

Spacecraft	Frame	Lat. (Deg.)	Long. (Deg.)	Picture Height (km)	Picture Width (km)	Sun Elevation Angle (Deg.)	Negative Generation
Apollo 7	5-1621(1)	19.92N	18.54E	120	150	14	5
ERTS-A							
RBV	1010-08425-1(1)	20.18N	18.20E	185	185	31	4
MSS	1064-08425-6(1)	20.15N	18.25E	185	185	36	4
Mariner 9	6391738(9,**)	21.90N	213.90W	439	897	32	3
	8982649	29.43	221.09	565	721	32	
	9054539(2)	29.50	211.67	561	718	32	
	9126429	29.70	202.46	560	719	33	
	7651453(3,*)	24.54	216.94	528	684	27	
	7651593(3)	23.58	204.95	632	732	17	
	7651103	17.05	216.45	430	554	31	
	7722993(4)	17.35	208.07	430	555	32	
	7723278(9,**)	16.90	204.30	570	651	28	
	6391803(5,*)	27.30	213.20	480	1007	28	
	13496013(6)	24.18	213.06	61	76	9	
	13496083(7)	24.97	213.19	64	79	9	
	13496118(7)	24.53	213.02	641	825	10	
	13496293(8)	31.61	209.84	69	87	15	
	13496363(8)	31.89	211.04	72	90	15	

(1) Emi Koussi, Figures 2,8,9
(2) Hecates Tholus, Figure 3
(3) Elysium Mons, Figures 3,5
(4) Albor Tholus, Figure 3
(5) Elysium Mons
(6) Elysium Mons, Figure 5
(7) Elysium Mons, Figures 6,8,9
(8) Hecates Tholus, Figure 4
(9) Albor Tholus
* Photogrammetric pairs
**

FIGURE CAPTIONS

Figure 1: Geologic Sketch Map: Tibesti Volcanic Province, Chad, Africa. Regional setting for volcano Emi Koussi (EK, lower right). Other volcanoes are: Toussidé (To), Timi (Tm), Trou au natron (TN), Sosso (S), Yirrigué (Y), Abéki (A), Mousgou (M), Voon (V), Yéga (Ye), Oyoye (Oy), Toon (T), Tieroko (Ti), Dadoi (D).
(Map after Vincent (1970) and Gese et al. (1963)).

Figure 2: ERTS Photograph: Emi Koussi and surroundings, Earth. Earth Resources Technology Satellite multispectral scanner photograph of southeastern Tibesti showing Emi Koussi in lower right. Volcano is about 70 km in diameter with 12 × 15 km caldera. Recent basalts appear very dark in this infrared photograph. Massive valley incision occurred at the beginning of the Pleistocene. Portions of the Yéga, Oyoye, Toon, and Tieroko volcanoes can be seen in the upper left section of the image. For photographic support data, see Appendix and Table 1.

Figure 3a: Geologic Sketch Map: Elysium Volcanic Province, Mars. Regional setting for Elysium Mons, Hecates Tholus and Albor Tholus. Note location of volcanoes on the crest of a broad, topographic high, with tectonic depressions aligned perpendicular to contours at maximum regional topographic gradient. Hecates Tholus, with a form reminiscent of a classic volcanic

dome, is probably 8-10 km above the 6.1 mbar mean martian pressure surface; Elysium Mons is about 20 km above that surface. General topography from Christensen (1974), with detailed topography from Hord et al. (1974) and from photogrammetry based on the method described by Blasius (1973).

Figure 3B: Photomosaic of Elysium Volcanic Province, Mars. Mercator-projected photomosaic of Mariner 9 frames showing Elysium volcanic province. Images processed by the Image Processing Laboratory of the Jet Propulsion Laboratory. Note distinct boundary of Hecates Tholus, and diffuse boundaries of the other two volcanoes.

Figure 4: Photomosaic and Terrain Sketch Map of Hecates Tholus (Mars).

4A: Photomosaic of Mariner 9 high-resolution frames showing part of the Hecates Tholus volcanic dome (left) and Elysium Plains (right). Illumination is from the left.

4B: Sketch map of Hecates Tholus region. Large embayment of dome in lower center of map may be a secondary caldera or impact crater modified by erosional processes. Crater at far right is believed to be of impact origin because of its circularity, concentric rim terracing, and the radial texture of the surface exterior to the rim. Note differences between crater and central caldera at left center. Volcanic flows near the crater may have been formed from fissure eruption provoked by the impact event, but more likely were formed before the impact occurred, and are

covered by impact ejecta distinguished from the volcanic material by the radial texture. Slight textural differences in the plains surface at the volcano's edge may indicate late channel activity and deposition at channel mouths. The channeling is believed to be volcanic.

Figure 5: Elysium Mons: Low Resolution.

Left: Mercator projection of Elysium Mons with topographic point network and contours. Contour interval is 2 km (resolution of photogrammetric data = ± 1.5 km). Summit arbitrarily chosen as zero altitude. Data may contain residual overall tilt of no more than 2 km across entire frame. Sun from lower left.

Right: Near vertical view of Elysium Mons, with lighting from upper right. Note subdued ridged plain immediately north of volcano.

Figure 6: Elysium Mons: High Resolution

Two-frame mosaic, sun from left. Caldera approximately 15 km in diameter, 1 km deep in northwest. Large (5 km) crater at southeast caldera rim is believed of impact origin. Channels connected to caldera are thought to have a volcano-tectonic origin. Large black line at top of mosaic is a data drop. For support information, see Appendix and Table 1.

Figure 7: Size-Frequency Cratering Curves for the Elysium Volcanic Province.

7A: Crater counts on high-resolution photographs of

Elysium Mons reveal extremely large slope for craters smaller than 1.5 km diameter, corresponding to craters of volcanic origin. Correlation between slope for larger craters (seen at both high and low resolution) and other cratered surfaces (c.f., Soderblom et al., 1974) suggests they are of impact origin.

7B: Crater populations on the Elysium and Tharsis plains, on Hecates Tholus and on Olympus Mons illustrate the range in relative ages of these volcanic landforms. The insert shows the normalized population of 4-10 km craters, which have been used to assign relative ages to surfaces over the entire planet (Soderblom et al., 1974). The error bars in both figures are statistical representations of the random nature of crater counts (square root of N for small N), and are slightly overestimated.

Figure 8: Comparison of Emi Koussi and Elysium Mons.

8A: Emi Koussi.

Top: Sketch Map of Emi Koussi made on enlargements of ERTS RBV and MSS and Apollo 7 photographs. Physical features from low-sun film product; geologic contacts from ERTS MSS infrared and color differenced data. Identification of rock types based on tentative correlation with field map of Geze et al. (1963).

Bottom: Enlargement of Apollo 7 frame 5-1621 showing region mapped. Note deeply dissected flanks of volcano,

craters, and cinder cones.

8B: Elysium Mons

Top: Sketch Map of Elysium Mons made on enlargements of Mariner 9 photography. No distinct units were mappable, but several distinguishable elevation levels within caldera may correlate to phases of activity. "Ringed" craters may have extended, raised rims and shallow interiors, suggestive of the form predicted by McGetchin and others (1974) for martian cinder cones.

Bottom: Enlargement of Mariner 9 frame DAS13496083 showing region mapped. Surface of volcanic flank shows low, subdued mounds and radial pattern, possibly caused by volcanic ash mantling flows of viscous lava, and numerous craters and crater chains.

Figure 9: Comparison of Spacecraft Imaging Data.

Four sources of photographic data are compared here. ERTS RBV and MSS are smoothed by ground reconstruction equipment and were taken at relatively high sun angles. Apollo 7 data is from color film and Mariner 9 from vidicon, both at low sun angles. For discussion of imaging systems, see Appendix.

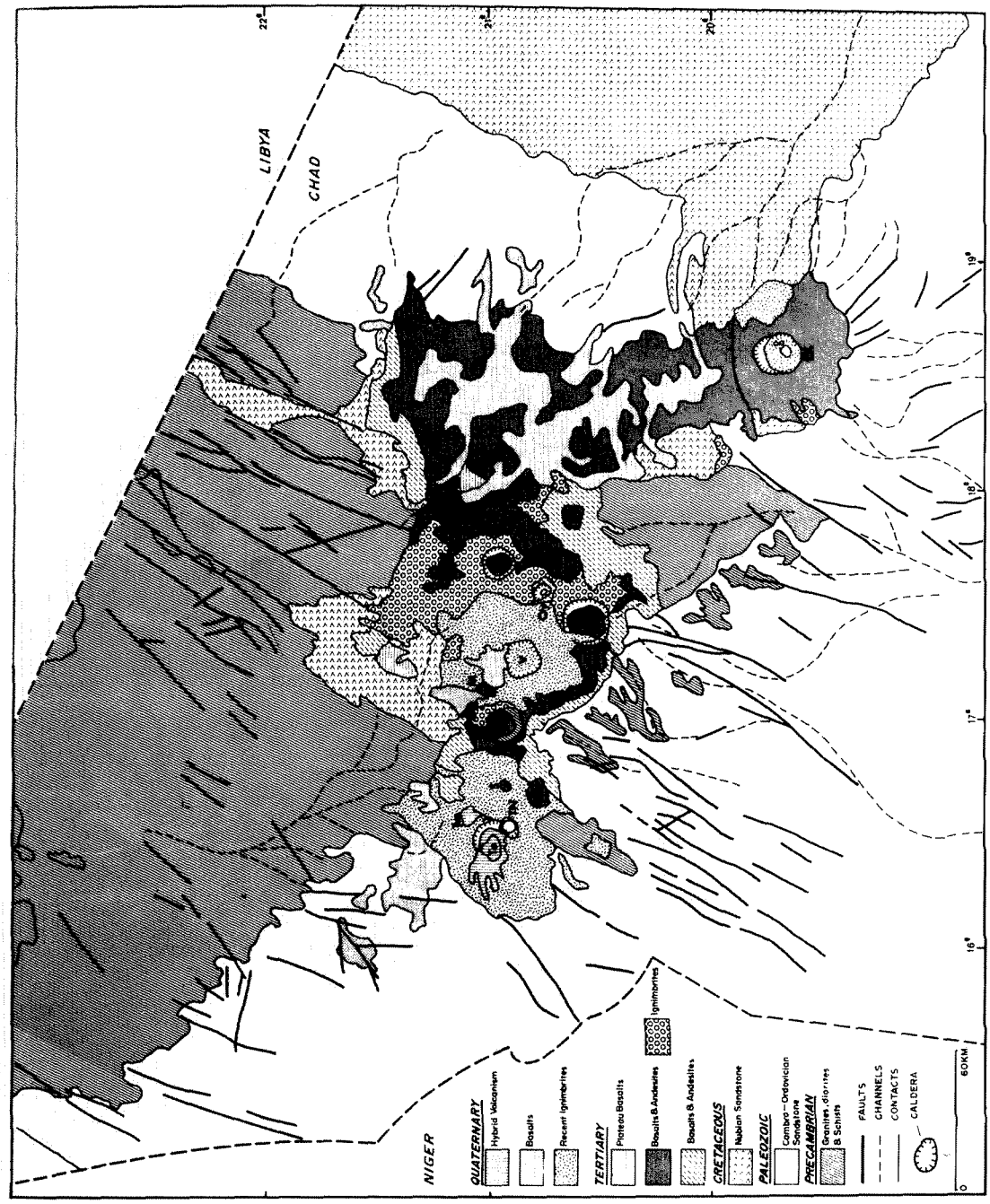
LIBYA
CHAD
NIGER
22°
21°
20°
19°
18°
17°
16°
QUATERNARY
Hybrid Volcanism
Basalts
Recent Ignimbrites
TERTIARY
Plateau Basalts
Basalts & Andesites
Ignimbrites
Basalts & Andesites
CRETACEOUS
Nubian Sandstone
PALEOZOIC
Cambro-Ordovician Sandstone
PRECAMBRIAN
Granites, diorites & Schists
FAULTS
CHANNELS
CONTACTS
CALDERA
0
60KM

Figure 1

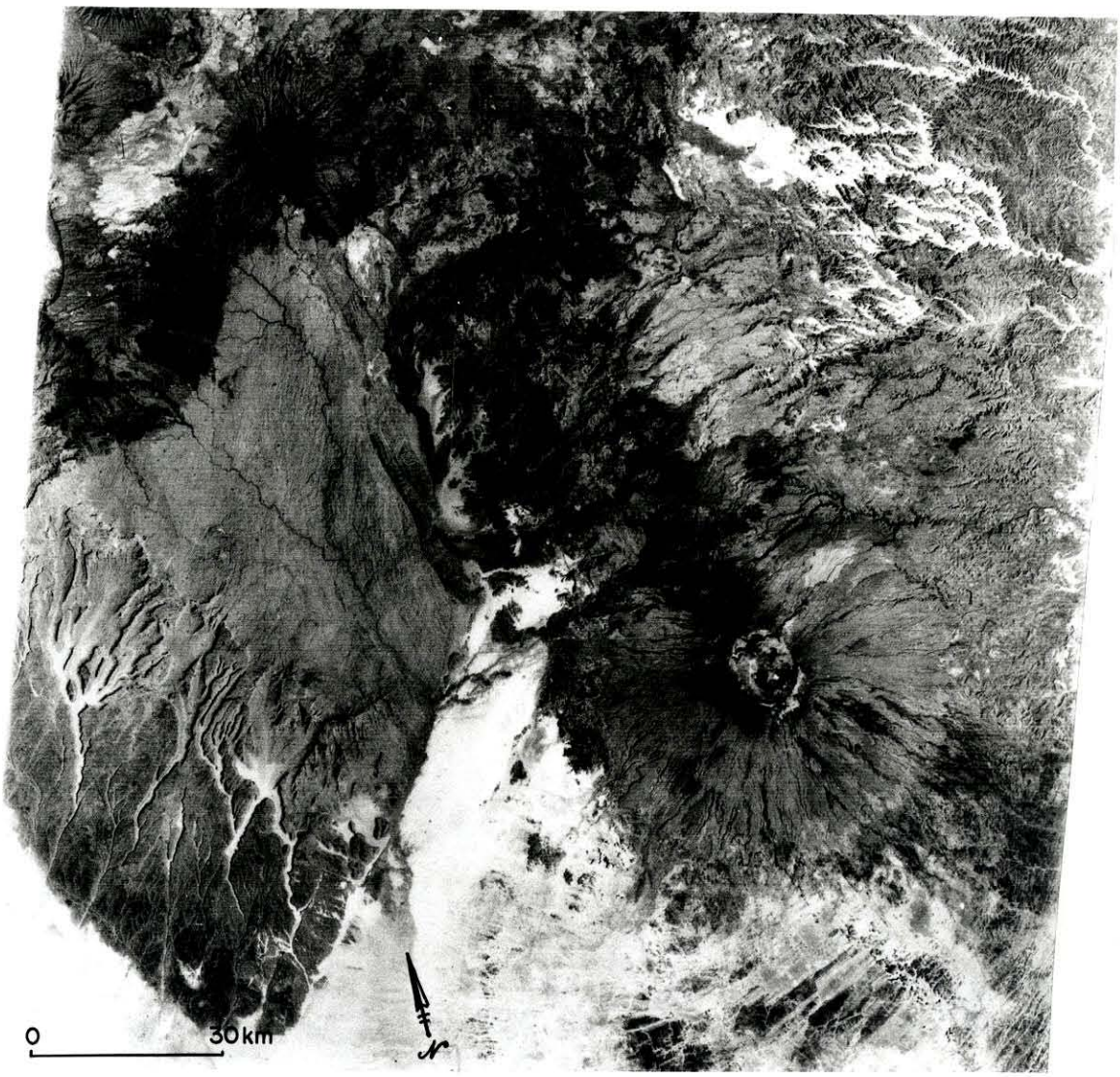

Figure 2

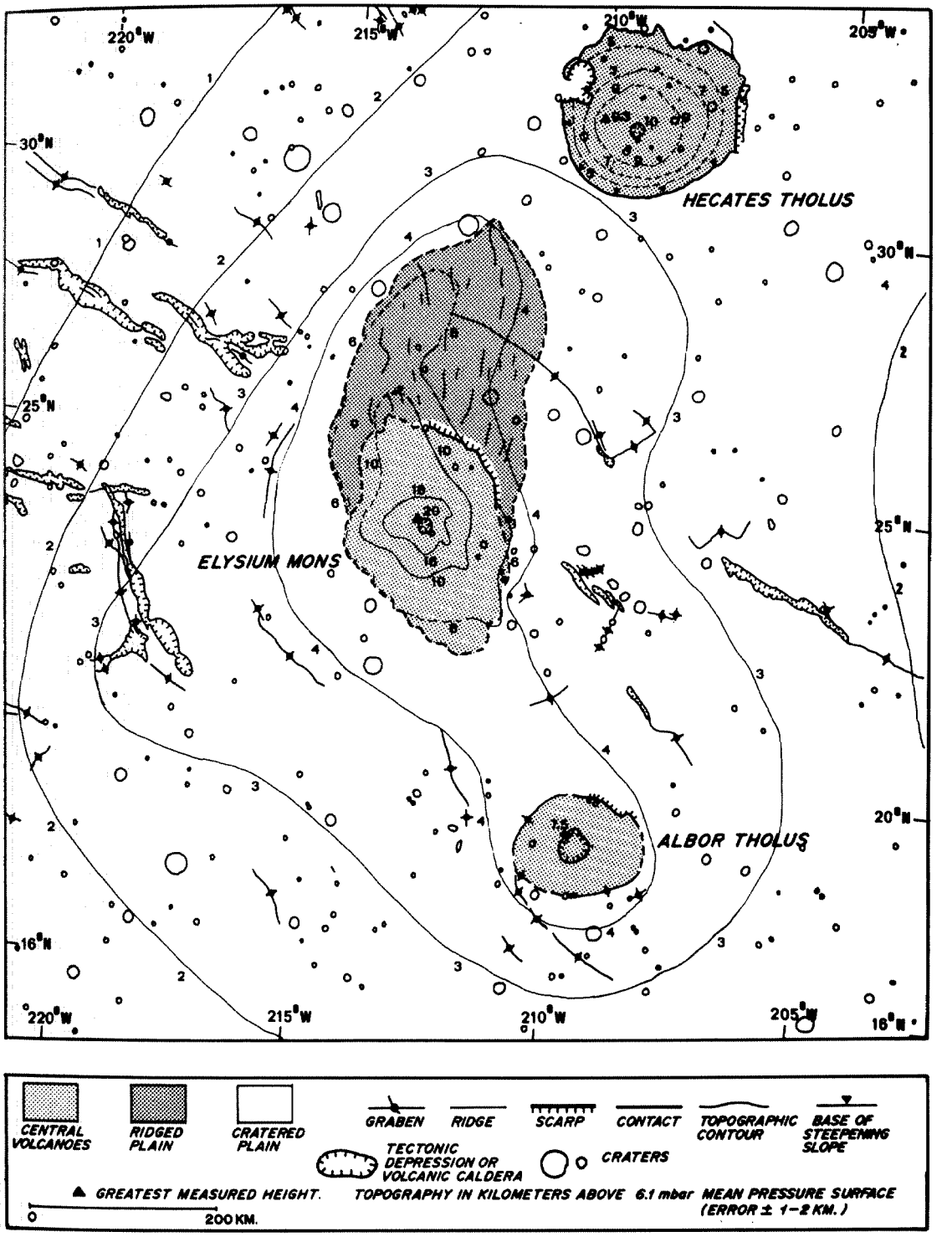
220°W
215°W
210°W
205°W
30°N
25°N
20°N
16°N
HECATES THOLUS
ELYSIUM MONS
ALBOR THOLUS
CENTRAL VOLCANOES
RIDGED PLAIN
CRATERED PLAIN
GRABEN
RIDGE
SCARP
CONTACT
TOPOGRAPHIC CONTOUR
BASE OF STEEPENING SLOPE
TECTONIC DEPRESSION OR VOLCANIC CALDERA
CRATERS
GREATEST MEASURED HEIGHT.
TOPOGRAPHY IN KILOMETERS ABOVE 6.1 mbar MEAN PRESSURE SURFACE (ERROR ± 1-2 KM.)
200 KM.

Figure 3A

Figure 3B

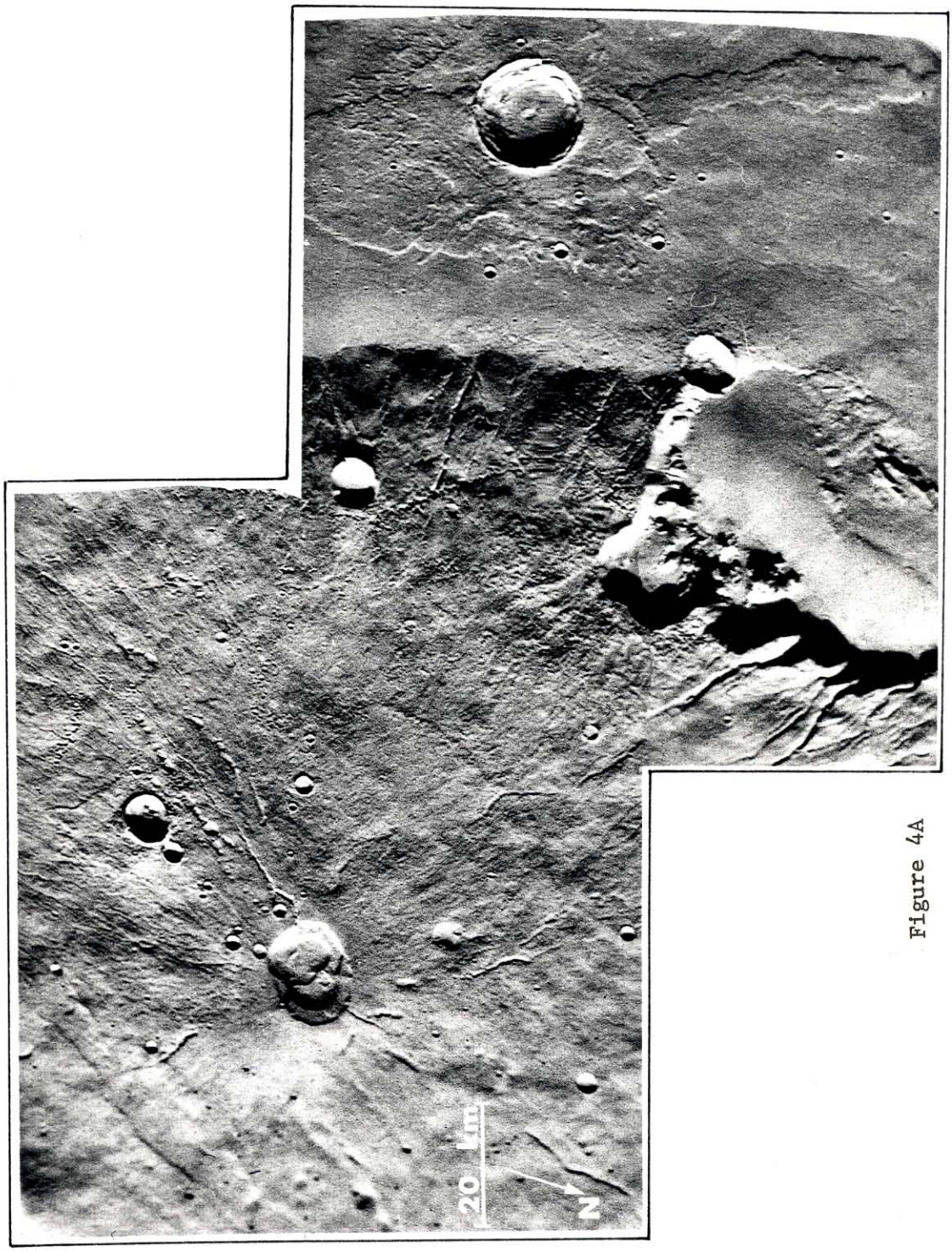

Figure 4A

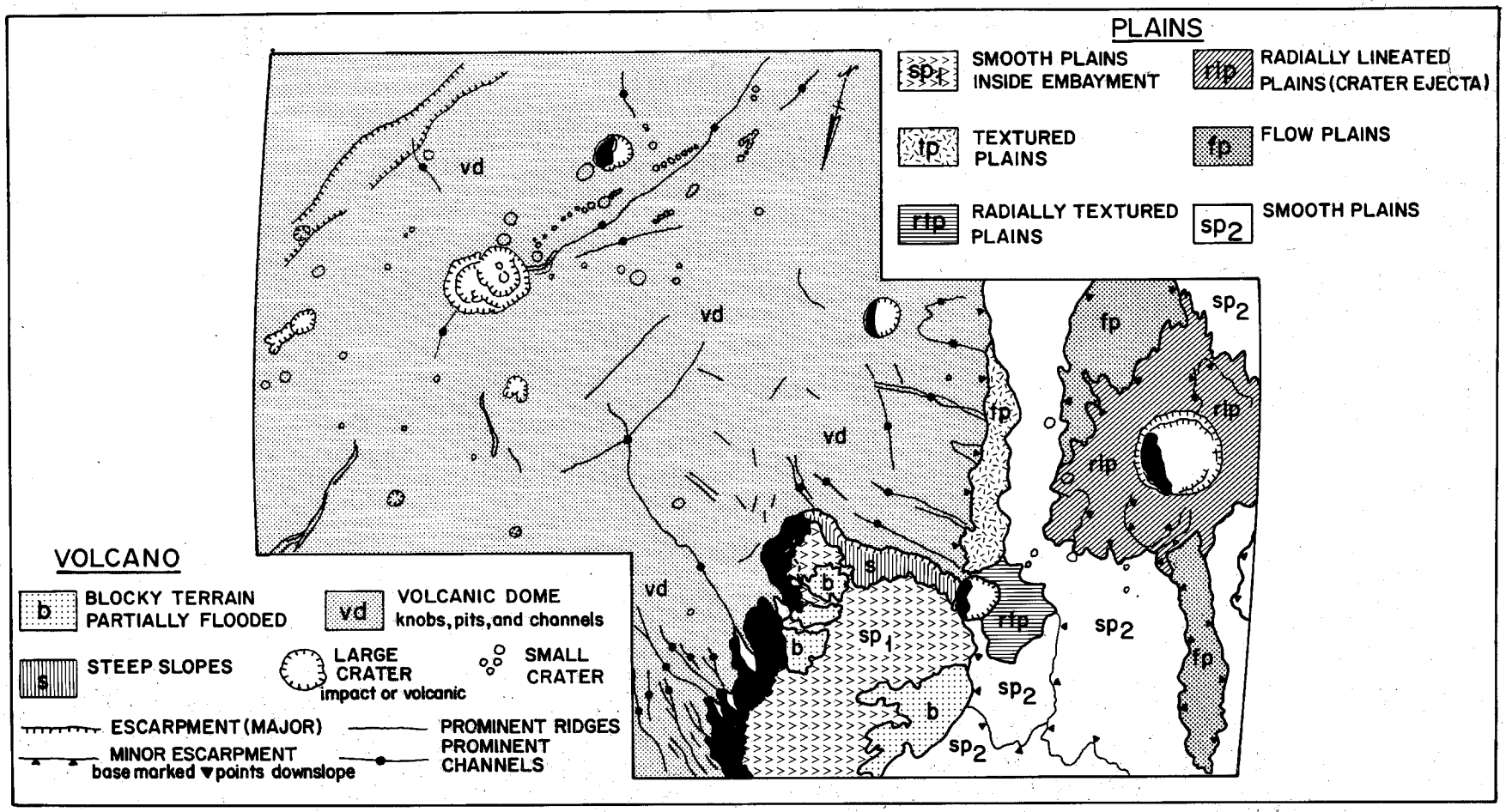
PLAINS
SMOOTH PLAINS INSIDE EMBAYMENT
RADIALLY LINEATED PLAINS (CRATER EJECTA)
TEXTURED PLAINS
FLOW PLAINS
RADIALLY TEXTURED PLAINS
SMOOTH PLAINS
VOLCANO
BLOCKY TERRAIN PARTIALLY FLOODED
VOLCANIC DOME knobs, pits, and channels
STEEP SLOPES
LARGE CRATER impact or volcanic
SMALL CRATER
ESCARPMENT (MAJOR)
PROMINENT RIDGES
MINOR ESCARPMENT base marked ▼ points downslope
PROMINENT CHANNELS
vd
b
s
fp
rlp
sp1
sp2

Figure 4B

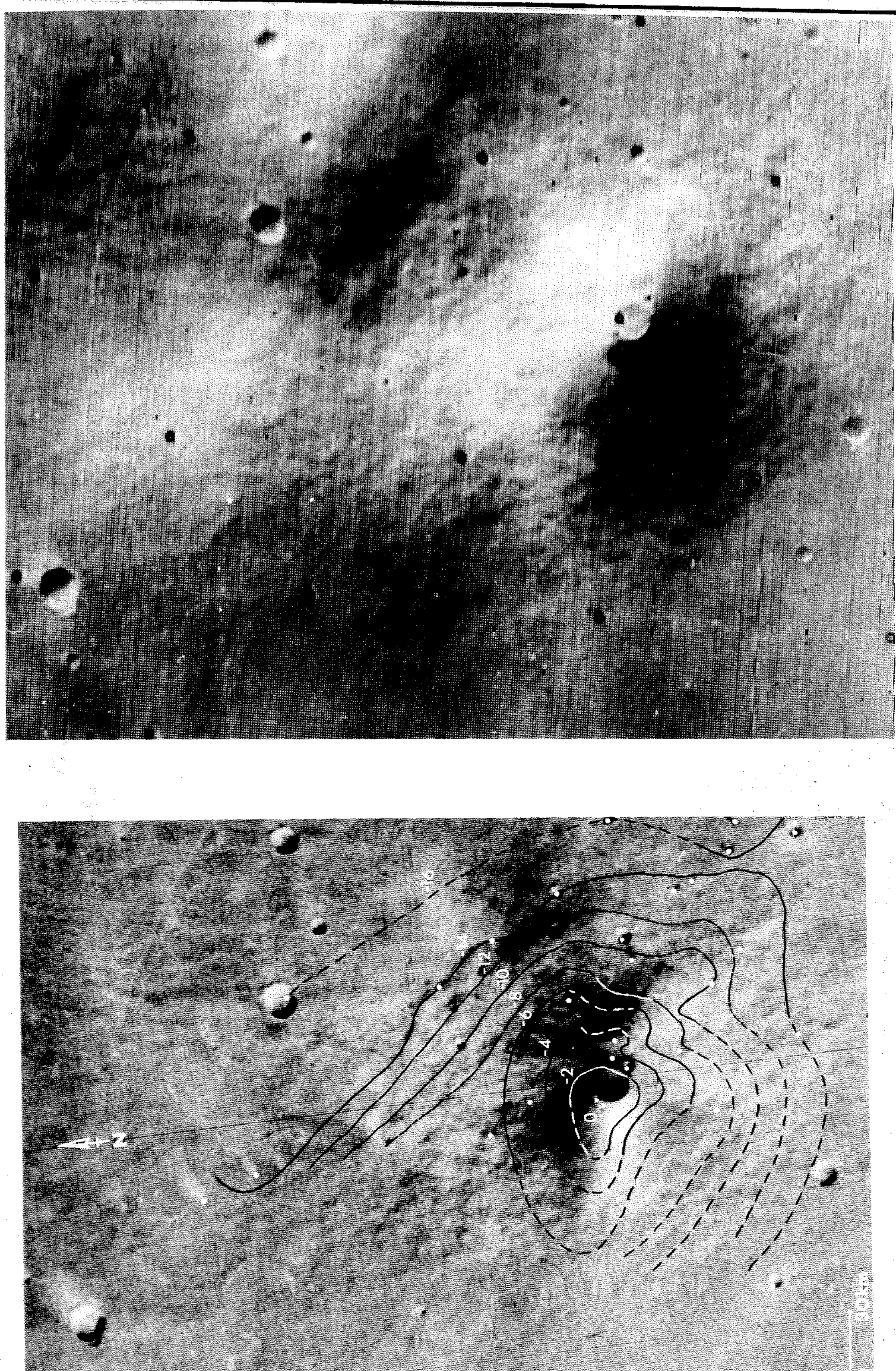

Figure 5

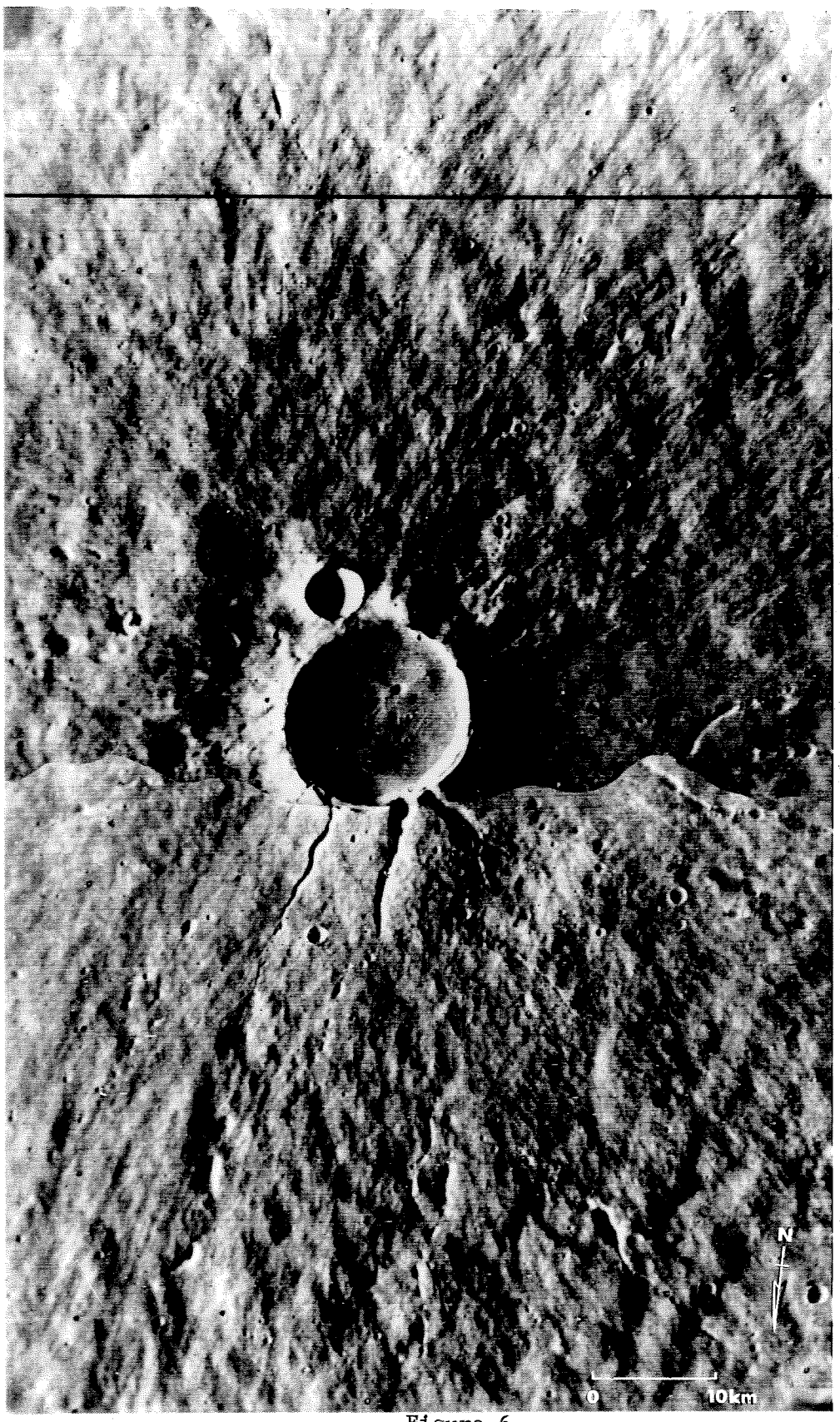

Figure 6

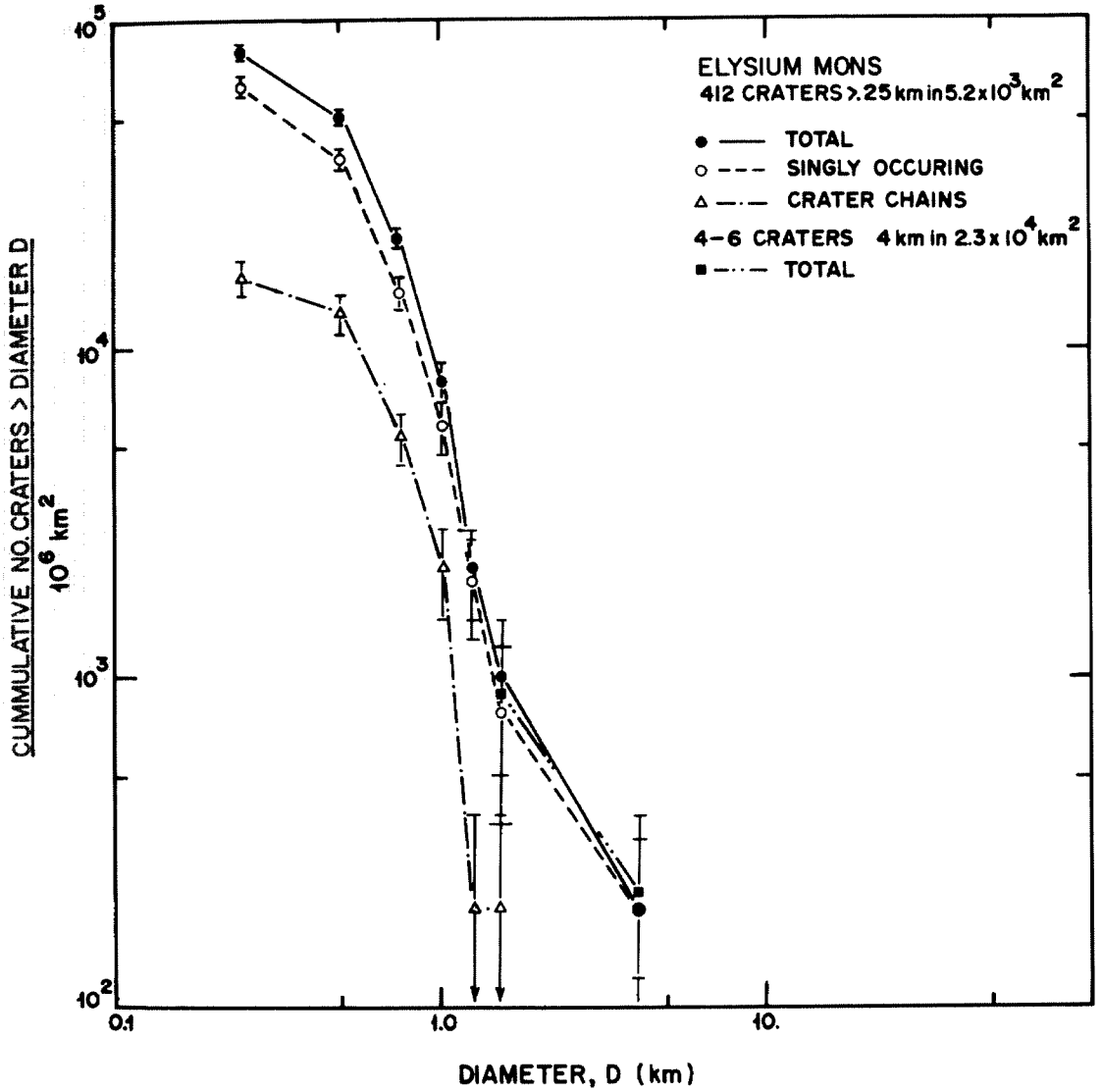
ELYSIUM MONS
412 CRATERS >.25 km in 5.2x10^3 km^2
TOTAL
SINGLY OCCURING
CRATER CHAINS
4-6 CRATERS 4 km in 2.3x10^4 km^2
TOTAL
CUMMULATIVE NO. CRATERS > DIAMETER D
10^6 km^2
10^5
10^4
10^3
10^2
0.1
1.0
10.
DIAMETER, D (km)

Figure 7A

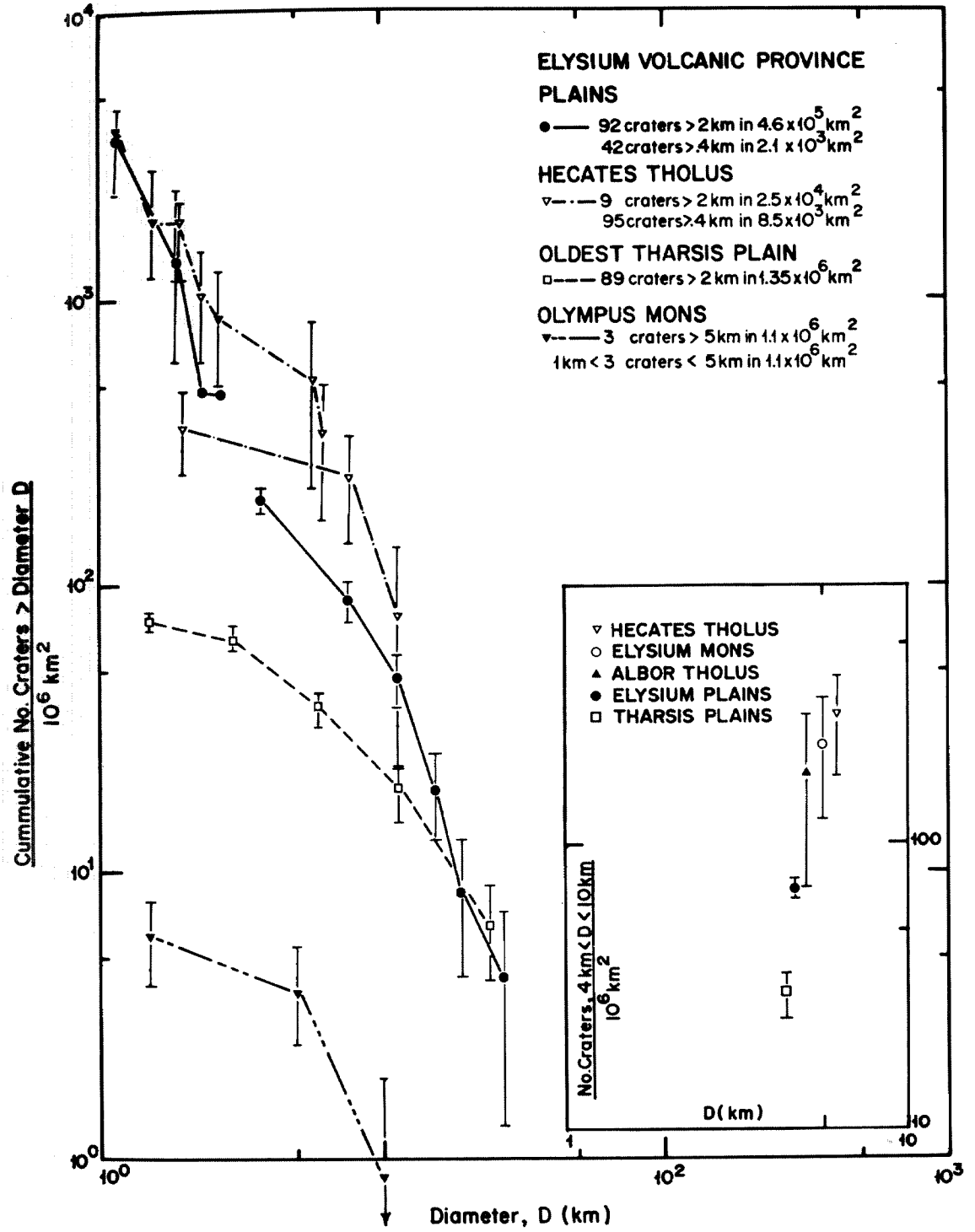
ELYSIUM VOLCANIC PROVINCE
PLAINS
92 craters > 2 km in 4.6 x 10^5 km^2
42 craters > 4 km in 2.1 x 10^3 km^2
HECATES THOLUS
9 craters > 2 km in 2.5 x 10^4 km^2
95 craters > 4 km in 8.5 x 10^3 km^2
OLDEST THARSIS PLAIN
89 craters > 2 km in 1.35 x 10^6 km^2
OLYMPUS MONS
3 craters > 5 km in 1.1 x 10^6 km^2
1 km < 3 craters < 5 km in 1.1 x 10^6 km^2
Cummulative No. Craters > Diameter D
10^6 km^2
Diameter, D (km)
HECATES THOLUS
ELYSIUM MONS
ALBOR THOLUS
ELYSIUM PLAINS
THARSIS PLAINS
No. Craters, 4 km < D < 10 km
10^6 km^2
D (km)

Figure 7B

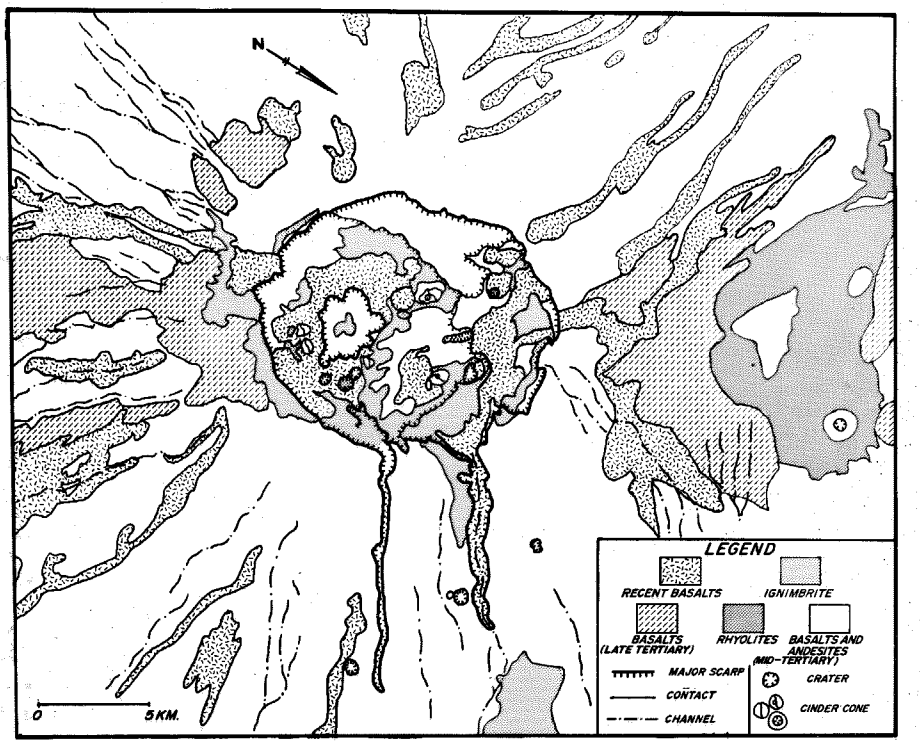
N
LEGEND
RECENT BASALTS
IGNIMBRITE
BASALTS (LATE TERTIARY)
RHYOLITES
BASALTS AND ANDESITES (MID-TERTIARY)
MAJOR SCARP
CONTACT
CHANNEL
CRATER
CINDER CONE
0
5KM.

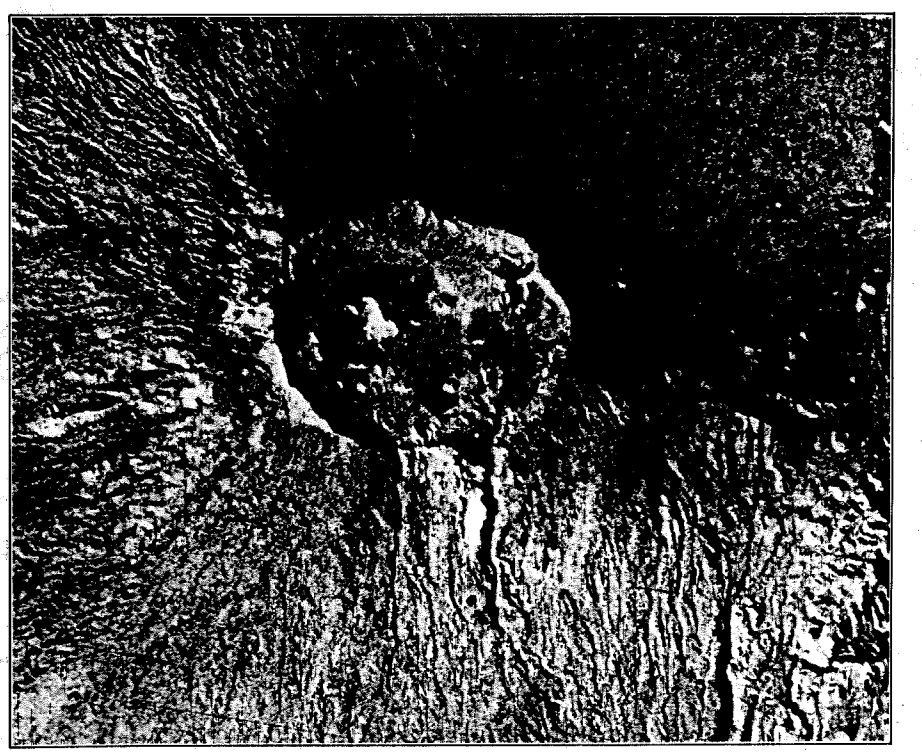

Figure 8A

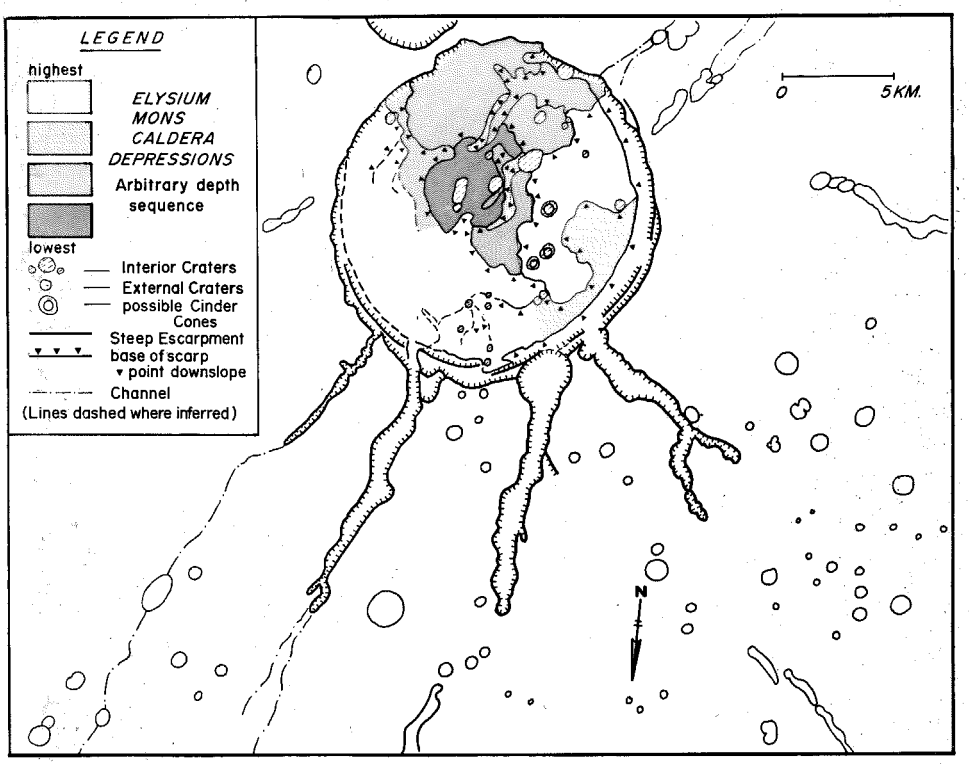
LEGEND
highest
ELYSIUM MONS CALDERA DEPRESSIONS
Arbitrary depth sequence
lowest
Interior Craters
External Craters
possible Cinder Cones
Steep Escarpment
base of scarp
▾ point downslope
Channel
(Lines dashed where inferred)
0
5KM.
N

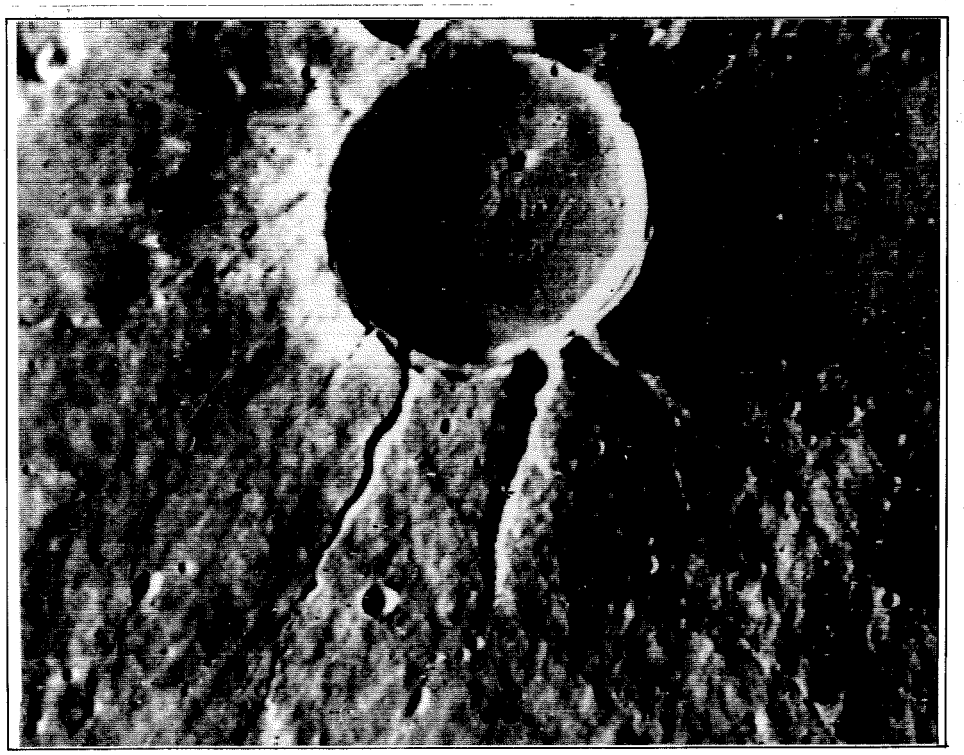

Figure 8B

ERTS RBV Band 3

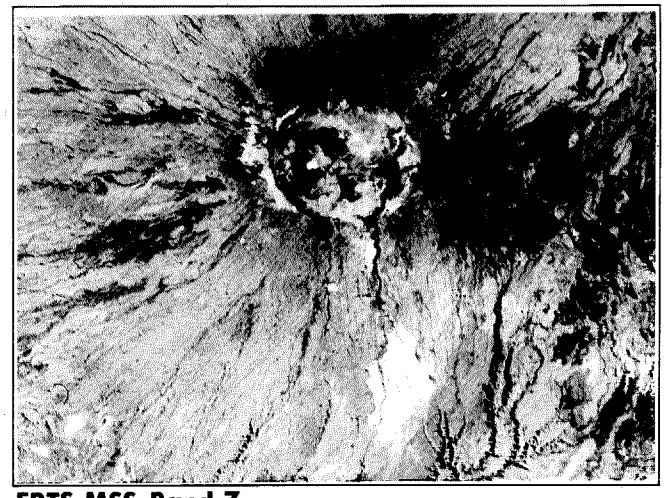

ERTS MSS Band 7

APOLLO 70mm FILM

MARINER 9 VIDICON

Figure 9

Part 2. Age of Martian Channels

Introduction

Of landforms revealed to the Mariner 9 spacecraft during its global reconnaissance of Mars in 1971 and 1972, four have evoked much interest from both the scientific community and the lay public. Discovery of gigantic volcanoes within Montes Tharsis and of the enormous Valles Marineris chasms, which was followed closely by recognition of sedimentary layered deposits in the polar regions, has stimulated extended discussion on the evolution of the atmosphere, surface, and interior of Mars. However, the most dramatic and controversial features remain the large, often sinuous channels so reminiscent of terrestrial river channels.

In the years since the completion of the Mariner 9 mission, strong differences have developed, and have not yet been resolved, concerning the mode of channel formation. Owing to limitations within imagery of kilometer resolution, the same feature is often cited as a "type example" by authors presenting opposed points of view. Unfortunately, higher resolution photography, when available, often provides as much confusion as clarification. Furthermore, each martian channel has its own specific characteristics, so that discussions tended to revolve around single examples. Only recently has an attempt been made to develop a general categorization scheme (Sharp and Malin, 1975). Although again based on "type examples", this scheme will be used to limit the discussion in this paper to a few specific types of channels. The types to be discussed comprise part of the exogenic family of channels termed "outflow" and "runoff", which are believed to be the result of the flow

of a liquid across the surface of Mars. The considerations of this paper are, however, independent of the mechanism for channel genesis.

The focus of this paper is upon the equally important question of channel age. Initially, it was believed that they were extremely young because of their fresh appearance and the paucity of superposed impact craters (cf, Masursky, 1973; Hartmann, 1973). Early crater counts seemed to indicate ages similar to those of the Tharsis volcanoes and south polar layered deposits, suggesting that Mars had undergone recent geological and, presumably, climatological changes. Estimates of absolute age, based on an impact flux enhanced by as much as a factor of 25 relative to the moon, ranged from tens of millions to hundreds of millions of years. Current interpretation, based on the recognition of more craters and on the reduction of the Mars-to-moon enhancement factor, would increase these ages by an order of magnitude (Soderblom et al., 1974; Blasius, 1975).

This paper will draw upon new crater counts and the principle of superposition to enlarge the data base for interpretation of relative age relationships between martian channels and other surface features. Implications of these relative ages and a possible absolute timescale will be discussed in a separate speculative section.

General Properties of Channels

The exogenic outflow, runoff, and fretted channels considered herein are defined by Sharp and Malin (1975) (Fig. 2) as follows:

> Outflow Channels: These are mostly large features that start full-born from localized sources. They are broadest and deepest at the head and decrease in size distally. Some appear to be scoured and display features suggestive of massive catastrophic flooding.

Runoff Channels: Such channels typically start small and increase in size and depth distally. The headwaters usually have tributary branches. Configurational control by crustal structures can be strong.

Fretted Channels: These are steep-walled features with wide smooth concordant floors. Planimetric configuration can be complex, with irregularly indented walls, integrated craters, and control by linear crusted structures, presumably fractures, often evident. Isolated butte- or mesa-like outliers are common, and extensive lateral integration of adjacent channels has occurred locally.

Many channels cited herein are hundreds of kilometers long, several kilometers wide, and as much as a kilometer deep. Their geographic distribution is shown in Figure 1 and given in Table I. Two major characteristics are apparent in their geographical and geological relationships: 1) with the exception of the Elysium channels, all exogenetic channels lie within the more heavily cratered portion of Mars, and 2) many of the channels appear associated with margins of the heavily cratered terrains. In addition, data from Sagan et al., (1973, Fig. 1) suggest that channels are most abundant in, if not restricted to, temperate and tropical latitudes. Runoff and outflow channels seem to head generally in areas of rough, irregular topography. In particular, outflow channel source areas are principally areas of chaotic terrain (see e.g., Sharp, 1973) and irregular regions of low, hummocky relief interpreted as regions of lithospheric seepage (Sharp and Malin, 1975). Fretted channels show no evidence of specific source regions, but some appear to head in craters or in features at least superficially resembling craters associated with modified chaotic terrain.

Among outflow channels, the Elysium features are unusual in appearing to head in elongate depressions of probable volcano/tectonic origin.

These channels are, however, easily distinguished from the many other endogenic channels which occur within the volcanic provinces by diagnostic features described by Sharp and Malin (1975). The Elysium channels discussed in that paper, however, are large volcano-tectonic features, not the smaller, sinuous, low relief features of concern in this paper.

Features Superimposed on Channels

The classical technique for determining relative age relationships between various landforms on extraterrestrial planetary surfaces involves the determination of the number of craters formed upon such surfaces. This procedure rests upon two assumptions; that the cratering processes are time-dependent and that they act everywhere in the same manner, and that the surfaces faithfully retain the craters, or modification by any degradational process is uniform over all surfaces.

On Mars, as on the moon, most craters are believed to be of impact origin, although volcanic craters may be important locally (see, e.g., Blasius, 1975; Malin, 1975). It seems reasonable to assume that the impact process is time-dependent and acts isotropically on all regions of Mars. However, it is not clear that martian degradational processes act uniformly over the entire planet. Indeed, the opposite seems more likely, for variations in small crater populations led to the identification of debris blankets which mantle the martian surface poleward of the 30th parallels (Soderblom et al., 1973).

One of the weaknesses of determining relative ages of some surfaces by cratering statistics is the small number of craters. Geologic

provinces encompass finite areas, and it is often difficult to find enough craters of the desired size to insure interpretative reliability.* Three ways have been commonly used to deal with this problem. The first is to work with craters in a well-populated size range, in practice usually those on the order of 0.1 to 1.0 km in diameter. This is not usually satisfactory on Mars because the resolution of the Mariner 9 cameras is in this range and craters of this dimension are easily disguised by mantling. The second method sums all craters of specified sizes on many small areas and divides by the sum of the areas. If the areas have had a uniform history, there should be no inherent statistical problems, and this is the method most frequently used in martian studies (Hartmann, 1974). Unfortunately, processes on Mars are known to be non-uniform, and this method therefore yields an average more youthful than the greatest age but older than the youngest. In addition, the youngest age may not reflect the genetic age of formation of the feature, but the time when the surface underwent environmentally controlled degradation which may be independent of the feature which is

---

*Error bars on crater counts can quantify a number of variable parameters, but most frequently refer to the discriminability of craters near the limit of resolution of a given size (what is the probability that all the craters in the given area have been counted?) and the statistically random property of the extra-planetary source (what is the probability of a given area containing a specific number of craters of a certain size?). The former process is extremely difficult to assess, because it is a complicated function of scene contrast, optics resolution, image motion, and a whole catalog of problems associated with the generation of the image. The latter is much more easily derived, if one assumes the process of impacts to really be random. In that case, crater counts become simply another type of counting experiment and are treatable using Poisson statistics. Thus the standard deviation error bar (1 sigma) is just the square root of the total number counted.

modified. The final method is to accept the large errors associated with small populations and to compare the study areas to nearby locations to reduce the possibility of regional variations and to reduce any systematic errors in the counting technique. This method has been used successfully on the moon (Malin, 1974) and on Mars (Blasius, 1975; Malin, 1975) to acquire relative age relationships.

Hartmann (1974) has written the most recent and extensive analysis of martian channel ages. He utilizes two independent crater count methods. At Mangala channel, he notes that only one crater as large as 2.5 km in diameter is seen in five high-resolution photographs with a total channel area of 2200 km. Estimating that one such crater is formed on Mars every $1\text{-}8\times10^4$ years based on a Mars/lunar flux enhancement ratio which ranges from 8:1 for the more youthful age to 1:1 for the older age, he determines that there is a significant probability that Mangala is on the order of 6×10^8 to 5×10^9 years old. In the same work, to avoid "statistics of one", Hartmann sums 31 craters (diameter > .25 km) visible on five unspecified channels, divides by the total area, and produces a size-frequency curve. By referencing this incremental crater frequency diagram to theoretical isochrons previously derived, Hartmann estimates a "modal or mean age" for his five channels of about 10^8 years.

In the present study, over 80 craters ranging in size from 0.25 to 16 km were counted on five channels representative of the 20 or so major channels on Mars. Not included were the cratered channels of the chaotic and fretted terrains because of the difficulty in delineating between

the channels and the smoother areas of the chaotic and fretted landforms. Table II lists photographic data, number and size of craters, and the approximate area of each section of channel. Also listed are similar statistics for some nearby unchanneled surfaces (Tables III and IV).

Comparison of the absolute numbers of craters within the channels, using procedures similar to those of Hartmann (1974), yields "ages" similar to the one he determined for Mangala. For example, the channel Ladon (23°S, 28.5°W, Fig. 3) has two craters between 4 and 8 km in diameter within an area of approximately 6000 km, which requires an age from 1.0 to 8×10^9 years to acquire significant probability, comparable to Hartmann's values of 6×10^8 to 5×10^9 years for Mangala. Similar calculations for the other channels in Table I yield similar results. Most of the channels appear to have cratering ages which may be on the order of billions of years. It must be noted that an absolute crater age for the channels is dependent on the impact rate assumed and cannot be uniquely determined by these methods. Figure 4a compares the summed crater frequency populations from this work with Hartmann's martian cratering isochrons and channel data, and shows the general similarity of the two data sets. A less controversial determination of relative ages is shown in Figure 4b, where the cumulative crater populations on channels is compared to that on the surfaces surrounding the channels, on the oldest plains unit, and on an old volcanic plains unit.

It is important to ask if any other landforms or deposits are superposed on channels. At least two types of mantles can be seen in places

to lie over the channel topography in Mariner 9 photography. One is the major plains units of the northern hemisphere, and the second is the sub-polar debris mantles described by Soderblom et al. (1973).

A major distinction in surface morphology on Mars exists between cratered "uplands" in the southern half of the planet and relatively uncratered "lowlands" in the northern half. Several papers have set limits on the position of these lowland plains deposits within the overall stratigraphic history of Mars (Soderblom et al., 1974; Jones, 1974; Carr et al., 1973; McCauley et al., 1972). Thus, if one could place the channels relative to the plains units, the channels could be related to the general scheme of martian chronology. The location of many channels near boundaries between major physiographic provinces would seem to make this a feasible task. Unfortunately, such is not the case because most Mariner 9 photography is of insufficient resolution. Even when a photograph might be able to show clear-cut relationships between plains units and channels, debris mantles obscure the contact. The following two examples illustrate these limitations and are indicative of the type of data available for analysis.

Figure 5 shows an unnamed channel located at the boundary between heavily cratered terrain and a less cratered plains near 0-5°N, 60.8°W. The plains unit comprises the eastern part of the Lunae Planum plateau, which has been determined by independent analyses to be the oldest post-uplands terrain (Soderblom et al., 1974; Jones, 1974; Chapman, 1974; Arvidson, 1974). The channel, 450 km long, 12 km wide, debouches northward down a regional slope from an area of chaotic terrain (10^4 km^2)

and has features which place it in the outflow category of exogenic channels. Some 50 km below the head of the channel, it divides into two, north-trending, roughly parallel branches. The eastern branch follows along the terrain boundary and appears to tap other, small chaotic regions. It is approximately 400 km long. The western branch lies some 40 km to the west, within the plains unit.

The morphology of these channels changes as they cross from one terrain to the other. The western branch fades in apparent topographic relief north and west of the fork and the western wall of the east branch also appears subdued or missing. An attendant crater-like form connected to the western branch immediately west of the divide, is barely visible, suggesting comparable burial. About 100 km north of the divide, both the eastern and western branches reacquire more definite topographic form, although remaining subdued. Eventually both channels dwindle and die within the plains unit. These characteristics suggest that the material of the plains overlie many portions of the channels, with the occasional resurgence of form the result of incomplete burial by the thin, volcanic units which are evidenced by mare-like ridges within the local area.

Similar arguments apply to the Elysium channels, where narrow angle high-resolution frames show an extremely subdued apparent cross-section suggestive of burial by incoherent material. If the shallow appearance of these channels were the result of the inability of an unconsolidated material to preserve the channels, it would be difficult to explain the apparent steepness of the channel walls; thus burial is

considered a more likely alternative. In this case, however, debris mantles (to be discussed shortly) may be complicating the situation.

A second example is the mouth of Mangala as shown at high resolution (Fig. 7). Mangala is distinctive in that it is one of the few channels that terminates at an abrupt cliff. Although not visible in Figure 7, flow fronts and mare-like ridges are seen on the nearby plains surface, suggesting a volcanic origin. The concordance of the channel bed and the plain suggests that either a large portion of the plain near the channel mouth is alluvial, or that the presumably volcanic plains have flooded over portions of the channel and its deposits. The slight albedo feature near the mouth of the channel may be evidence of alluviation, but cannot be distinguished from other light albedo markings of probable eolian origin. Evidence for eolian-related albedo features is seen in the two small craters with dark streaks on the plain beneath the channel. It appears possible, however, that the darker plains material north of the channel mouth has embayed the lighter material. It is concluded that the plains are primarily of volcanic origin and have flooded and buried the Mangala channel deposits.

Further study of Mangala reveals a possible extension of the channel for 460 km south of the presumed source area (Fig. 6). If this is indeed part of the Mangala system, then the highly cratered plain transecting the mid-portion of the original channel is younger than the channel, making Mangala extremely old.

Debris mantles may have played a role in the evolution of the martian surface forms. Soderblom et al. (1973) have postulated the

presence of sub-polar blankets which modify small crater abundances, crater morphology, and central peaks at latitudes greater than 30-40° in both hemispheres. They estimate the thickness at from .1 to 1 km and speculate that the materials are derived from the polar sedimentary deposits. Subsequently, Soderblom et al. (1974) suggest that the equatorward boundary of this mantle moves north and south in phase with the periodic obliquity variations described by Ward (1973, 1974). They recognized four zones -- deeply mantled poleward of +40° and -40°, thinly mantled from around -15° to +40° and largely unmantled from -15° to -40°. These mantles are useful in setting age limits on the youngest channel features.

Debris mantles may be responsible for the seeming lack of detection of channels south of 40°. Two channels within a few degrees of the mean boundary of the mantle (and also near a probable source of dust - the Hellas Basin) are shallow and subdued (Fig. 8). Narrow-angle frames of one of these channels display features listed by Soderblom et al. (1974) as characteristic of mantling (Fig. 9). Blanketing of channels north of the average mantle boundary attests to the variability of the location of the mantle.

Nearly all channels studied show local effects of mantling, usually in slight but distinct changes in the morphology of the small, superposed craters. In some instances, the effects are strong, in others they are less evident. Evidences of mantling are strongest in areas where crater morphology and number deviate most strongly from normal, suggesting greater thickness in mantling debris.

The Elysium channels (Figs. 10 and 11) represent a major deviation from the debris-mantle explanation for subdued forms in some channels. The Elysium channels appear to be extremely shallow, and this was attributed in a previous section to mantling by a volcanic plains unit. However, crater morphologies and other features suggest the presence of a patchy mantle over the entire Elysium region. Is this mantle composed of lava flows or a tuff or ash, or could it be of non-volcanic origin? The channel floors appear extremely smooth and the walls are steep but low in relief. This suggests that the channel floor is buried beneath some thick mass of material. If it were eolian in origin, it might be expected to be easily transported away from the channel. In addition, the rough texture of the surrounding surface appears different from others seen on Mars where the origin of the debris is more clearly eolian. Exhuming craters in particular look distinctly different, as if the material under which they have been buried were more resistant than seen elsewhere. The explanation for the form of the Elysium channels proposed here is that they are blanketed by a terrain-conforming, moderately resistant mantle, possibly a tuff associated with the more silicic magmas proposed for the Elysium volcanic field (Malin, 1975).

To summarize:

1. A significant number of craters are superposed on channels.
2. Although the numbers of craters are less than on the surrounding surfaces, they are comparable to the population of craters on older martian plains.

3. A few channels, in no other way differing from other channels, appear to be covered by older plains material.
4. Debris mantles locally cover many channels.

Channels Superimposed on Other Features

The oldest terrain on Mars is characterized by large craters, basins and basin-related structures, and intercrater plains and is dominant in the southern hemisphere (McCauley et al, 1972; Carr et al., 1973; Soderblom et al., 1974). In this section, the relationships between channels and the older craters will be examined.

As noted, (McCauley et al., 1972; Milton, 1973; Sharp and Malin, 1975), a large number of channels extend out from regions of chaotic terrain. Although the largest of these chaotic areas are irregularly shaped, many are roughly circular, and clearly occupy craters (Figs. 12,13). Separate areas of chaos are often connected by broad flat-floored channels which usually circumvent but occasionally cut through the walls of craters that pock the surface between them. In tangentially grazing encounters, the channels appear to erode crater rims by undermining and collapse. However, the eastern part of Ares channel encounters two craters nearly headon and appears to have breached their rims (Figs. 13). Mangala, an outflow channel not associated with chaotic terrain, also appears to have breached two, relatively subdued, 30-km craters, one over 180 km downstream from the head of the channel (Figs. 2,6).

Ma'adim, a large runoff channel in a densely cratered region (Fig. 2) appears to have attacked craters through both grazing and

headon erosion. Two 30-km craters are breached some 150 km above the mouth of the channel, and about a quarter of the rim of another 30-km crater has been trimmed away by the channel. Nirgal, another runoff channel in a somewhat less densely cratered area, breaches a 20-km crater at its mouth.

The best examples of fretted channels are in a region of fretted terrain near 38°N, 340°W (Fig. 12). Here it appears that numerous craters have been joined by the fretting process, so that they have to have been integrated with the channels by both tangential cutting and perpendicular breaching.

Although Mars has many large basins, only one, Hellas, has visibly associated channels. Two large channels, both immediately east of the basin, are consequent upon the basin topography (Fig. 8). Both are aligned downslope, and have formed around and through the mountainous features associated with the basin structure.

While craters and basins are among the oldest landforms, seventy-five percent of the most heavily cratered area consists of a relatively smooth rolling plains which occupies the area between craters. Called by various authors "plateau plains" or "heavily cratered plains" these inter-crater areas will be here called "inter-crater plains." The possible origin and makeup of these plains is currently under study (Wilhelms, 1974; Malin, 1975). Although the morphologies of channels developed within these plains bear strongly on both their origin and the nature of the underlying materials, this discussion will be limited to age relationships (for a more detailed treatment, see e.g., Malin, 1975).

Most channels within the heavily cratered regions of Mars are necessarily developed within the intercrater plain, since these plains cover the most area. Additionally, no large channels are seen in areas where the surface is essentially saturated with large craters. Channels are thus younger than the materials that underlie the plains and younger than the processes which formed the plains.

To summarize:

1. The oldest features on Mars -- the large craters, basins, and inter-crater plains -- all predate the major channels visible on the surface.
2. By implication, the processes of chaos formation and fretting were operative at the time of channeling.

Discussion

How old are the martian channels and what is their place in martian history? The reader is forewarned that this section presents interpretations of an increasingly speculative nature.

The first objective of any dating process is to place features in relative order. Since major channels are found only within relatively old heavily cratered regions, one concludes that they are either older than the plains which cover the remainder of the planet, having been buried or destroyed in the plains-making process, or that channels originate through processes operative only in cratered regions. Such a process would have to be lithospheric, and this seems unlikely since young volcanic plains devoid of channels must be underlain by older crust in which the process would presumably be active. Thus, the

interpretation that channels are older than the plains units is favored. This conclusion is supported by the observation of plains and crater relationships to channels already described. Subsequent to the creation of large craters, basins, and the inter-crater plains came the formation of portions of the chaotic and fretted terrains and associated channels. Some of the channels predate the formation of the oldest volcanic plains. The channels are therefore among the older features of the surface of Mars.

Minimum age of channels is less clearly defined. Superposed craters and the mantled appearance of channels and indenting craters indicate that most channels cannot be young in an absolute sense. Aside from small, fretted channels discussed by Sharp and Malin (1975), the only evidence suggesting that some channels are young involves a single 2.5-km crater which indents one part of a strand of a Mangala channel and appears to be truncated by another strand (Hartmann, 1974) (Fig. 14). Hartmann argues in favor of this sequence of events because of: 1) the apparent non-circularity of the crater on its eastern rim and 2) the appearance of bright rays of the crater superposed on the older but not the younger channel strand. Since appearances in Mariner 9 photographs can be deceiving, a number of computer-enhanced versions of the frame in question have been prepared. From these frames the following conclusions are reached. The non-circularity of the crater is apparent only. When corrections for viewing geometry and removal of artifacts associated with the filtering algorithm used in the computer processing are made, no deviation from circularity is detectable. In addition,

when one considers that many craters display some polygonality, any argument based on departures from perfect circularity must be suspect. The special image processing further suggests that the ray system is most likely photometric shading associated with slight changes of slope, accentuated by the enhancing process practiced on all Mariner photos. This is supported by the rarity of rays associated with martian craters, probably because of subsequent erosional or depositional activity. Craters with rays are never seen without continuous ejecta blankets, and the absence of such blankets around this crater suggests that it is not rayed. These considerations throw doubt on Hartmann's (1974) assignment of a relatively youthful age to some of the activity in Mangala channel.

Finally, it is theoretically possible to assign absolute ages to the channels using cratering curves currently in vogue. Using Hartmann's (1973, 1974) curves, the channels do not appear to be substantially younger than 10^8 years. Using a flux comparable to the moon's (Soderblom et al., 1974), ages in excess to that of the solar system are obtained, suggesting that the channels date from the period when the bombardment of Mars was in excess to that of a linearly extrapolated flux. This period, called the "end of heavy bombardment" or "terminal bombardment", occurred on the moon around four billion years ago. Soderblom et al. (1974) propose a similar history and timescale for Mars, which could make the channels about four billion years old.

In conclusion, the channels on Mars appear to be old, in some places older than the oldest volcanic plains unit. No evidence for

recent channel activity has been found. This supports the assertion of Sharp and Malin (1975) that the channels reflect an ancient period in martian history separated from the present by billions of years. The temporal association of chaotic and fretted terrain, areas of lithospheric seepage, the channels and the intercrater plains unit suggests possible connections exist between the processes which formed these landforms. These will be discussed in a subsequent work (Malin, 1976).

REFERENCES

Arvidson, R. E., Morphologic classification of martian craters and some implications, Icarus 22, 264-271 (1974).

Blasius, K. R., Geology of the great volcanoes of the Tharsis region of Mars, Ph.D. dissertation, California Institute of Technology, Pasadena, California 91125 (1975).

Carr, M. H., H. Masursky, and R. S. Saunders, A generalized geologic map of Mars, Jour. Geophys. Res. 78, 4031-4026 (1975).

Chapman, C. R., Cratering on Mars: I. Cratering and obliteration history, Icarus 22, 264-271 (1974).

Hartmann, W. K., Martian cratering: IV. Mariner 9 initial analysis of cratering chronology, Jour. Geophys. Res. 78, 4096-4116 (1973).

Hartmann, W. K., Geological observations of martian arroyos, Jour. Geophys. Res. 79, 3951-3357 (1974).

Jones, K. L., Evidence for an episode of martian crater obliteration intermediate in martian history, Jour. Geophys. Res. 79, 3917-3932 (1974).

Malin, M. C., Lunar red spots: Possible pre-mare materials, Earth and Planetary Sci. Lett. 21, 331-341 (1974).

Malin, M. C., Investigation of surface features of the planet Mars, Ph.D. Thesis, California Institute of Technology, Pasadena, California 91125 (1976).

McCauley, J. F., M. H. Carr, J. A. Cutts, W. K. Hartmann, H. Masursky, D. J. Milton, R. P. Sharp, and D. E. Wilhelms, Preliminary Mariner

9 report on the geology of Mars, Icarus 17, 289-327 (1972).

Masursky, H., An overview of geologic results from Mariner 9, Jour. Geophys. Res. 78, 4029-4030 (1973).

Milton, D. J., Water and processes of degradation in the martian landscape, Jour. Geophys. Res. 78, 4037-4047 (1973).

Sagan, C., O. B. Toon, and P. J. Gierasch, Climatic change on Mars, Science 181, 1045-1049 (1973).

Sharp, R. P., Mars: Chaotic and fretted terrains, Jour. Geophys. Res. 78, 4073-4083 (1972).

Sharp, R. P. and M. C. Malin, Channels on Mars, Geo. Soc. Am. Bull. 86, 593-609 (1975).

Soderblom, L. A., T. J. Kreidler, and H. Masursky, Latitudinal distribution of a debris mantle on the martian surface, Jour. Geophys. Res. 78, 4117-4122 (1973).

Soderblom, L. A., C. D. Condit, R. A. West, B. M. Herman, and T. J. Kreidler, Martian planetwide crater distributions: Implications for geologic history and surface processes, Icarus 22, 239-263 (1974).

Ward, W. R., Large-scale variations in the obliquity of Mars, Science 181, 260-262 (1973).

Ward, W. R., Climatic variations on Mars: I. Astronomical theory of insolation, Jour. Geophys. Res. 79, 3375-3386 (1974).

Wilhelms, D. E., Comparison of martian and lunar geologic provinces, Jour. Geophys. Res. 79, 3933-3941 (1974).

Table I: Large Martian Channels

Channel Name or Region	Latitude	Longitude	Type (after Sharp and Malin, 1975)
Deuteronilus (D)	36 N	343 W	fretted
Deuteronilus (D)	36 N	330 W	fretted
Elysium (E)	37 N	220 W	outflow(?)
Kasai (K)	27 N	69 W	modified fretted
KASAI (K)	23 N	67 W	modified fretted
Lunae Planum (LP)	2 N	60 W	outflow
Xanthe (X)	6 N	47 W	runoff
SHALBATANA (S)	5 N	44 W	modified outflow
SIMUD (Si)	5 N	36 W	modified outflow (chaotic terrain)
TIU (T)	10 N	32 W	modified outflow (chaotic terrain)
ARES (A)	7 N	20 W	outflow
Arabia (Ar)	7 N	329 W	runoff
AUQAKUH (Aq)	30 N	300 W	fretted
HUO HSING (HH)	30 N	293 W	fretted
Elysium (E)	28 N	225 W	outflow
MANGALA (Man)	7 S	151 W	outflow
NIRGAL (N)	28 S	40 W	runoff (fretted?)
Eos (Eo)	15 S	38 W	outflow
LADON (L)	23 S	28 W	outflow
Margaritifer (Mar)	15 S	25 W	outflow
Tritonius (Tr)	4 S	246 W	fretted
Gomer (G)	3 S	234 W	fretted
AL QAHIRA (Al)	18 S	197 W	runoff (fretted?)
MA'ADIM (Maa)	21 S	182 W	runoff
Hellas (H)	36 S	270 W	outflow (runoff)
Hadriacum (H)	40 S	253 W	outflow

Capital letters = named channels
Lower case letters = unnamed channels

Table II: Channels and Intercrater Plains

Camera	DAS	Area(km)^2	Number of craters per increment (km) in channel (craters on adjacent plains are in parentheses)								
			<.5	.5-1	1-2	2-4	4-8	8-16	16-32	32-64	64-128
Mangala Channel											
B	9628644	627(800)	1(1)	1(1)							
B	9628924	380(1740)	1(1)	(1)					(2)		
B	12499645	1200(300)	2	3(2)	(1)						
B	12499715	500(1000)	2(4)	1	(2)						
B	12499785	200(1200)	(6)	(1)	1(1)						
Ares Channel											
A	7830583	3.6×10^4(15.9×10^4)				(8)	2(8)	2(10)	(4)	(4)	(1)
B	7758803	825(1450)	2	3(3)	1(1)	(1)	(1)				
B	9233289	1145(500)	2	3(2)	2				(1)		
B	12362181	1000(2100)	1(6)	1(3)	(2)	(2)	(2)	(1)			
B	12362251	1670(1600)		2(3)	4(3)	(1)					
Ma'adim Channel											
A	6606703	8500				2(59)	2(43)	(39)	(25)	(9)	(1)
	6606773	(2.3×10^5)									
Elysium Channels											
B	8910724	700(3500)	5(10)	2(4)	1(4)	(1)					
B	10313804	1100	7(11)	5(9)	6(6)						
B	10313874	(5500)									
Ladon Channel											
A	6426803	5700(1.15×10^5)				1(20)	2(12)	(7)	(2)	(2)	(2)
B	9376438	3000	2	4(3)	1	0(1)	2				
B	9376504	(3000)									

Table II (Continued)

	B-CAMERA			A-CAMERA					
	<.5	.5-1	1-2	2-4	4-8	8-16	16-32	32-64	64-128
Number of craters	25(39)	25(32)	16(20)	3(93)	8(75)	2(57)	(34)	(15)	(4)
Total area	10677 (22690)			57395 (515650)	55025 (510550)	51200 (506100)	(506240)	(504000)	(504000)
Number of craters/10^6km^2	2341.5 (1718.82)	2341.5 (1410.31)	1498.55 (881.45)	52.27 (180.35)	145.39 (146.90)	39.06 (112.63)	- (67:+6)	- (29.76)	- (7.94)
CHANNELS									
Cumulative number of craters	66±8	41±6	16±4	13±4	10±3	2±1.4			
Cumulative number of craters/10^6km^2	6200±750	3800±600	1500±375	240±66	183±55	36±26			
PLAINS									
Cumulative number of craters	91±9.5	52±7.2	20±4.5	278±17	185±14	110±10	53±7.3	19±4.4	4±2
Cumulative number of craters/10^6km^2	4000±420	2300±320	880±200	550±33	365±27	220±20	105±15	38±8	8±4

Table III: Lunae Planum Plateau Plains (0°, 68°W)

DAS	Area	<.5	.5-1	1-2	2-4	4-8	8-16	16-32	32-64
7399213	2268	2	3	5	2	1			
7399353	2408	3	11	9		1			
7399703	4292	1	7	5	1		1		
7471243	2365		7	4	2				
7471068	206,255				46	7	2	6	1
7471138	207,966				66	9	5	4	
7471278	225,540				35	16	5	4	
Totals	11333	6	28	23	5	2	1		
	639761				147	32	12	14	1
cumulative number of craters		65±8	59±7.7	31±5.5	8±3	3±1.7	1±1		
					206±14	59±7.7	27±5.2	15±4	1±1
cumulative number of craters/10^6km^2		5700±700	5200±700	2750±480	700±250	265±150	88±88		
					320±20	92±12	42±8	23±6	1.6±1.6

Table IV: Oldest Tharsis Volcanic Plain (30°N, 122°W)

DAS	Area	<.5	.5-1	1-2	2-4	4-8	8-16	16-32	32-64
8370889	4408	23	8	3	1				
6967418	235,277			6	10	4	2		
6967768	357,780			8	6	5	6	5	
7039728	357,576				17	5	2	2	
8370854	401,921				5	11	7	2	
Totals	4408	23	8	3	1				
	1,349,554			14	38	25	17	9	
cumulative number of craters		35±6	12±3	4±2	1±1				
				103±10	89±9	51±7	26±5	9±3	
cumulative number of craters/10^6km^2		7900±1400	2700±700	900±450	227±227				
				76±7	66±7	38±5	19±4	6.7±2.2	

FIGURE CAPTIONS

Figure 1: Airbrush Shaded Relief Map of Mars.

Mercator projection showing location of largest martian channels (for key to abbreviations, see Table I). Large channels are named; unnamed channels are usually shorter and narrower. Map prepared by U.S. Geological Survey and Lowell Observatory, Flagstaff, Arizona.

Figure 2: Examples of Exogenic Channels (after Sharp and Malin, 1975).

2A: Outflow Channel. A-frame mosaic of Mangala Vallis (350 km long, 10 km wide) located 151°W, 5°S (DAS 6822728, 6822792).

2B: Runoff Channel. Ma'adim Vallis (>700 km long, 15 km wide) located 182°W, 21°S (DAS 6606708, 6606778). A-frame mosaic taken from 1700-km altitude.

2C: Fretted Channel. Unnamed channel in Deuteronilus (750 km long, 20 km wide) located at 343°W, 36°N. (DAS 9378149, 9378289).

Figure 3: Ladon Valles (28°W, 23°S).

3A: A-frame of Ladon Valles, showing location of B-frame mosaic (Fig. 3B). Channels debouch into large basin to the north (DAS 6426808).

3B: B-frame mosaic of Ladon Valles. Numerous craters are seen on the channel formations, the largest about 8 km in diameter. The images have poor definition owing to high sun conditions (sun elevation angle = 70°; 50° phase angle). Rotation of top frame is the result of spacecraft and scan

platform motion. (DAS 9376439, 9376509).

Figure 4: Crater Counts on Martian Channels.

Left: Incremental crater counts, after Hartmann, 1974. Error bars are rms standard deviations.

Right: Cumulative crater counts, comparing crater populations on the channels with the populations on the surfaces immediately adjacent to the channels (intercrater plains), on the Lunae Planum plateau plains, and on the most heavily cratered portion of the Tharsis volcanic plain. Note that the counts on B-frames cluster together, as noted by Soderblom et al. (1974), who suggest the small crater population is controlled by eolian debris blankets. Note, too, the relative position of the craters seen on A-frames suggests an age for the channels comparable to that of the older plains unit, the Lunae Planum.

Figure 5: Unnamed Channel near Lunae Planum (60°W, 2°N).

Left: Mariner 9 A-frame mosaic showing channels which traverse the boundary between heavily cratered uplands and a moderately cratered plains (the Lunae Planum plateau). These outflow channels appear subdued and in places sections are missing within the plains. It is suggested that the channels are overlain by volcanic material. (DAS 7471138, 7471208, 7471558, 7542958, 7543028).

Right: Sketch map of unnamed channel, showing location of channel with respect to terrain boundaries.

Figure 6: Mangala Vallis (151°W, 5°S).

Left: Mariner 9 A-frame mosaic showing possible extension of channel some 400 km beyond the hummocky region near middle left. The extension is characterized by an east-facing escarpment with small conformal island-like ridges along the southern reach. The west-facing portion of the channel is no longer visible, suggesting removal, perhaps by burial by volcanic plains. The large numbers of craters superposed on the plains immediately east of the visible channel indicate significant antiquity, and the channel would necessarily be older if it is covered by these plains. (DAS 6822658, 6822728, 6822798, 8297424, 8297494).

Right: Sketch map of Mangala Vallis, with channel extension in light tone.

Figure 7: Mangala Vallis - mouth area.

Stereo pair of Mariner 9 high resolution frames, orthographically projected, showing the mouth of Mangala channel. The lack of contrast is the result of poor illumination conditions -- 67° sun elevation angle, 20° phase angle. The dark material north of the escarpment appears to embay the lighter material near the mouth, suggesting that the alluvial features which might be expected to accompany a large channel are buried by the plains material. Note at the extreme right the incision of the crater floor (DAS 10686114 (left); 9556549 (right)).

Figure 8: Unnamed channels near the Hellas Basin (270°W, 36°S).

8A: Photomosaic of Mariner 9 A-frames showing extremely subdued topography of two channels near a region of thick debris mantling. Channel on left is abruptly terminated in a large depression on the flanks of a possible volcanic construct. The right channel continues headward some 1000 km. Low contrast photographs are the result of poor illumination conditions (sun elevation angle = 48°, phase angle = 45°). (DAS 6031098, 6031168, 6031238).

8B: Sketch map of Hellas channels, showing location of channels and position of B-frame mosaic (Figure 9).

Figure 9: Unnamed channel near Hellas Basin.

High resolution photomosaic of Mariner 9 B-frames, showing subdued nature of channels near Hellas. Landforms show features diagnostic of mantling -- gently rolling smooth surfaces, subdued crater rims, "elevated" or filled crater floors, and faint crater ejecta blankets. Channel floor shows some evidence of streamlining. Slumps and suture-like grooves mark the channel banks. Possible lineations related to superposed crater ejecta are seen in the upper right portion of the mosaic (DAS 8908629, 8908699, 8908769, 8908839).

Figure 10: Unnamed Channels in Elysium (225°W, 30-35°N).

10A: Mariner 9 A-frame photomosaic showing the Elysium channel systems west of the Elysium volcanoes. The large,

channel-like forms were interpreted as volcano/tectonic depressions of endogenic origin by Sharp and Malin (1975). Light areas appear moderately to heavily mantled; dark areas seem relatively unmantled (DAS 7579568, 7579708, 8910834).

10B: Sketch map of Elysium channels. Dark tone represents areas of subdued, mantled appearance (designated mp for mantled plains). Two areas covered by B-frames are marked. (Note that both are within mantled regions although they have been left clear for greater visibility).

Figure 11: B-frames of the Unnamed Channels in Elysium.

11A: Two high resolution frames and one partial almost form a complete photomosaic (DAS 8910729 (Top), 10313809, 10313879). Note the shallow appearance of the channel (large width to depth ratio), the rough texture of the surrounding terrain and the large number of craters superposed on the channel. Also note streamlined as well as rectilinear islands.

11B: Single B-frame showing mantled texture of plains and subdued nature of Elysium channels. The proposed explanation for the phenomena seen here is that the channels and surrounding terrain are covered by a blanket of weakly consolidated material (possibly a tuff) presently being eroded (DAS 8910869).

Figure 12: Tiu and Simud Valles - Chaotic Terrain (34°W, 5-10°N). Mariner 9 A-frame photomosaic of chaotic terrain and

associated channels. Note the large number of craters superposed on the floor of the chaotic terrain/channels. Chaos appears to develop within craters with greater ease than within the surrounding intercrater plains. Many areas show a progressive disintegration of landscape, from smooth, unaltered terrain, through a structurally controlled fractured zone, to areas of progressively greater fracturing and landform degradation. A resistant cap-rock may promote the visual appearance by fracturing as unconsolidated materials are removed from beneath. Many craters appear to be encountered tangentially by the chaotic terrain and the channels. Some craters appear resistant to the erosional mechanism (DAS 7686808, 7686878, 7686948).

Figure 13: Ares Channel and Associated Chaotic Terrain (20°W, 7°N). Mariner 9 frames show two forms of chaotic terrain in association with the largest of martian channels, Ares Vallis. South of the channel is an irregular region of chaos; west of the channel is a circular region, occupying the interior of what may be a large ($\sim$ 200 km) crater. Note that the Ares channel breaches headon two craters immediately west of the main branch of the channel (DAS 7830518, 7830588).

Figure 14: Crater Superposed on Mangala Vallis.

Crater cited by Hartmann (1974) as evidence for recent flow of material within Mangala channel. Each image represents a portion of DAS 12499790 from line 350 to line 600, sample

500 to sample 720. A, B, and C have undergone Mariner 9 standard processing, presenting a shading corrected, vertically high pass filtered, and horizontally high pass filtered images, respectively. The crater appears polygonal and is apparently rayed on the left. D presents a specially processed image, with the high frequency features boosted through the use of a modulation transfer function-related restoration filter. The crater no longer appears polygonal and the rays are resolved as terrace benches. E is a sketch map of the area, where p stands for plains, t for terraced channel walls, ch for channel floor, and c is the crater.

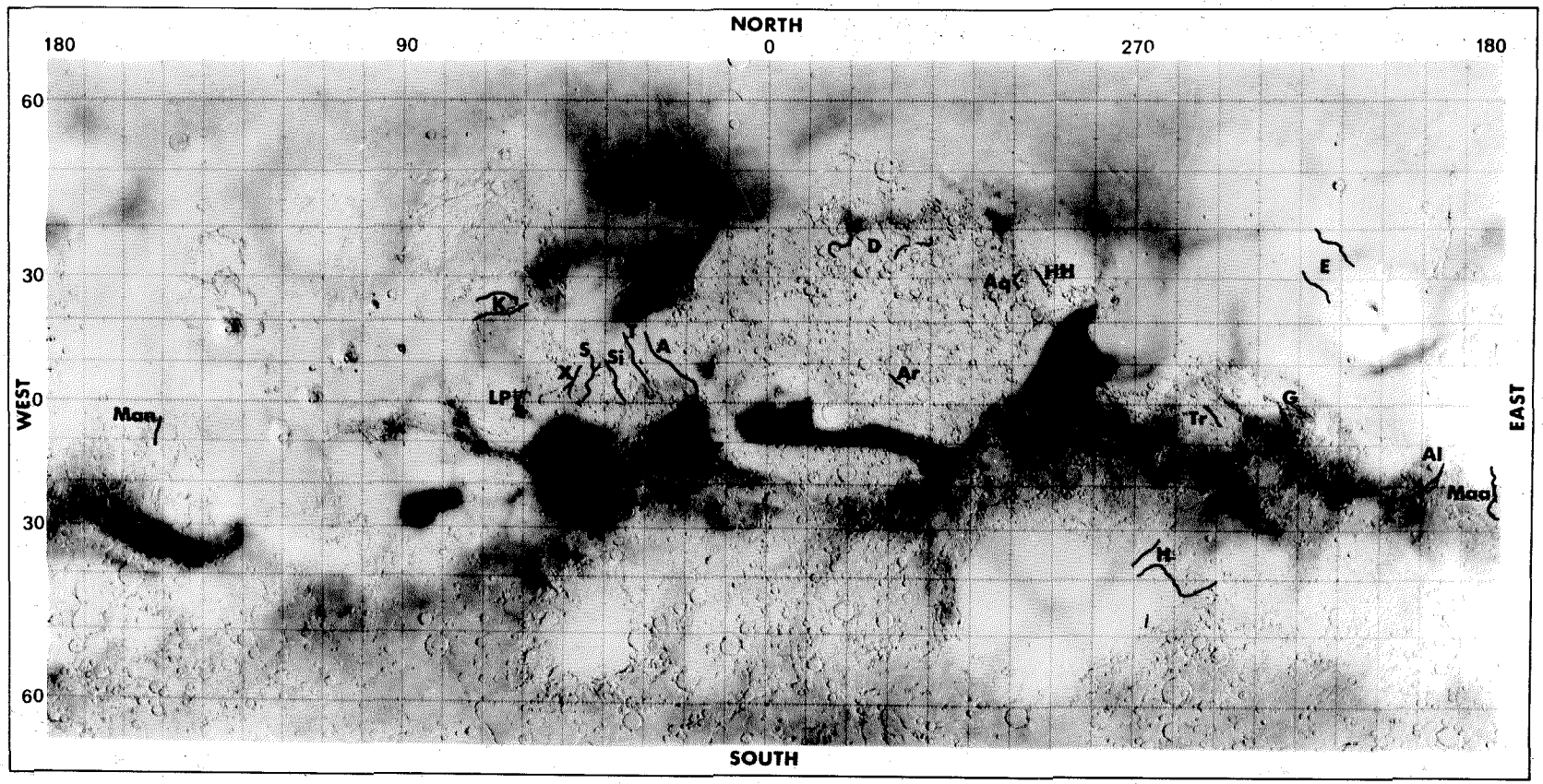
NORTH
180
90
0
270
180
60
30
0
30
60
WEST
EAST
SOUTH
D
Aq
HH
E
K
S
Si
A
X
LP
Ar
Man
Tr
G
Al
Maa
H

Figure 1

Figure 2A

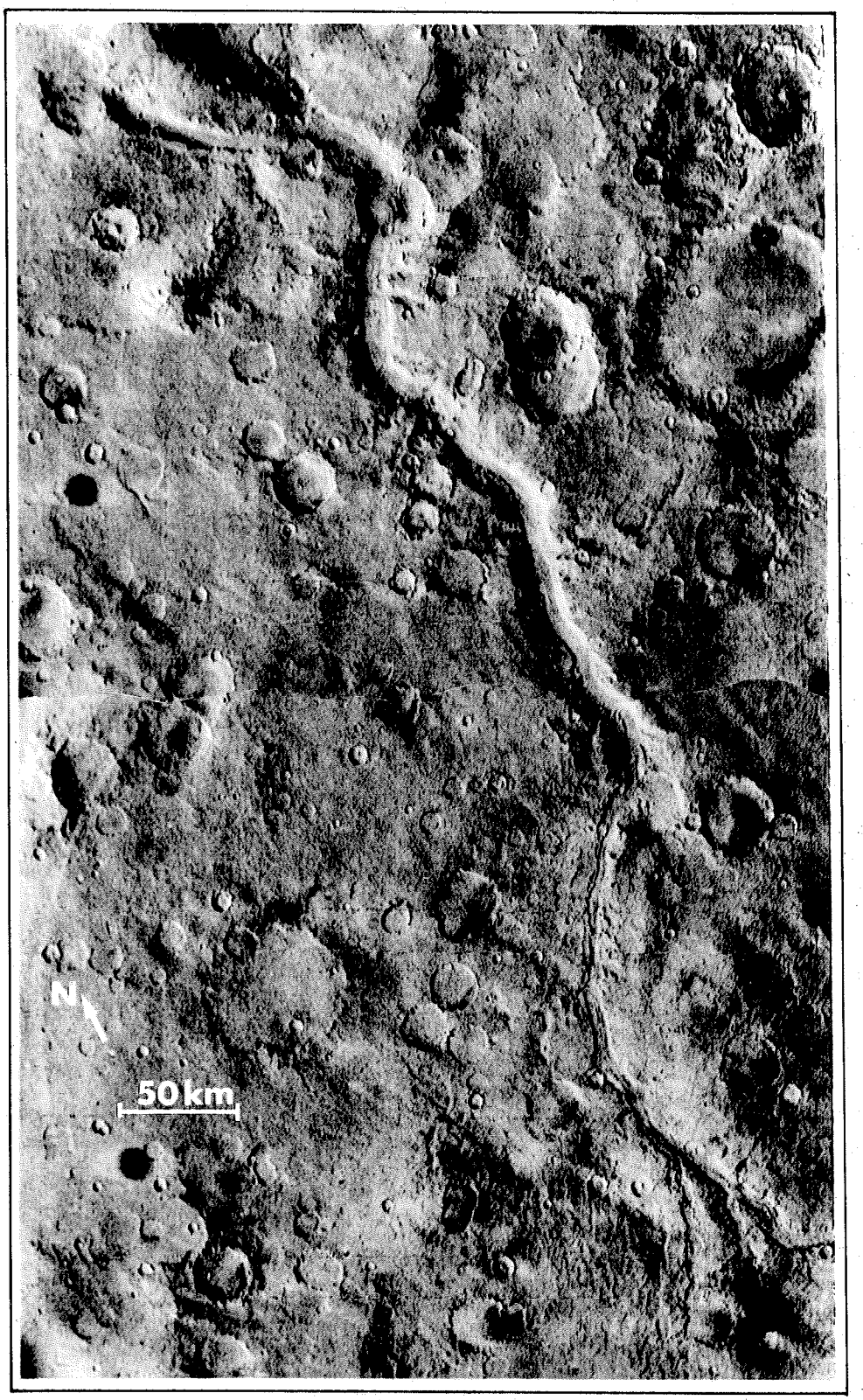

Figure 2B

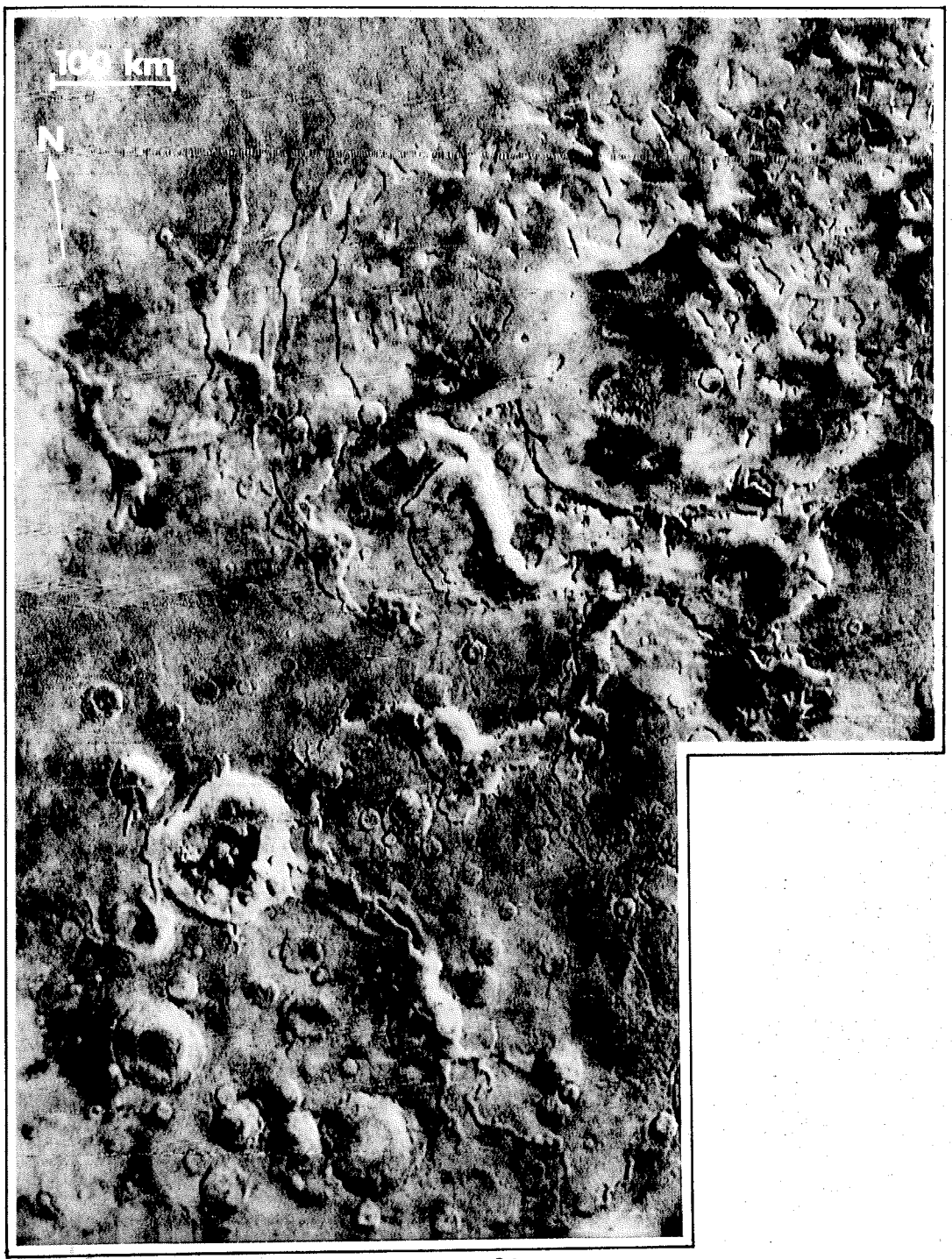

Figure 2C

Figure 3A

Figure 3B

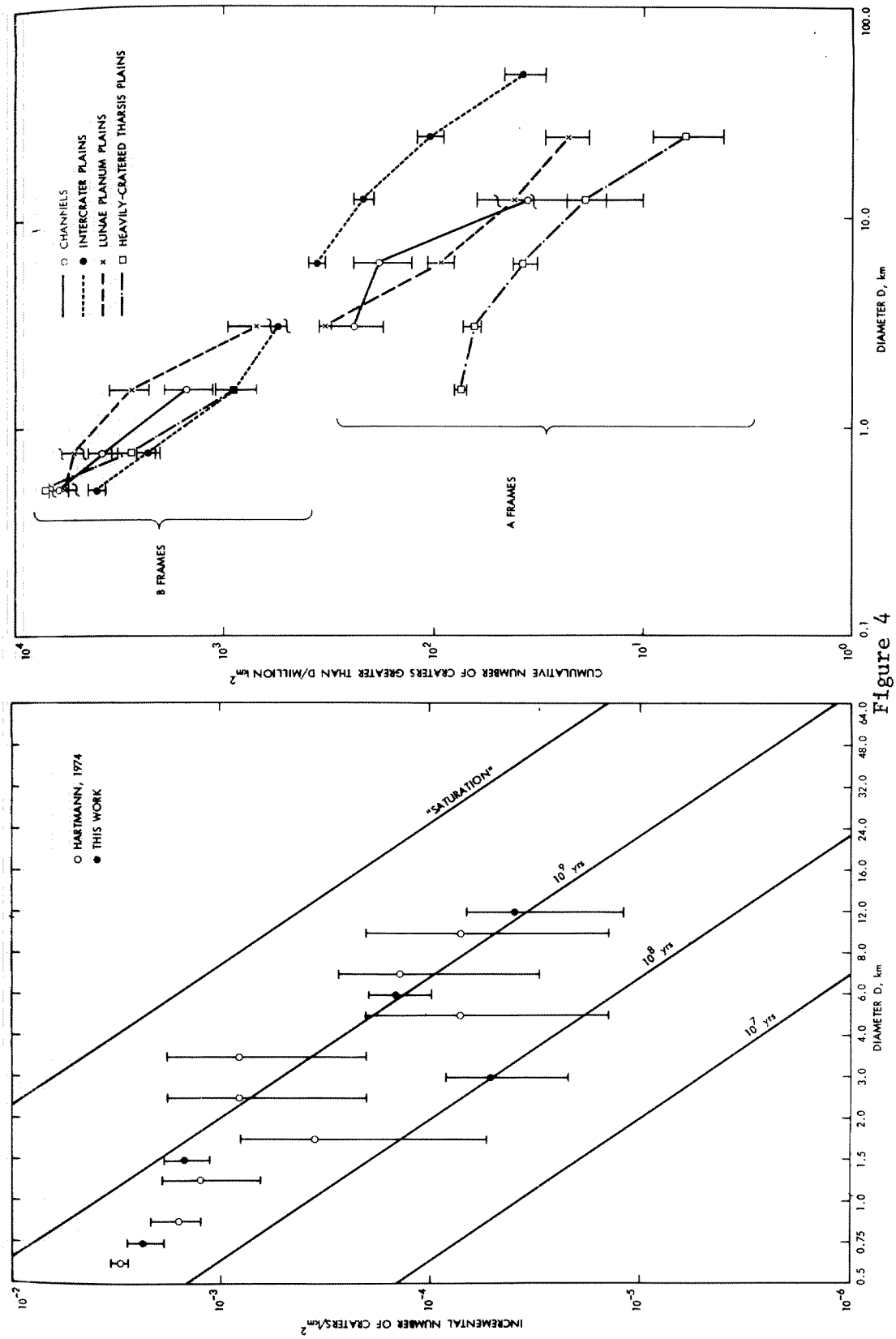
CUMULATIVE NUMBER OF CRATERS GREATER THAN D/MILLION km²
DIAMETER D, km
CHANNELS
INTERCRATER PLAINS
LUNAE PLANUM PLAINS
HEAVILY-CRATERED THARSIS PLAINS
B FRAMES
A FRAMES
INCREMENTAL NUMBER OF CRATERS/km²
HARTMANN, 1974
THIS WORK
"SATURATION"
10⁹ yrs
10⁸ yrs
10⁷ yrs

Figure 4

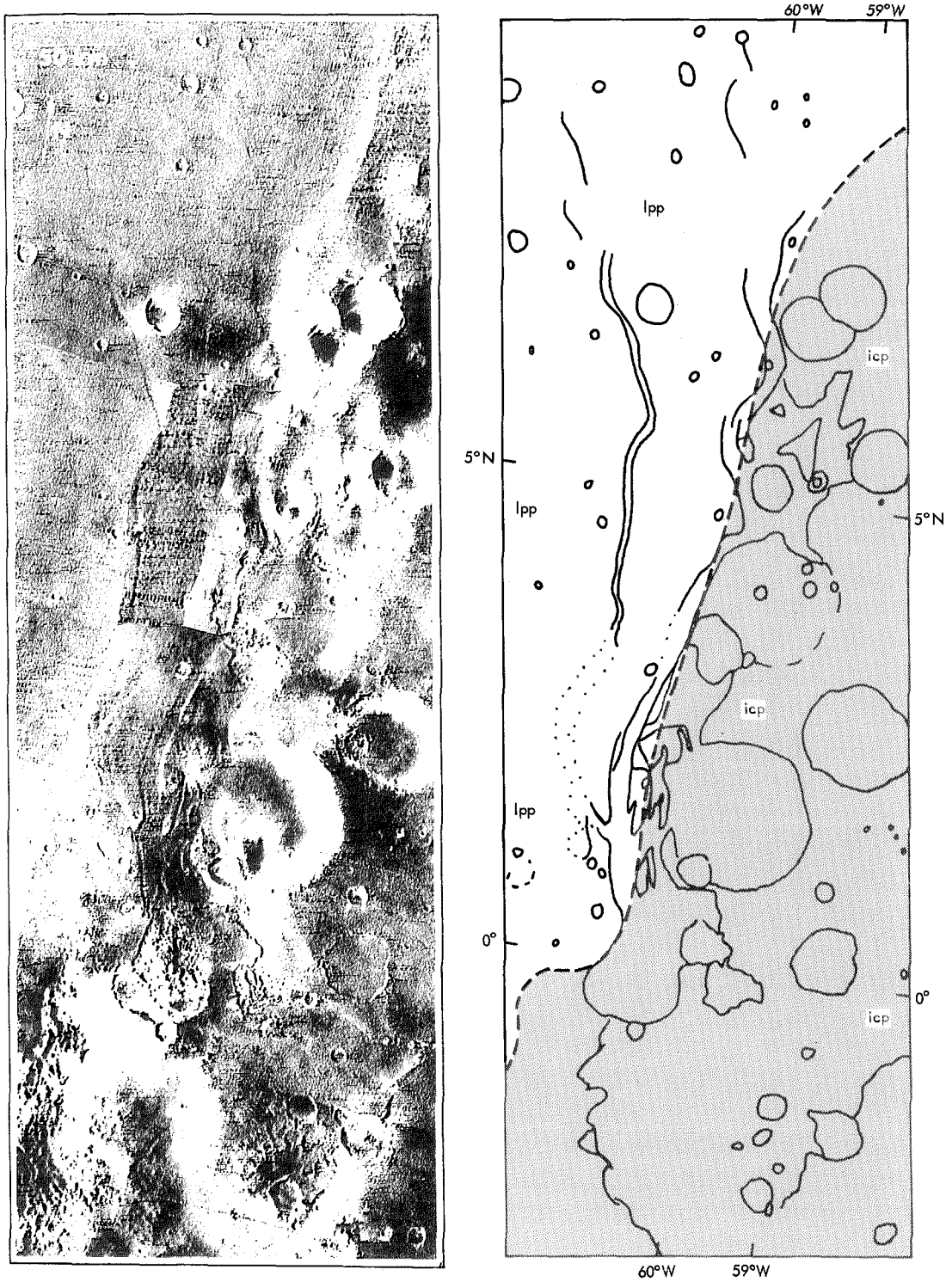

Figure 5

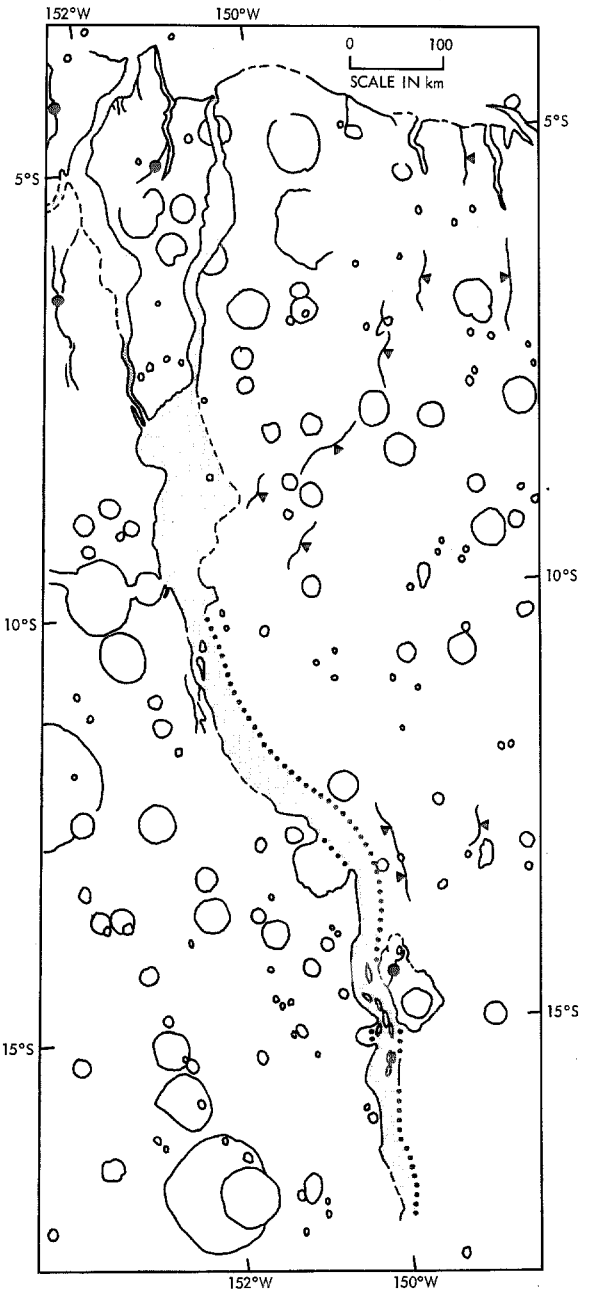

Figure 6

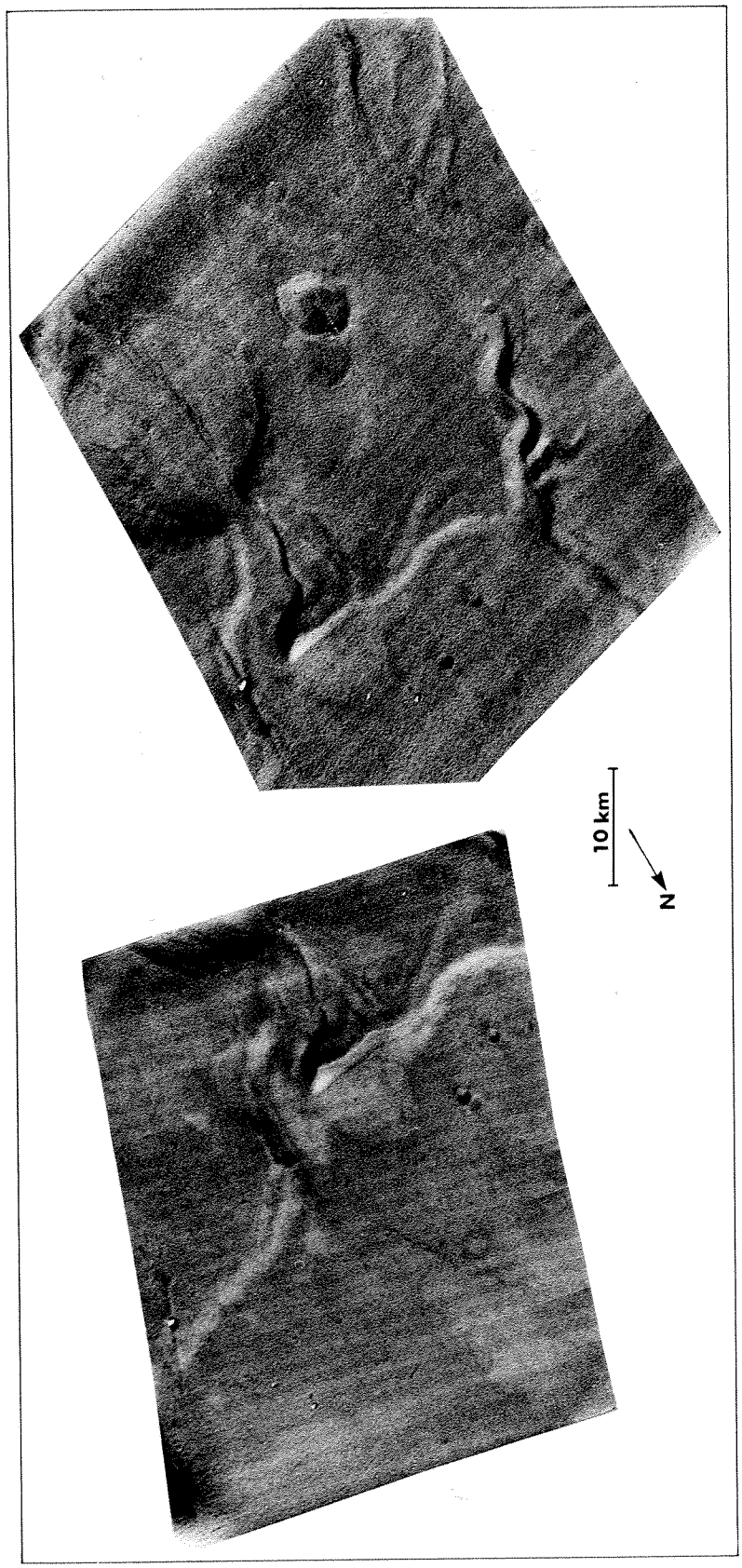

Figure 7

Figure 8A

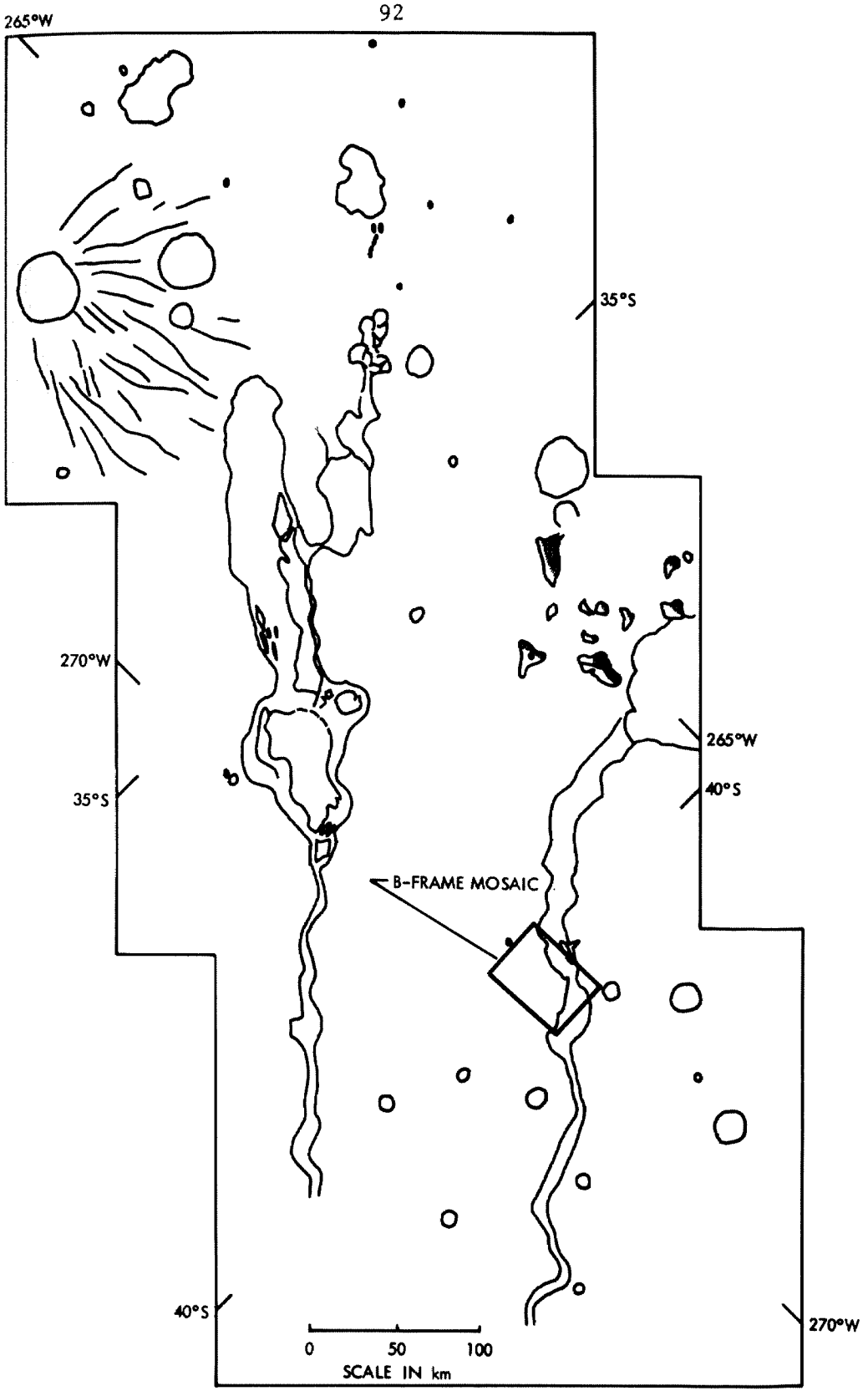
265°W
35°S
270°W
265°W
35°S
40°S
B-FRAME MOSAIC
40°S
270°W
0
50
100
SCALE IN km

Figure 8B

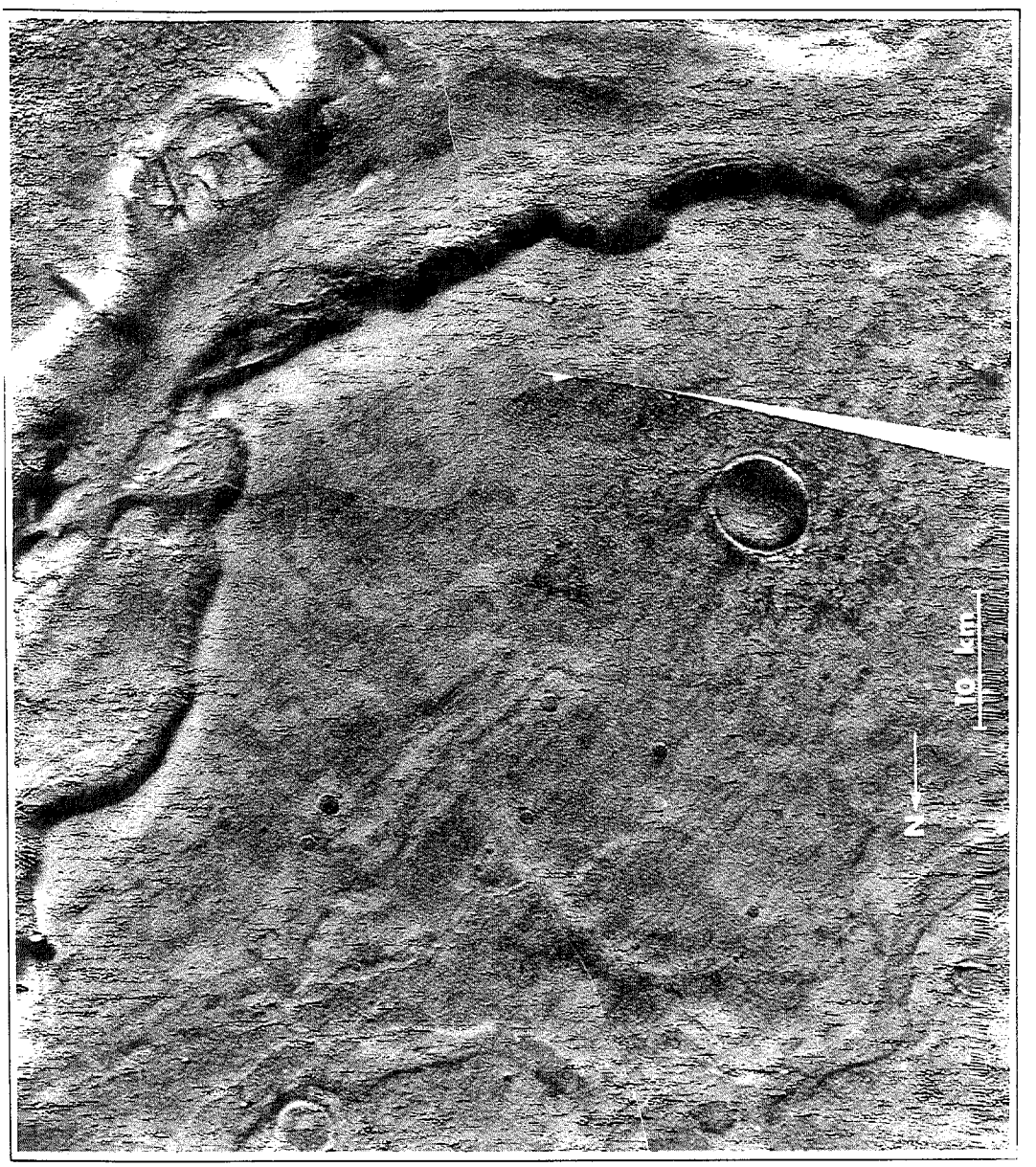

Figure 9

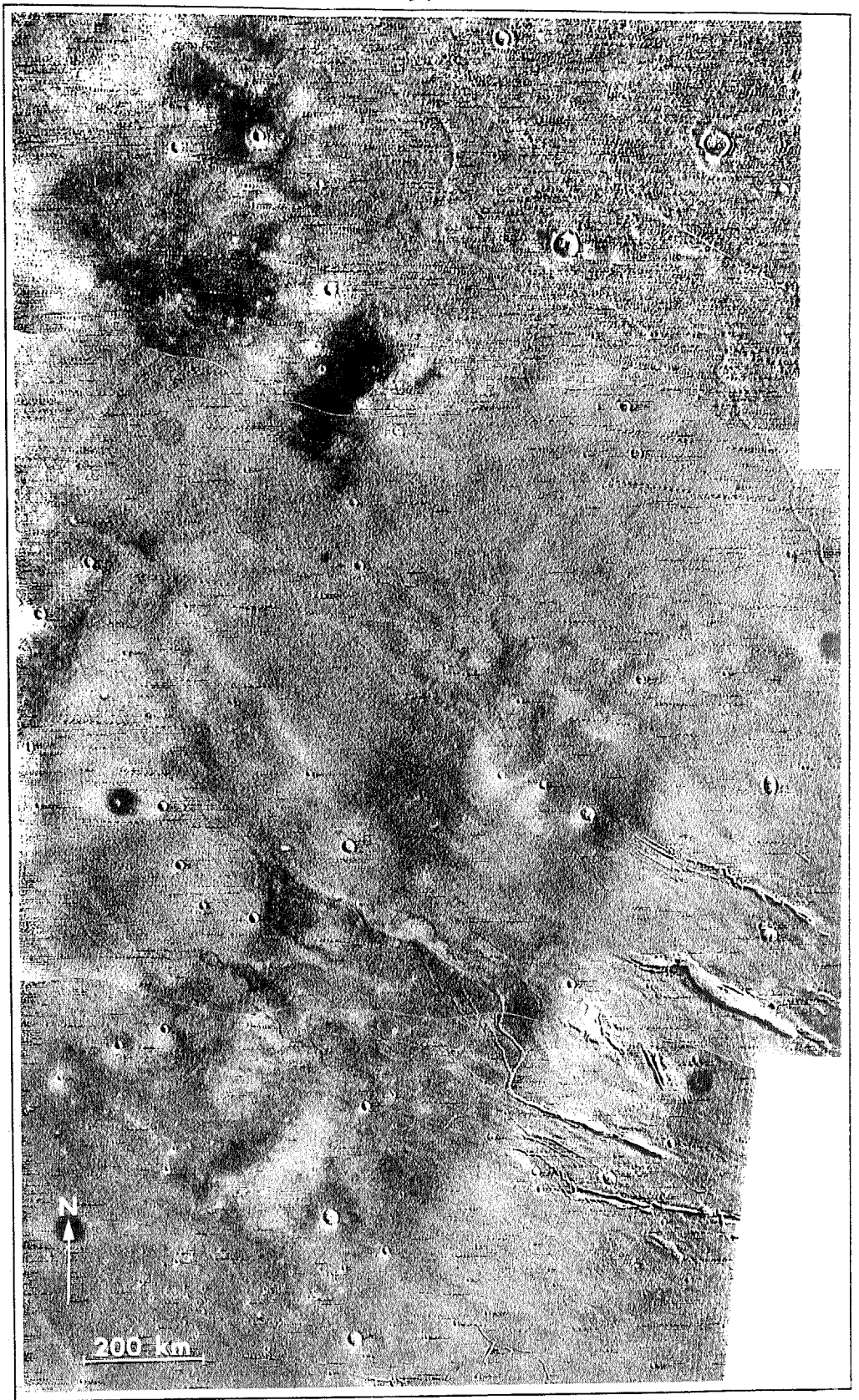

Figure 10A

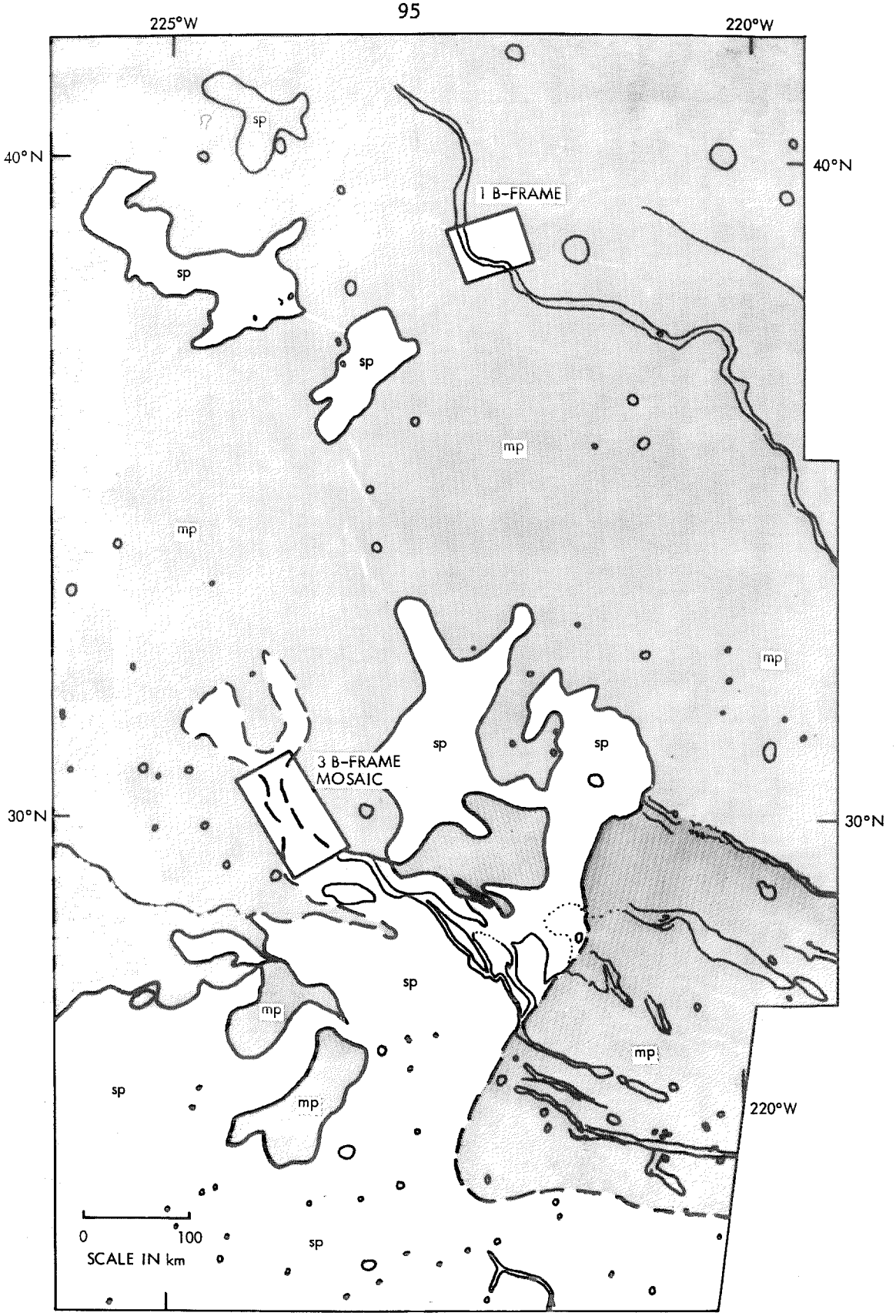
225°W
220°W
40°N
30°N
1 B-FRAME
3 B-FRAME
MOSAIC
sp
mp
0
100
SCALE IN km

Figure 10B

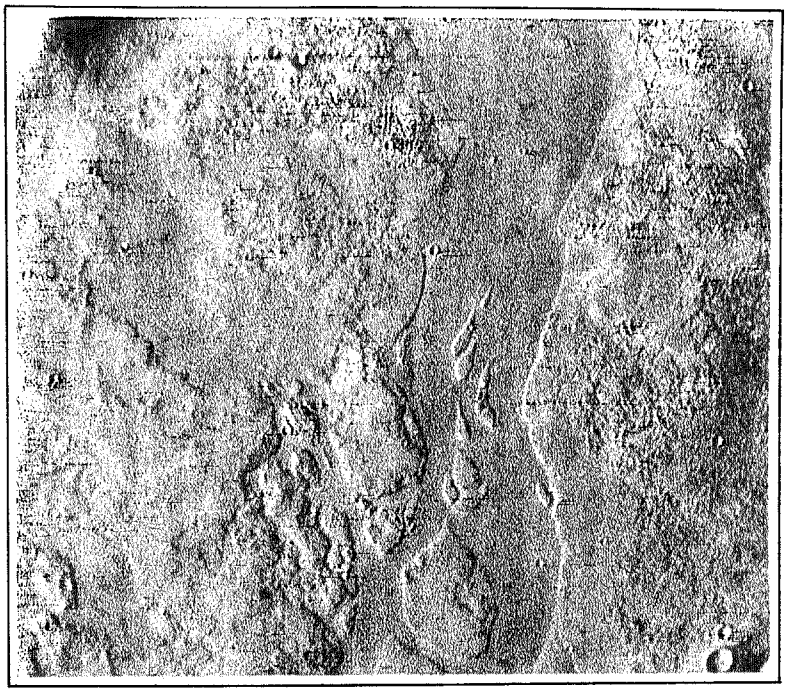

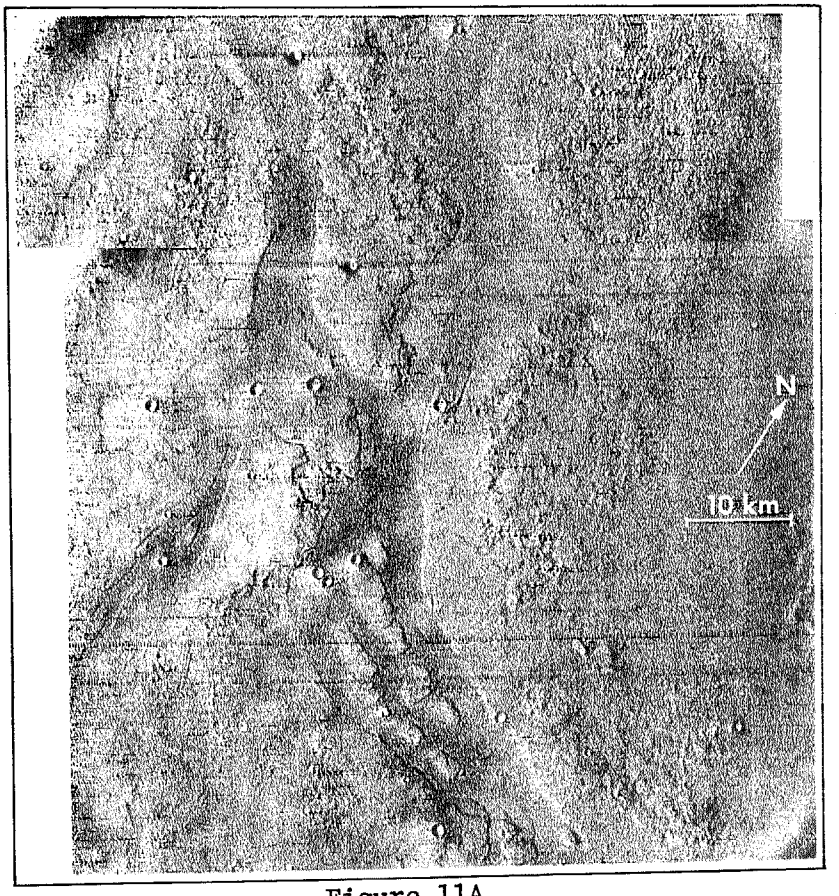

Figure 11A

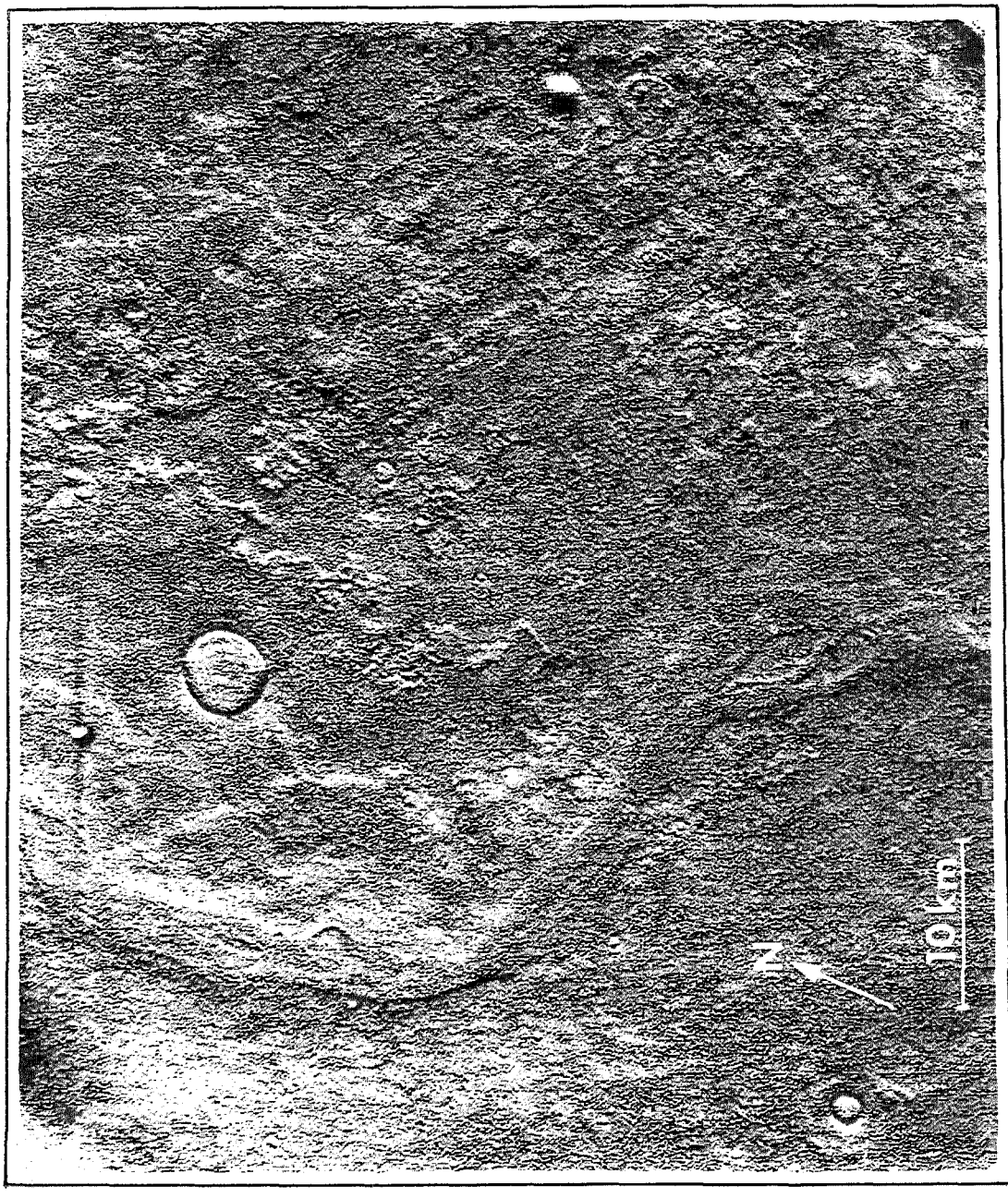

Figure 11B

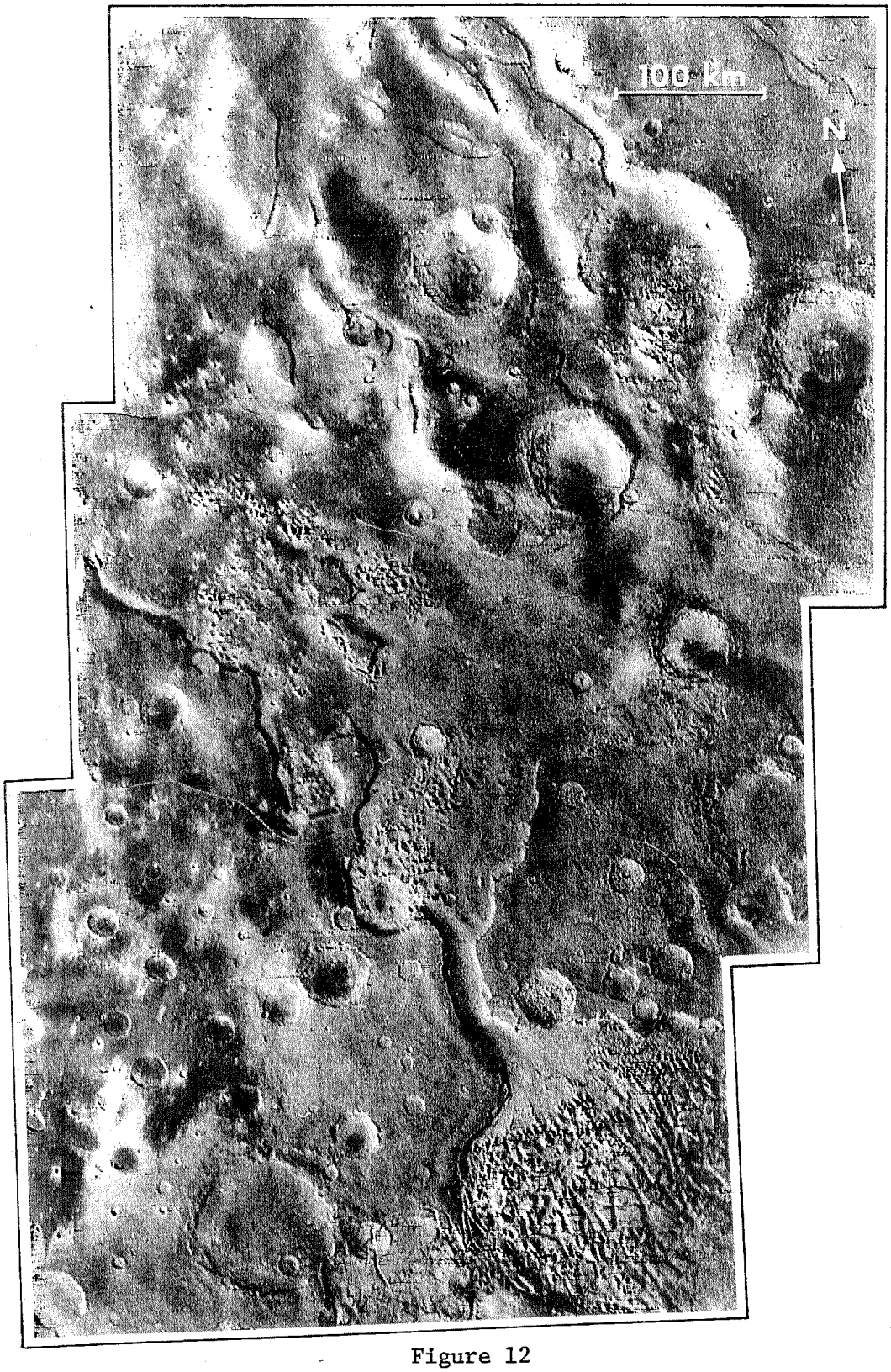

Figure 12

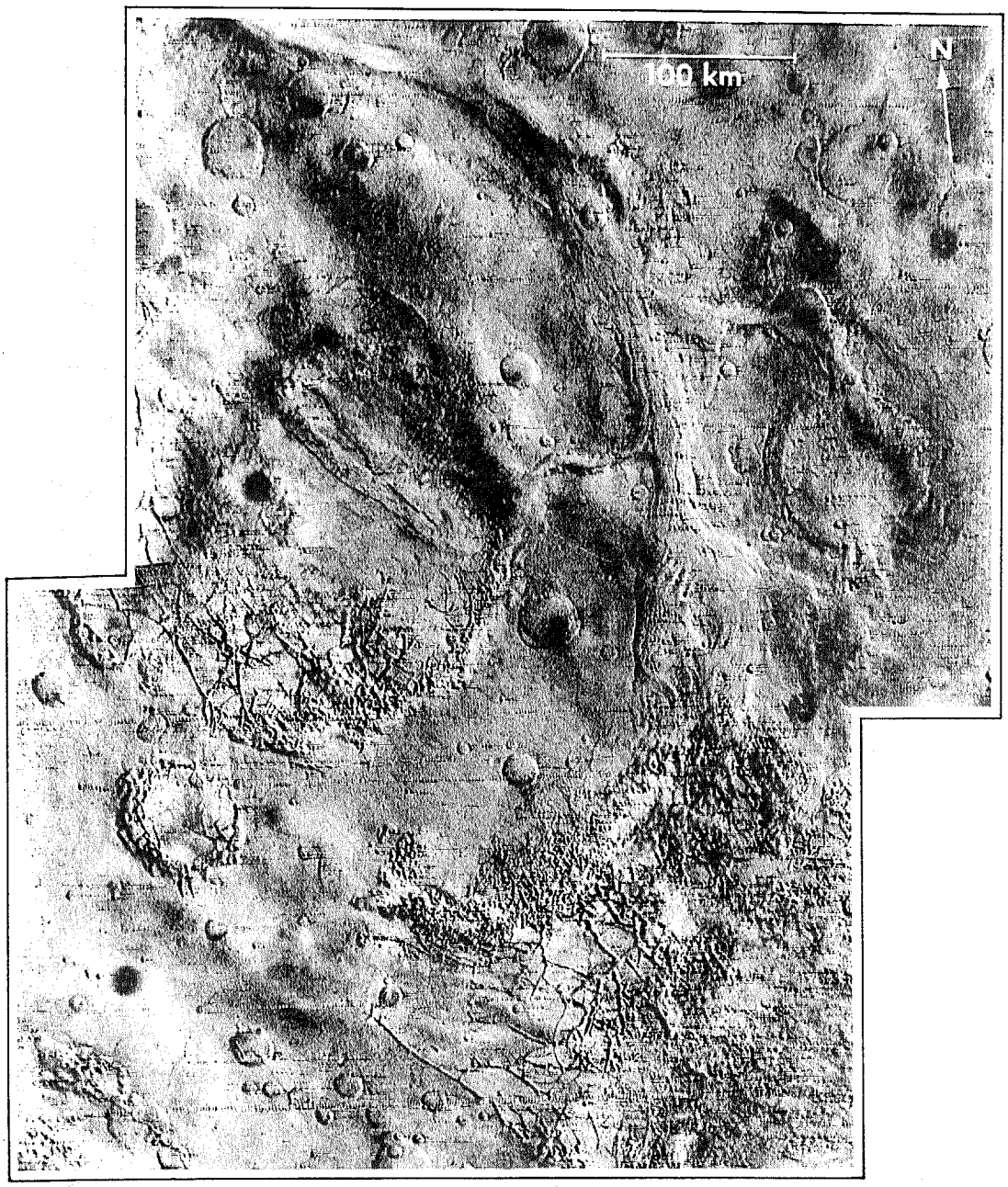

Figure 13

A

B

C

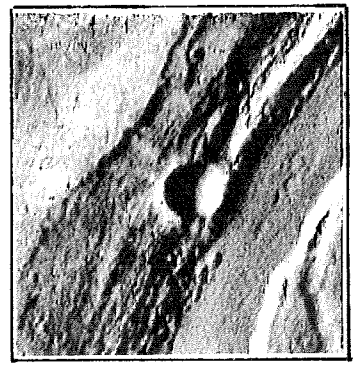

D

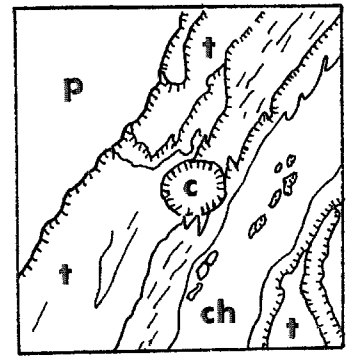

E

Figure 14

Part 3. Nature and Origin of Intercrater Plains on Mars

Introduction

Craters on Mars have been studied since first revealed in the Mariner 4 photographs transmitted to Earth in 1965. Although initial studies emphasized the many lunar-like aspects of the martian crater population, the deficiency of smaller craters and attendant variations in size-frequency diagrams suggested non-lunar processes had acted on the craters. Mariners 6 and 7 returned more and better data on martian craters and clearly showed not only that the surface was unsaturated with large craters (i.e., on the order of 50-km diameter), but that there was less than an equilibrium population (i.e., a surface where crater erosion is dependent on the impact of smaller objects). This suggested large-scale degradation independent of specific process. Initially, it was proposed that the degradation reflected post-cratering atmospheric processes (Murray et al., 1971). However, Chapman et al., (1959) reported crater morphologies which suggested that the degradation of the craters occurred in part during the epoch of crater formation. Subsequent studies of Mariners 6, 7 and 9 photographs support this suggestion (Soderblom et al., 1974; Chapman, 1974; Arvidson, 1974).

It is proposed here that the relatively smooth, crater-deficient areas within the cratered terrains on Mars (denoted intercrater plains, Fig. 1) are constituted of ancient stratified consolidated and unconsolidated materials, including large amounts of volatiles. They are among the oldest terrane units presently visible on Mars. An atmosphere significantly denser than the present one probably existed during their formation.

This paper will present observational evidence which bears on the above proposals for the nature and origin of the intercrater plains. After discussion of the evidence cited in support of previous views, further morphologic features of the plains will be examined to document the diversity of plains-forming materials and processes. In the discussion section, the set of speculative proposals will be developed.

Current Hypotheses

Three processes have been proposed to create and distribute the material of the intercrater plains (Fig. 1). One is that the materials represent impact-generated debris distributed by ballistics and by fluidized "base-surge" phenomena (Chapman et al., 1969; Cintala et al., 1975). Another specifies large-scale atmospheric redistribution of impact debris and weathering products (Chapman et al., 1969; Murray et al., 1971). The third involves the formation of large volcanic plains similar to those in the younger terrains of the northern hemisphere of Mars (Wilhelms, 1974). All three alternatives involve deposition rather than erosion, the former being a far more likely process to produce the observed sharp contacts, visible layering, and equal floor elevations inside and outside of craters (Wilhelms, 1974).

There are two main hypotheses for the formation of the intercrater plains: 1) that they are eolian, or 2) that they are volcanic. Used in this context, eolian refers to any process of transport above the surface; thus, the first two of the previously mentioned processes fall within this genetic category.

The first hypothesis proposed was that of eolian origin. Leighton

et al. (1967) and later Murray et al. (1971) cite the smooth plains, degraded large craters and pristine small craters as evidence of a post-large crater, pre-small crater erosional or depositional period involving widespread lateral transport of material. Chapman et al. (1969) cite evidence of a range of degradational states for the large craters to place the modification at a time commensurate with crater formation. The evidence in these early works was in most cases circumstantial, and only with the planetwide coverage of Mariner 9 were good examples found to support the interpretations (Soderblom et al., 1974; Arvidson, 1974). Figure 2 shows regions of cratered terrain with a range of crater degradation portrayed. Regional differences have been attributed to more recent blanketing, exhumation, and erosional phenomena sufficient to significantly modify smaller craters, but to have had only a modest effect on the larger craters. While this is not specific evidence for an "atmospheric" origin, it suggests deposition of relatively unconsolidated debris associated with an ancient period of martian history.

The second alternative, proposed by Wilhelms (1974) is that the plains are predominantly volcanic. The evidence he cites is straightforward: similarity of features within the plains unit with comparable lunar features. Two categories of evidence are presented -- the flooding of craters near the margins of large, youthful volcanic plains and the presence of lunar-like ridges. Figure 3 shows a wide-angle view of the margin of the Cryse Planita with uplands immediately south (14°N, 50°W). Features such as flow fronts (Fig. 4) and ridges (Fig. 5) suggest a volcanic origin

similar to lunar maria for Cryse and other lightly-cratered plains. The transition between these plains and the uplands shows partially filled and remnant "ghost" craters similar to those filled by the lunar mare basalts. Since these features are also seen deep within the cratered terrains as manifestations of the intercrater plains/craters ensemble, an argument can be made for similar genesis (i.e., older volcanic units).

More evidence is shown in the ridges seen throughout the intercrater plains. Although not ubiquitous, these ridges are abundant enough to rank as a major landform of the plains. Figure 5 shows some examples. Ascribed to volcanic processes by lunar analogy (Wilhelms, 1974), it is important to note that the similarity is to lunar highland ridges, rather than to mare ridges, and that the "ridges" are one-sided scarps. Figure 5 compares lunar mare and highland ridges with "ridges" of the martian smooth plains and intercrater plains. It is clear that the escarpments of the intercrater plains are indeed more like those of the lunar highlands, whose origin is still uncertain (Hodges, 1973; Howard and Muehlberger, 1973; Scott, 1973; Mattingly et al., 1973; Young et al., 1973). They also resemble the recently discovered escarpments on Mercury (Murray et al., 1974). The current explanations for the lunar highland escarpments center on thrust faults or flow fronts, although neither origin can explain all the data. Of course, one process and subsequent ridge-form on one planet may not necessarily be applicable to another planet, but the detailed similarity is suggestive.

Wilhelms has chosen to separate two distinct types of intercrater plains: the "plateau" plains and the plains of the heavily cratered

terrain. He apparently distinguishes the two primarily on the basis of crater frequencies, although the cratering statistics of Soderblom et al. (1974) and Mutch (personal communication, 1974) do not seem to indicate any great differences. On the qualitative observation of somewhat fewer craters and on the apparent burial and embayment of a moderate number of the larger craters, Wilhelms places the plateau plains intermediate in age between the heavily cratered terrain and the old, crater-deficient volcanic plains of the Lunae Planum.

All discussions of origin of intercrater plains have included disclaimers indicating the complexity of the problem and implying that more than one process was at work. Both Wilhelms (1974) and Soderblom et al. (1974) mention eolian, volcanic and fluvitile processes among others. In lieu of specific evidence which might exclude one of the alternatives, a complex history would seem reasonable. In the following sections, other features of the intercrater plains are examined for such evidence.

Morphologies of the Intercrater Plains

Surface features

As discussed initially by Murray et al. (1971), the surface of the intercrater plains at low resolution is essentially smooth and featureless. At higher resolution, however, a number of landforms can be seen. Some of these are associated with ephemeral, possibly polar-derived debris mantles (Soderblom et al., 1973), while others appear to be more deeply rooted. In general, the regions between craters are characterized by low, rolling topography, becoming hummocky in regions. Small craters are abundant, especially in swarms of associated secondaries.

In some regions, many of the larger craters (~ 20 km) have smooth, steep, convex-appearing interior walls and no ejecta, while in other nearby regions, the morphology changes to rough, blocky slumping interior walls and extensive ejecta blankets (Fig. 6). These differences appear to represent not only latitudinal variations (as might be expected for blanketing by polar-derived debris blankets (Soderblom et al., 1973, 1974), but also longitudinal variations (perhaps in the materials in which the impacts occurred). In equatorial regions, where numerous lineations which resemble gullies mark the surface, the texture of the intercrater plains becomes quite rough (Fig. 7). Irregular features of positive and negative relief and discontinuous albedo markings create a surface of confusing complexity. No diagnostic traits indicative of materials or processes are clearly visible, and few features can be traced any great distance.

Perhaps more outstanding than the surface of the intercrater plains are the indications of the subsurface as revealed through erosional processes which have penetrated into the unit. The geographically limited formation of the chaotic, fretted and troughed terrains (Sharp, 1973a,b) and channels (Sharp and Malin, 1975) within the intercratered plains has revealed important information about the materials of the plains unit and about the erosional processes. It is this new information which bears most directly on the nature and origin of the intercrater plains.

Fretted terrain

Fretted terrain occurs in localized regions along the margin between cratered "uplands" and uncratered "lowlands" on Mars. A complete description of the features of fretted terrain can be found in Sharp (1973b). Two features are of particular interest to the present discussion. The first concerns the mode of transport of debris developed by the fretting process and the second involves the limitation of vertical incision of the intercrater plains unit. Figure 8a shows the development of fretted "channels" within the intercrater areas. At high resolution (Fig. 8b) the fretting process can be seen to have removed crater-filling material along its course but to have left untouched terrain immediately adjacent to the channel. Portions of small craters intercepted by the channels are still intact while other parts have been completely removed. This can be attributed to the resistance to erosion of the crater rims (possibly the result of shock lithification), to the gentleness of the fretting process, and to the ease of removal the debris produced by fretting. It is inferred that the materials into which the erosion occurred were essentially unconsolidated.

In most cases, floors of fretted channels exceed in depth floors of adjacent craters (Fig. 9), while craters integrated with the channels have concordant floors. This uniform depth of erosion appears throughout the intercrater plains, as has been noted by several Mariner 9 investigators (Sharp, 1973b; L. A. Soderblom and D. Wenner, personal communication, 1973), and will be shown elsewhere in this work in association with other erosional terrains.

Chaotic terrain

Chaotic terrain is confined primarily to a region within ±15° of the equator between 0° and 60°W, an area informally called the "Cryse Trough" because of its topographic form (a broad depression, trending roughly north-south and paralleling the Tharsis Ridge). Sharp (1973b) defines chaotic terrain as regions with "rough floor topography featuring a haphazard jumble of large angular blocks" with "arc-shaped slump blocks on [the] bounding escarpments." Although some areas of chaotic terrain are irregular in shape, others are clearly circular and crater-like. Some are in fact contained within craters (Fig. 10).

As noted previously in the fretted terrain, the erosion of the chaotic terrain appears to have three main attributes: 1) material was effectively removed from the chaotic regions with little effect on the surrounding terrain; 2) chaos developed to a depth greater than that represented by the floors of large craters; and 3) integrated regions of chaotic terrain and channels have concordant floors (Fig. 10). Material removal may have been less complete or effective than in fretted regions, a point indicated by the gradation from smooth channel floors to the rough, jumbled positive floor topography of the chaos. The restricted vertical development suggests that the erosional processes are effective to a limited depth. It is again inferred that the materials were only slightly consolidated, although the irregular blocks and the gradational transition from the smooth intercrater plain to the degenerated landform may imply more consolidated capping materials.

Channels attributed to fluidal action

Some of the most intriguing features on the martian surface are the large sinuous channels, and the most controversial problem associated with the channels is that of their origin. Although several alternatives have been proposed (Schumm, 1974; Carr, 1974), the favored origin is that of fluid erosion (Milton, 1973; Baker and Milton, 1974; Sharp and Malin, 1975). Channels of this nature are almost entirely restricted to the cratered terrain/intercrater plains, and provide yet another means of probing the subsurface of the plains.

Baker and Milton (1974) have developed a case for the origin of some channels by catastrophic floods, as have Sharp and Malin (1975). The best example of such a channel is Mangala. The morphological similarity to the channeled scablands in Washington State, formed by the catastrophic release of the ice-dammed Pleistocene Lake Missoula (Bretz, 1923; 1969), is striking. The scablands developed in two types of materials: the Palouse loess deposit and the basalts of the Columbia Plateau which were covered by the loess. The massive floods stripped away the loess to form wide channels, and incised into the bedrock floors of these scabland channels as deep as 200 m.

Figure 11a shows a portion of the Mangala channel suggestive of catastrophic flooding. Two features within this photograph bear directly on the materials of the plains unit. First, note that the craters on unchanneled terrain are subdued and appear blanketed while those on channel deposits are more pristine in form. This suggests at least a superficial mantle of loose material has been eroded. Second,

note the stripped and scoured appearance along the margin and in large isolated patches, and the smooth channel floor. This suggests the patchy removal of a blanket of loose debris and incision into a more resistant material. Further downstream, a braided section of channel may represent in part unconsolidated channel deposits eroded during the terminal stages of the flood (Fig. 11b). Similar features are seen within the Ares channel.

In these cases, while the process of removal appears to have been more violent than in the fretted or chaotic regions, evidence is strong for at least some unconsolidated fine material being a constituent of the intercrater plains.

Layers within the plains

Layering of subsurface materials is seen in several places within the cratered hemisphere of Mars. In most cases, the visibility of the layers is marginal, the four following examples being representative of the range in perceptibility of the features.

The best and most obvious occurrence of layered material outside of the polar layered deposit occurs within the Ganges Chasma of the Valles Marineris (Fig. 12). Rising above the interior floor of the 750-km long, 170-km wide and 2-km deep chasm is a mesa-like island of layered material which is about 2-km thick (D. Dzurisin, personal communication, 1974). The summit of the layered mesa is essentially level with the surface of the intercrater plain into which the chasm is formed. It is possible that these layered materials are not representative of the intercrater plains unit in which the chasm has formed, since the walls

of Ganges Chasma do not show the abundant layering seen in the intra-trough mesa. The layered material of the mesa would then most likely represent a post-chasm deposit which has subsequently been partly removed. Since the layered deposit is as thick as the plains unit, it is difficult to imagine processes that could essentially fill the chasm to its brim, and then remove the material. It seems more likely that the visible layers in the mesa represent some inhomogeneity within the plains material, which is evidenced by the differences from the wall layering. The nearly complete removal and the appearance of slope gullies which head in "weeping layers" suggests a loosely consolidated material possibly rich in volatiles (Sharp and Malin, 1975).

Elsewhere in the Valles Marineris, layers are seen within the wall formations (Fig. 13). A distinct dark unit seems to cap the sequence, consistent with the smooth plain surface being a later volcanic material covering the older, intercrater plains unit. Mare-like ridges on the plains immediately north (Lunae Planum) and south (Syria, Sinai Panitia) reinforce this impression. In the walls of the canyons, beneath the sharp, darker brink, broad bands of alternating light and dark albedo (relative albedos -- the absolute differences may be quite small) suggest layering, as do the differences in outcrop expression which occur downslope. Such layering is seen in several widely separated locales extending over the entire length of the Marineris system, some 3000 km. The layered materials may not be entirely members of the intercrater plains unit, but since the eastern end of the Valles are within the intercrater plains unit, while the mid and western regions are within smoother, younger plains units, a laterally gradational change

consistent with the burial of the intercrater plains by younger volcanics is suggested.

Nearly halfway around the planet, at 26°S, 140°W near the Sirenum Fossae, where a smoother volcanic plain "laps" onto older intercrater plains, a graben has cut into the materials (Fig. 14). Dark and light strata are seen within the walls and on "islands" within the graben. The surface to the northwest reveals a number of low, lobate escarpments (probably lava flow fronts) which cover and are cut by a series of small horst and graben which parallel the main tectonic feature. To the southeast, a similar plain surrounds a highly textured region of much lower albedo. It is suggested here that the dark stratum and this one dark surface region are older material which has been covered by lighter plains units.

Finally, in the braided region of the Mangala channel, slight, very faint lineations with contour-like configuration (Fig. 11) may indicate layering within that region of intercrater plains. Note particularly the "resistant" knobs located on several "islands".

Exhumation of cratered surface and lower level boundary of intercrater plains

Perhaps the most dramatic evidence for the nature of the intercrater plains unit is shown in Figure 15. It shows an "island" within the gigantic channel Kasai, approximately 3-4 km high, whose surface is at the same relative elevation as the Lunae Planum plateau plains into which the channel is cut. Note the crater being exhumed from beneath

the retreating cliff of the island. Although Baker and Milton (1974) attribute this channel to catastrophic flooding, the remarkable state of preservation of not only the crater's wall, but of its interior features attests to the gentle character of the exhumation and erosional processes. This preservation also suggests that the 3-km thick deposit neither affected the crater during accumulation nor during the period prior to erosion. As noted by Baker and Milton, the walls of Kasai and of this particular island show stratification nearly identical to that seen in other regions. This suggests a connection between this otherwise isolated feature and the greater area of intercrater plains.

There are several other examples of crater exhumation within the intercrater plains, although the Kasai crater is by far the best. One is within the channel Shalbatana and is shown in Figure 16. This crater-like form is less distinct and perhaps more eroded than the Kasai crater. Although Sharp and Malin (1975) classified Shalbatana as an outflow channel of flood origin, their difficulty in explaining a channel volume/source volume ratio of unity caused them to propose a polygenetic origin. A complex origin does in fact seem to be more reasonable in light of the Shalbatana crater.

Another example is a crater-like form, seen only at low resolution, on the floor of Ganges Chasma (Fig. 12). Its light rim deposits stand above the dark floor material of Ganges but is some 1.5 km beneath the rim of the chasm. It cannot be conclusively demonstrated that this feature was once overlain by materials as represented by either the walls or layered deposits, but this conclusion seems plausible in light

of the close areal proximity and textural similarity to other features more clearly related to the intercrater plains unit.

A final observation concerning the cratered surfaces being exhumed from beneath the intercrater plains is the possible existence of a delineating stratum near the base of the unit. The dark floor of the Ganges Chasma occurs at an elevation of from 0 to -1 km relative to the 6.1 mbar pressure surface (Christensen, 1975). A similar dark unit is seen throughout the Valles Marineris whenever the floor reaches a depth of 0 to -1 km. As the surface of the plains into which the Valles have developed rises in altitude westward, the depth of incision increases, occasionally reaching but not penetrating below a dark unit at 0 to -1 km (Fig. 17). Eventually, the increase in surface elevation exceeds the increase in canyon depth and only patchy dark features are seen on the floor. The westernmost depths are between the 2- to 6-km levels, and no dark patches are visible. The Kasai and Shalbatana craters also appear developed within the 0 to -1 km surface, although it does not appear dark.

Discussion

This section will consist of a set of summary statements and conclusions and a series of progressively more speculative interpretations. The former are strongly suggested by the data; the latter are plausible extrapolations. It should be clear that the speculations may present only one of a number of possible alternatives.

The following statements summarize the observations presented in the previous sections:

1. Large craters show significant diversity in degradation, but most tend to be very degraded.
2. Some regions of intercrater plains are extremely subdued, with "flooded" craters.
3. Escarpments are seen in both high and low resolution images that are reminiscent of both lunar highland and mercurian scarps.
4. The processes of fretted and chaotic terrain formation remove material from channeled regions with little effect on surrounding terrain.
5. Fretted and chaotic terrains develop to depths greater than the depths of large, flat-floored craters.
6. Integrated regions of chaotic and fretted terrains have concordant floors.
7. A number of channels show evidence of stripping away of loose debris and scour of underlying resistant materials.
8. Several regions show subsurface layering.
9 A few craters are being exhumed from beneath thick deposits.

Two major conclusions can be derived from the observations presented above. First, that the landforms of the intercrater plains suggest a complex sequence of stratified units including both cohesive and relatively unconsolidated materials. Second, that the topmost unit varies from location to location across the surface of Mars. Both conclusions are independent of specific materials and processes which may be invoked to form the unit. They suggest that martian intercrater

plains are more complex than many investigators have portrayed. Any planetwide stratigraphy must recognize that complexity.

The data and above conclusions seem relevant to four topical speculations: 1) the nature of the materials; 2) the nature of plains formation; 3) the relationship between chaotic, fretted, and channeled terrains; and 4) considerations of an ancient martian crust. The first two will be discussed together, since problems relating environmental processes and constituent materials are nearly inseparable.

The surface of Mars appears to have been continually modified prior to and during the portion of heavy bombardment recorded in the most cratered regions. The resurfacing continued after the bombardment ceased, although its nature appears to have changed dramatically. Surface ridges and resistant wall outcrops suggest competent rock units, while scoured channels, widespread weakly consolidated strata, subdued morphology, and the ease of erosion suggest loose debris blankets. It is interesting to speculate that the enormous widths of the martian channels (relative to terrestrial examples) may be due to lateral erosion of looser, unconsolidated material along a more resistant bedrock. Volcanic plains seem to have formed throughout the period recorded by the intercrater plains unit and afterwards. The source and nature of the unconsolidated material, however, cannot be definitely established and appears to be unique to the intercrater plains. There seems to be too much loose debris too evenly distributed to be attributed to the cratering process alone. Thus an atmosphere appreciably greater than that presently observed on Mars, capable of transporting

considerable material both in suspension and through saltation and traction, is probable. Impact-generated debris (such as the lunar surface materials), weathering products, and volcanic ash are all probably constituent materials. Since the redistribution of this fine material appears to have terminated with the end of the heavy bombardment, it is necessary for Mars to have lost this early atmosphere at that time, through exospheric loss, surface recombination, or through some as yet unknown process.

Spatial and temporal development of chaotic and fretted terrains and channels within intercrater plains suggests that lithospheric volatiles believed necessary for their formation (Sharp, 1973b; Sharp and Malin, 1975) were supplied by the intercrater plains unit. These landscapes may reflect the temporary re-release of previously buried (or incorporated) atmospheric volatiles, or the release of juvenile volatiles. This suggests that the plains unit may be the residence for the ancient martian atmosphere, a possibility proposed in a different context by Fanale and Cannon (1971). This implies ancient and unique conditions for formation of these landforms, a conclusion similar to that arrived at through separate studies of channels (Malin, 1976; Sharp and Malin, 1975). Another point, the gentle nature of the erosion of fretted channels, suggests that this may be quite different from the channeling by catastrophic or longer-term flooding.

The final speculation concerns the observation of a 0 to -1.0 km "base level". Inspection of the planetary topographic model prepared by Christensen (1975) shows that, except in regions associated with

volcano/tectonic uplift (Tharsis and Elysium), the 0 to -1 km zone delineates the boundary between the cratered uplands and uncratered lowlands (Fig. 18). The transitional landform between these regions (fretted terrain) occurs within 1 km or so of this contour. In the northern plains between the volcano/tectonic uplifts, knobby terrains reminiscent of fretted terrain lie just above the 0 to -1 km zone, suggesting a ridge of pre-existing older terrain, currently eroded, surrounded by younger volcanic plains. Whether the altitude zone represents an environmental level (e.g., for permafrost, Sharp, 1973b; L. A. Soderblom and D. Wenner, personal communication, 1973), or an actual physical surface (as evidenced by craters) representing a discrete time-stratigraphic marker, is not apparent in the data presently available. However, it suggests the possibility of an ancient bedrock unit significantly older than the most cratered surface.

In summary, Mars appears to have had a complex early history, complete with significant atmospheric and some fluid erosion. Just as the polar layered deposits are believed to record the recent history of Mars (Cutts, 1973), so may the ancient layered deposits -- the intercrater plains -- record the most primitive history of Mars. Detailed studies of Martian stratigraphy in the distant future may be as intellectually rewarding as the studies of terrestrial stratigraphy are today.

REFERENCES

Arvidson, R. E., Morphologic classification of martian craters and some implications, Icarus 22, 264-271 (1974).

Baker, V. R. and D. J. Milton, Erosion by catastrophic floods on Mars and Earth, Icarus 23, 27-41 (1974).

Bretz, J. H., The channeled scablands of the Columbia plateau, Jour. Geol. 31, 617-649 (1923).

Bretz, J. H., The Lake Missoula floods and the channeled scablands, Jour. Geol. 77, 505-543 (1969).

Carr, M. H., The role of lava erosion in the formation of lunar rilles and martian channels, Icarus 22, 1-23 (1974).

Chapman, C. R., J. B. Pollack and C. Sagan, An analysis of Mariner 4 cratering statistics, Astron. J. 74, 1039-1051 (1969).

Chapman, C. R., Cratering on Mars: I. Cratering and obliteration history, Icarus 22, 264-271 (1974).

Christensen, E. J., Martian topography derived from occultation, radar, spectral and optical measurements, Jour. Geophys. Res. (in press) (1975).

Cintala, M. J., J. W. Head, and T. A. Mutch, Depth/diameter relationships for martian and lunar craters (abstr.), Transactions, Am. Geophys. Un. (EOS) 56, 389 (1975).

Cutts, J. A., Nature and origin of layered deposits of the martian polar regions, Jour. Geophys. Res. 78, 4231-4249 (1973).

Fanale, F. and W. A. Cannon, Adsorption on the martian regolith, Nature 230, 502-504 (1971).

Hodges, C. A., "Mare ridges and related studies: B. Mare ridges and lava lakes", Apollo 17 Preliminary Science Report (NASA SP-330), pp. 31.12-31.21. Washington: U.S. Government Printing Office, 1973.

Howard, K. A. and W. R. Muehlberger, "Mare ridges and related studies: C. Lunar thrust faults in the Taurus-Littrow Region", Apollo 17 Preliminary Science Report (NASA SP-330), pp. 31.22-31.25. Washington: U.S. Government Printing Office, 1973.

Leighton, R., B. C. Murray, R. P. Sharp, J. D. Allen, and R. K. Sloan, Mariner Mars 1964 Project Report: Television Experiment. I. Investigators' Report, Jet Propulsion Laboratory Technical Report 32-884, Pasadena: Jet Propulsion Laboratory (1967), 178 pp.

Malin, M. C., Investigation of surface features of the planet Mars, Ph.D. Thesis, California Institute of Technology, Pasadena, California 91125 (1976).

Mattingly, T. K., F. El-Baz and R. A. Laidley, "Observations and impressions from lunar orbit", Apollo 16 Preliminary Science Report (NASA SP-315), pp. 28.1-28.16. Washington: U.S. Government Printing Office, 1972.

Milton, D. J., Water and processes of degradation in the martian landscape, Jour. Geophys. Res. 78, 4037-4047 (1973).

Murray, B. C., L. A. Soderblom, R. P. Sharp, and J. A. Cutts, The surface of Mars: I. Cratered terrains, Jour. Geophys. Res. 76, 313-330 (1971).

Murray, B. C., M. J. S. Belton, G. E. Danielson, M. E. Davies, D. E. Gault, B. Hapke, B. O'Leary, R. G. Strom, V. Suomi, and N. Trask, Mercury's surface: Preliminary description and interpretation, Science 185, 169-179 (1974).

Schumm, S. A., Structural origin of large martian channels, Icarus 22, 371-384 (1974).

Scott, D. H., "Mare ridges and related studies: D. Small structures of the Taurus-Littrow region", Apollo 17 Preliminary Science Report (NASA SP-330), pp. 31.25-31.29. Washington: U.S. Government Printing Office, 1973.

Sharp, R. P., Mars: Troughed terrain, Jour. Geophys. Res. 78, 4063-4072 (1973a).

Sharp, R. P., Mars: Chaotic and fretted terrains, Jour. Geophys. Res. 78, 4073-4083 (1973b).

Sharp, R. P. and M. C. Malin, Channels on Mars, Geo. Soc. Am. Bull. 86, 593-609 (1975).

Soderblom, L. A., T. J. Kreidler, and H. Masursky, Latitudinal distribution of a debris mantle on the martian surface, Jour. Geophys. Res. 78, 4117-4122 (1973)

Soderblom, L. A., C. D. Condit, R. A. West, B. M. Herman, and T. J. Kreidler, Martian planetwide crater distributions: Implications for geologic history and surface processes, Icarus 22, 239-263 (1974).

Wilhelms, D. E., Comparison of martian and lunar geologic provinces, Jour. Geophys. Res. 79, 3933-3941 (1974).

Young, R. A., W. J. Brennan, R. W. Wolfe, and D. J. Nichols, "Mare ridges and related studies: A. Volcanism in the lunar maria", Apollo 17 Preliminary Science Report (NASA SP-330), pp. 31.1-31.11. Washington: U. S. Government Printing Office, 1973.

FIGURE CAPTIONS

Figure 1: Low Resolution View of Intercrater Plains on Mars. Mariner 6 wide angle photograph of Mars showing a large expanse of cratered terrain in Deucalionis Regio. The large crater, Flaugergues, is located near 17°S, 340°W and is about 200 km in diameter. Note the essentially smooth, featureless texture of the intercrater surface (Photo 6N21).

Figure 2: Craters of the Heavily Cratered Terrain on Mars.

2A: Two Mariner 9 A-frames illustrating the various morphologies of large craters in heavily cratered regions on Mars. Note the many subtle states of crater degradation. It has been suggested that the degradation of the large craters occurred concurrently with their formation (Chapman et al., 1969; Soderblom et al., 1974)(Top, DAS 6859268: centered 7.6°N, 321°W; Bottom, DAS 6858498: centered 24.8°S, 357°W).

2B: Two more Mariner 9 A-frames, showing craters in a variety of degradational states. (Top, DAS 6931298, 8.95°N, 311°W; Bottom, DAS 6930598: 18.3°S, 321°W).

Figure 3: Boundary between Smooth Plains and Intercrater Plains.

3A: Photomosaic of Mariner 9 A-frames showing the boundary between the Cryse Planitia and a region of cratered terrain near 14°N, 50°W. Note the buried and subdued craters in the zone between the smooth plains (upper right) and the intercrater plains (lower left). Note also the mare-like ridge in the smooth plains terrain (DAS 7543168, 7543238).

3B: Sketch map of smooth plains/cratered terrain (intercrater plain boundary, showing smooth plains (sp), intercrater plains (icp = heavy tone) and a transitional plains zone (tp = light tone). Similar relationships seen within the cratered terrain are cited by Wilhelms (1974) as evidence for a volcanic origin for the intercrater plains.

Figure 4: Flow Fronts on the Moon and Mars.

Photographs of flow fronts on the Moon (top) and Mars (bottom) are presented here at the same scale. The poor contrast of the Mars frame is probably the result of unfavorable viewing conditions (solar elevation angle = 47° as opposed to the lunar example, 17°). Features such as these demonstrate the likelihood of volcanic plains formation on Mars. Although no clearly discernible fronts are seen in the intercrater plains, the large range in relative ages of identifiable volcanic plains suggests volcanic processes may have been active during the formation of the intercrater plains. (Top: Lunar Orbiter V M161, centered at 32.7°N, 22°W; Bottom: Mariner 9 frame DAS 6966613, located near 17°S, 136°W).

Figure 5: Ridges and Scarps on the Moon, Mars and Mercury.

5(I): *Mare ridges on the Moon (top) compared with* smooth plains ridges on Mars (bottom), presented at the same scale. The general similarity in form suggests similar genesis, probably volcanic (Top: Apollo 17 metric camera M0454, enlargement of

frame centered near 19.5°N, 20.3°E, with a sun elevation angle of 5°; Bottom: Mariner 9 B-frame DAS 12901348 centered at 23.2°S, 244°W, sun elevation 20°).

5(II): Lunar highland (A), mercurian intercrater plains (C) and martian intercrater plains (D) escarpments, shown at same scale. B shows lunar example enlarged by a factor of 3 (see inset). These features are distinctly different from those of Figure 5(I) and most likely reflect different genetic processes. Lunar example (Lincoln-Lee Scarp, Apollo 17 landing site) has been interpreted by several lunar scientists (Howard and Muehlberger, 1973) as the result of faulting, as has the mercurian scarp (Discovery Scarp, Murray et al., 1974). A similar origin may apply to the martian scarps. (A: Apollo 17 M0793; B: AS17-150-23006; C: FDS528884 (Mariner 10) D: DAS 8009123 (Mariner 9)).

Figure 6: Variations in Crater Morphology within the Intercrater Plains Regions.

6A: Mariner 9 A-frame photomosaic showing areas photographed by B-camera. Frames rectified to Lambert Conformal projection. Note that frames b,c, and f are at approximately the same latitude, as are d and e. Instead of a latitudinal variation as seen by Soderblom et al. (1973) elsewhere on Mars, a longitudinal variation is suggested: steep, convex-appearing interior unterraced walls and little indication of ejecta blankets (b,c, and d) east of about 325°W (Type 1), and shallow,

blocky, terraced interior walls and pronounced ejecta blanket (e,f and Figure 8B) west of that longitude (Type 2). Although differences in crater size may be responsible for the morphologic differences, this seems unlikely, since only craters large enough to display the cited morphologic features are compared. The longitudinal variation suggested by the data may imply differences in the materials of the intercrater plains.

6B: Mariner 9 high resolution frame DAS 8263014, showing Type 1 crater morphology at 38°N, 307°W. Note the large number of small craters, probably secondaries formed by ejecta from a large fresh crater not shown in this photograph.

6C: Mariner 9 high resolution frame DAS 8191054, showing Type 1 morphology at 38°N, 316°W (photo same scale as B). Note small craters (secondaries?) and fretted channel at upper right.

6D: Mariner 9 high resolution frame DAS 8190914, showing Type 1 morphology at 30°N, 321°W. Note the escarpment at right that appears to traverse the crater wall and floor at bottom.

6E: Mariner 9 high resolution frame DAS 8118948 showing terraced crater morphology (Type 2) at 30°N, 330°W (photo same scale as D).

6F: Mariner 9 high resolution frame DAS 8047198 showing terraced morphology (Type 2) at 38°N, 334°W. Note extensive ejecta blanket and fretted channel at left.

Figure 7: High Resolution Photographs of Intercrater Plains in the Equatorial Region of Mars.

Two Mariner 9 B-frames showing the complex nature of the morphology of the intercrater plains in the martian equatorial regions. Escarpments, ridges, isolated hills, channel-like forms, and wave-like hummocks combine with craters and crater deposits to form a confusing pattern of topographic forms (Top: DAS 11620145, 16°S, 331°W; Bottom: DAS 8909609, 7.4°S, 245°W).

Figure 8: Fretted Channels and Craters: Relationship to Intercrater Plains

Top: Mariner 9 A-frame DAS 8119058 (36°N, 326°W) showing location of high resolution: B-frame on fretted channel.

Bottom: Mariner 9 B-frame DAS 8119093 showing terraced morphology (see Fig. 6) at 38°N, 326°W. Note the three main attributes of the process of fretting of the materials of the intercrater plains: 1) portions of crater rims survive the removal of surrounding material; 2) the fretting appears sharply defined (i.e., shows little effect immediately adjacent to the fretted area); and 3) a uniform depth of channel development.

Figure 9: Fretted Channels and the Intercrater Plains.

9A: Mariner 9 A-frame DAS 7975208 centered at 36°N, 345°W. This figure illustrates the three points shown in Figure 8 at a larger scale, and adds one more: that the fretting process

proceeds to a greater depth than the floors of the craters of the plains. Note the integration of craters by both tangential and headon encounters.

9B: Mariner 9 B-frame mosaic (DAS 9378189, 10650904, and 10650974) showing a portion of the fretted channel shown in Figure 9A. Note the concordant floor joining the fretted crater to the channel (middle left). Note, too, the resistant crater rims within the fretted channel (far right).

Figure 10: Chaotic Terrain and the Intercrater Plains.

These Mariner 9 photographs (DAS 7686808, 7686878 and 7686948) show the major aspects of the process of chaos formation within intercrater plains. Note: 1) the deterioration often appears confined initially to craters; 2) the effective removal of material in some regions, and the residue which survives in other regions; 3) the uniform appearance of channel and chaotic terrain depth; 4) that crater floors lie above the floors of the channels; and 5) the sharp boundaries between plains affected by chaotic terrain formation and those that are not. As in the case of fretted terrain, these observations suggest the effective removal of an essentially unconsolidated material, perhaps overlain by a more competent rock unit capable of resisting at least in part the erosion associated with chaos formation.

Figure 11: High Resolution Photographs of Mangala Vallis (5°S, 151°W).

11A: Mariner 9 B-camera frame DAS 12499650, illustrates two

interesting features which bear on the type of materials in the intercrater plains. Note the two small, subdued craters on the plains in the upper left portion of the frame, and compare these with the two similarly sized craters superposed on the channel formations in the upper right portion of the picture. The difference in morphology suggests a blanket covers the craters on the plain but not those on the channel. The second feature concerns the overall morphology of the channel, which is reminiscent of channeled scablands formed in Washington State, where loose material covered basalt bedrock. These two observations suggest the intercrater plains consist in part of loose material covering more resistant material.

11B: Mariner 9 B-frame (DAS 9628649) shows a portion of Mangala which is downslope from the first region. A most interesting feature of this region is the possible existence of layering or vertical structure evidenced in the terracing of some of the small "islands" and in the resistant knobs which top these "islands".

11C: Sketch Map of Figure 11B, indicating position of contour-like layering. Diagonal tone indicates pre-existing surface; light tone indicates deepest channel incision. X marks denote resistant knobs.

Figure 12: Layering in the Intercrater Plains: Ganges Chasma (6°S,50°W). Top: Mariner 9 A-frame (DAS 7614498) showing layered

deposit within Ganges Chasma. Note: 1) dark trough floor material possibly showing through "windows" in layered material north and east of B-frame rectangle; 2) light-colored hills rising above dark floor material, similar to layered material albedo; and 3) crater-like form west of layered mesa, indicated by "a".

Bottom: High resolution B-frame (DAS 9017619), showing the intra-trough mesa about 2 km high, whose summit is essentially level with the plain in which the trough formed.

Figure 13: Layering in the Intercrater Plains: Valles Marineris. Six Mariner 9 high-resolution B-frames illustrate the range in visibility of layers within the walls of the Valles Marineris. Each photograph is accompanied by a sketch showing the features identified as layering. In each case, the upper level plains surface is indicated by diagonal lines and an abbreviation (sp=smooth plain; icp=intercrater plain), and the lower level surface is indicated by a medium tone and abbreviation (ht=hilly terrain; cf=canyon floor). Featureless wall materials, possibly talus slopes, are left unmarked. Ridges and craters are marked, as are the ridges defining chutes near the brink of the walls.

13A & B: DAS 7398723 (7.5°S, 78°W)
13C & D: DAS 10132999 (6.7°S, 87°W)
13E & F: DAS 10492729 (1.5°N, 45°W)
13G & H: DAS 7614463 (8.6°N, 50°W)
13I & J: DAS 7326758 (7.3°N, 87°W)
13K & L: DAS 10204674 (6.6°N, 85°W)

Figure 14: Layering in the Intercrater Plains: Memnonia Fossae (24°S, 140°W).

14A: Mariner 9 A-frame (DAS 6966508) showing location of B-frame mosaic.

14B: Mariner 9 B-frame mosaic (DAS 9772004, 9772074, and 9772144) showing possible resistant, dark material outcropping beneath lighter material (ridge at center) and over light material on right (south) side of major graben. Note the sequence of flows and faulting on left side of graben.

14C: Sketch map of area shown in Figure 14B.

Figure 15: Crater Exhumation and the Intercrater Plains: Kasai Vallis (24°N, 61°S).

15A: Top: Mariner 9 A-frame mosaic (DAS 7399738, 7471698) showing location of B-frame mosaic within Kasai channel.
Bottom: Mariner 9 B-frame mosaic (DAS 10277409, 12866208) showing 8-km crater being exhumed from beneath the 3-km cliff of the intra-channel "island". Note preservation of crater. (Illumination in lefthand photo is from left; in righthand photo it is from the right).

15B: Mariner 9 B-frame (DAS 12866208) showing detail of buried crater.

15C: Mariner 9 B-frame (DAS 8945729) showing oblique view of partially buried crater.

Figure 16: Crater Exhumation and the Intercrater Plains: Shalbatana Vallis (7°N, 40°W).

Top: Mariner 9 A-frame (DAS 7614988) showing location of high-resolution B-frame within Shalbatana channel. Bottom: Mariner 9 B-frame (DAS 10492799) showing a crater-like form about 4 km in diameter being exhumed from beneath the layered wall of the Shalbatana channel (a). Sharp and Malin (1975) expressed concern in interpreting this channel as fluvial, because of the small source to channel volume ratio. This concern seems justified, since fluvial erosion would have probably destroyed the crater.

Figure 17: Elevation Profiles of the Valles Marineris. Ultraviolet spectrometer altitude profile for the Valles Marineris are shown here with ground tracks plotted on a photomosaic of the chasms. Note particularly in the eastern portion of the Valles Marineris that the depth of formation does not appear to exceed the zero kilometer elevation level and that the depth increases at roughly the same rate that the surface elevation increases. Only in the western portion of the Valles does the elevation increase become greater than the increasing depth. Wherever the canyon depth reaches about 0 km, the floor appears dark. In the east this is seen in many places, but as the floor elevation increases, only patches are seen of the low albedo material. It is possible that a dark base material underlies the material into which the Valles Marineris developed.

Figure 18: Map of 0 to -1 km Elevation Zone.

This map shows the 0 to -1 km elevation zone determined from radar radio occultation, UVS and photogrammetry. Note that except in regions of volcanic activity (Tharsis and Elysium, denoted VU) the erosional zone (ET) between the cratered terrain/intercrater plain and smooth plains follows this contour interval. The speculation presented here is that the 0 to -1 km contour zone signifies the presence of a discontinuity in the structure of the martian lithosphere. Although this discontinuity may be environmentally controlled (e.g., presence of a phase change of water from solid to liquid), the emergence of a cratered surface from beneath the intercrater plain at roughly this elevation suggests that the discontinuity is a real surface having important stratigraphic relation.

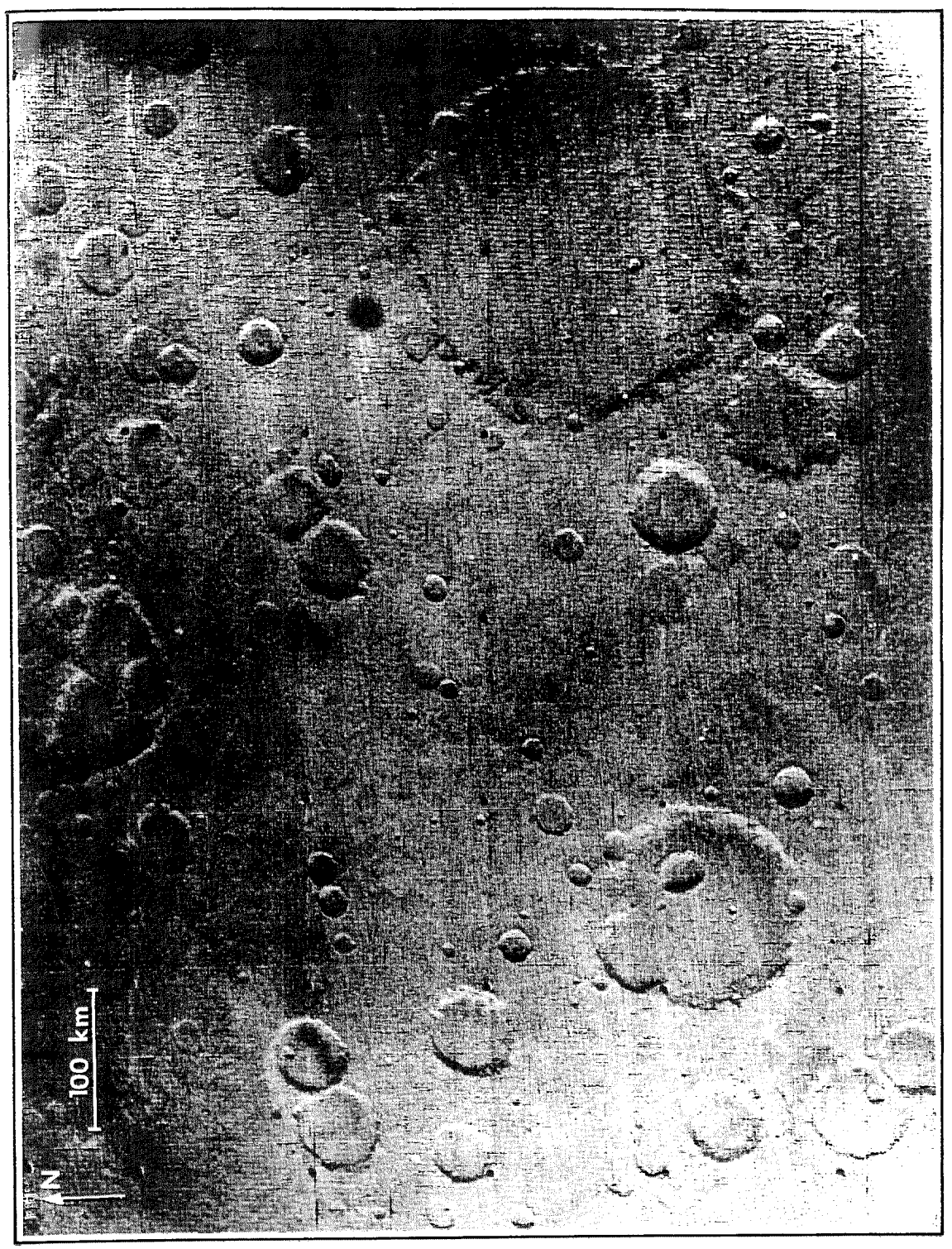

Figure 1

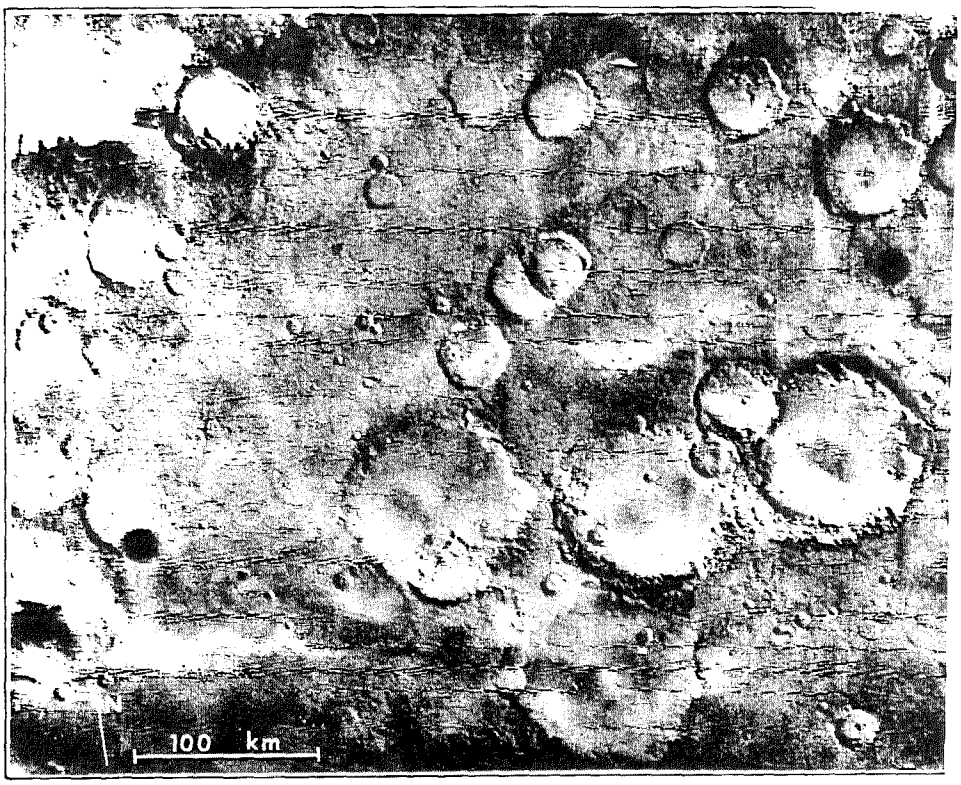

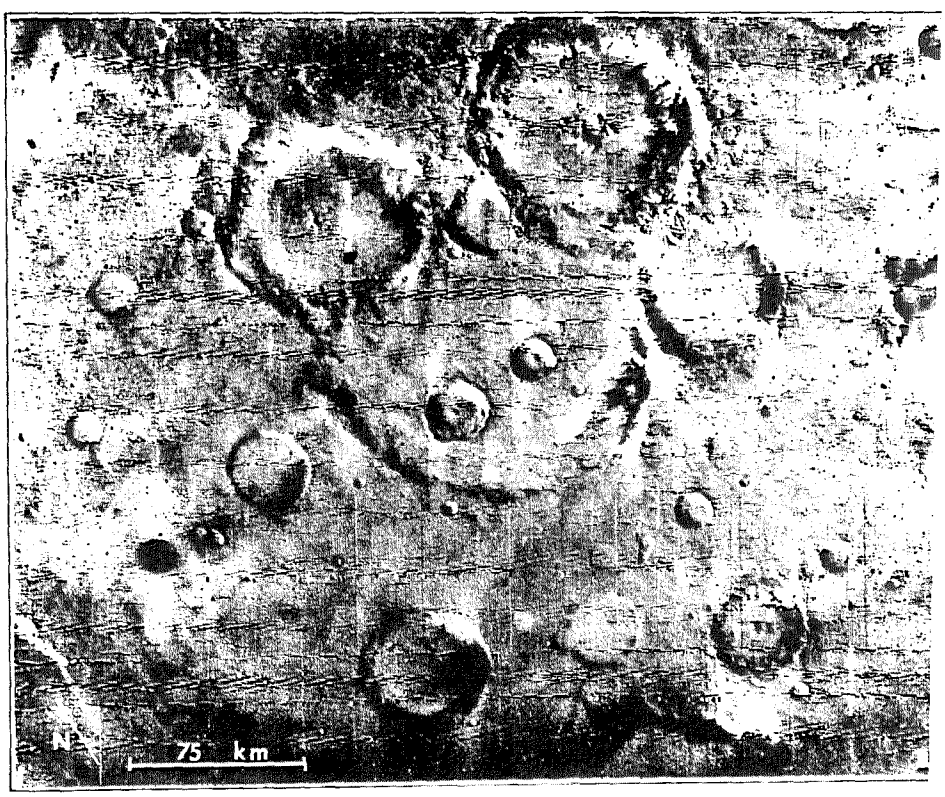

Figure 2A

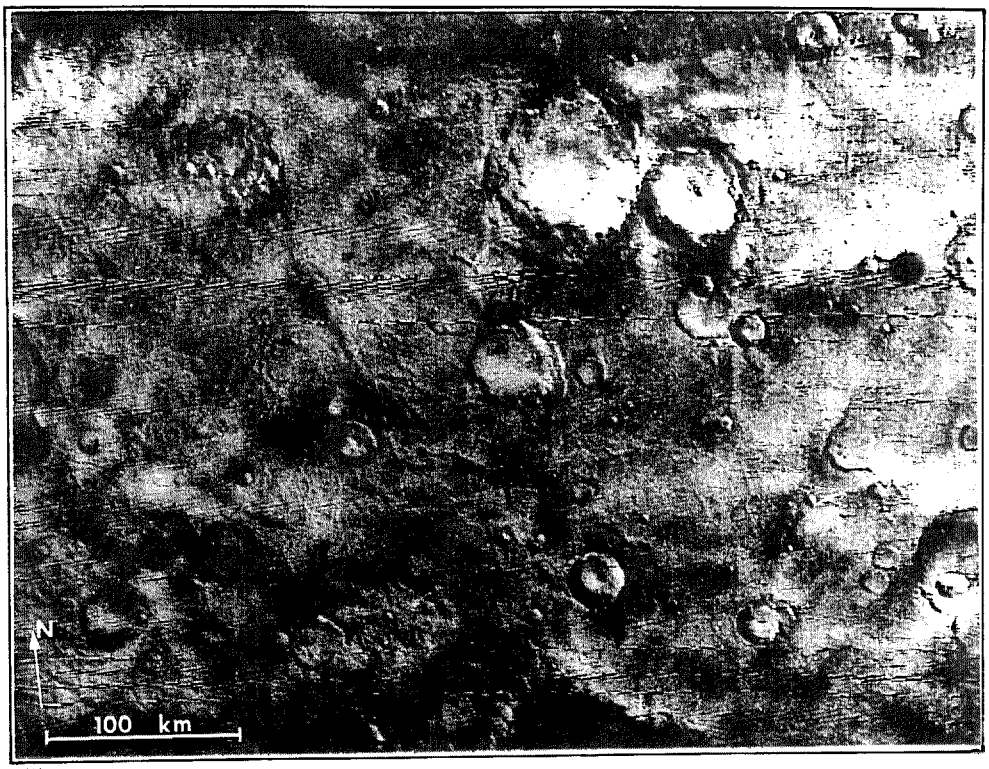

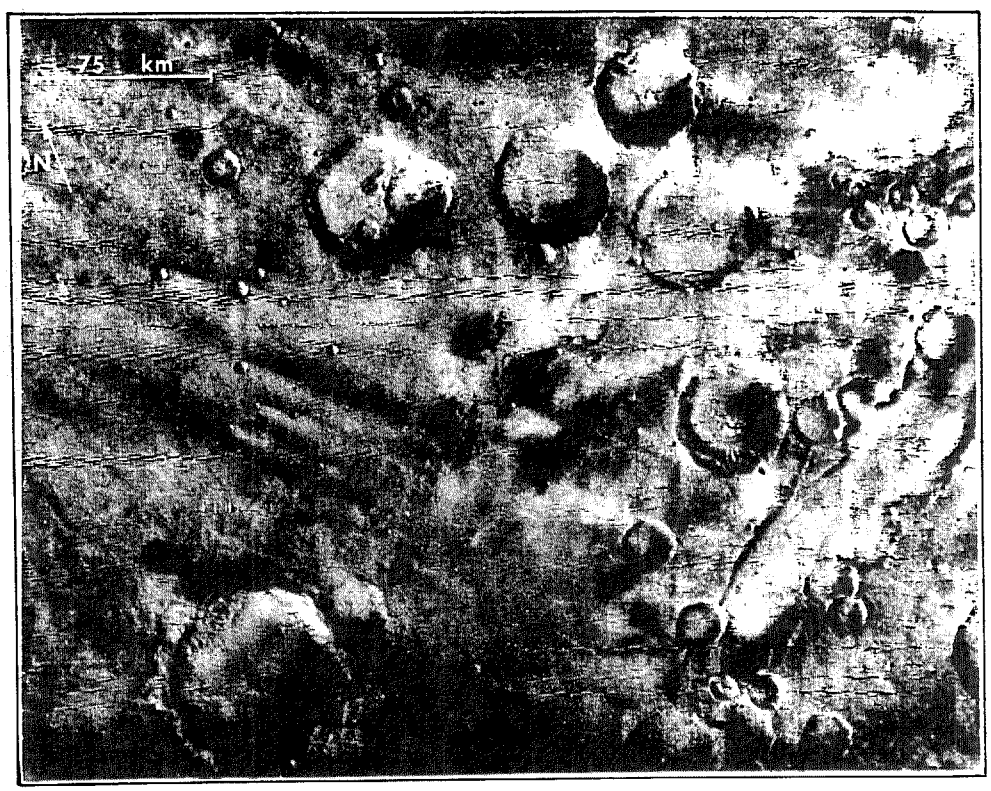

Figure 2B

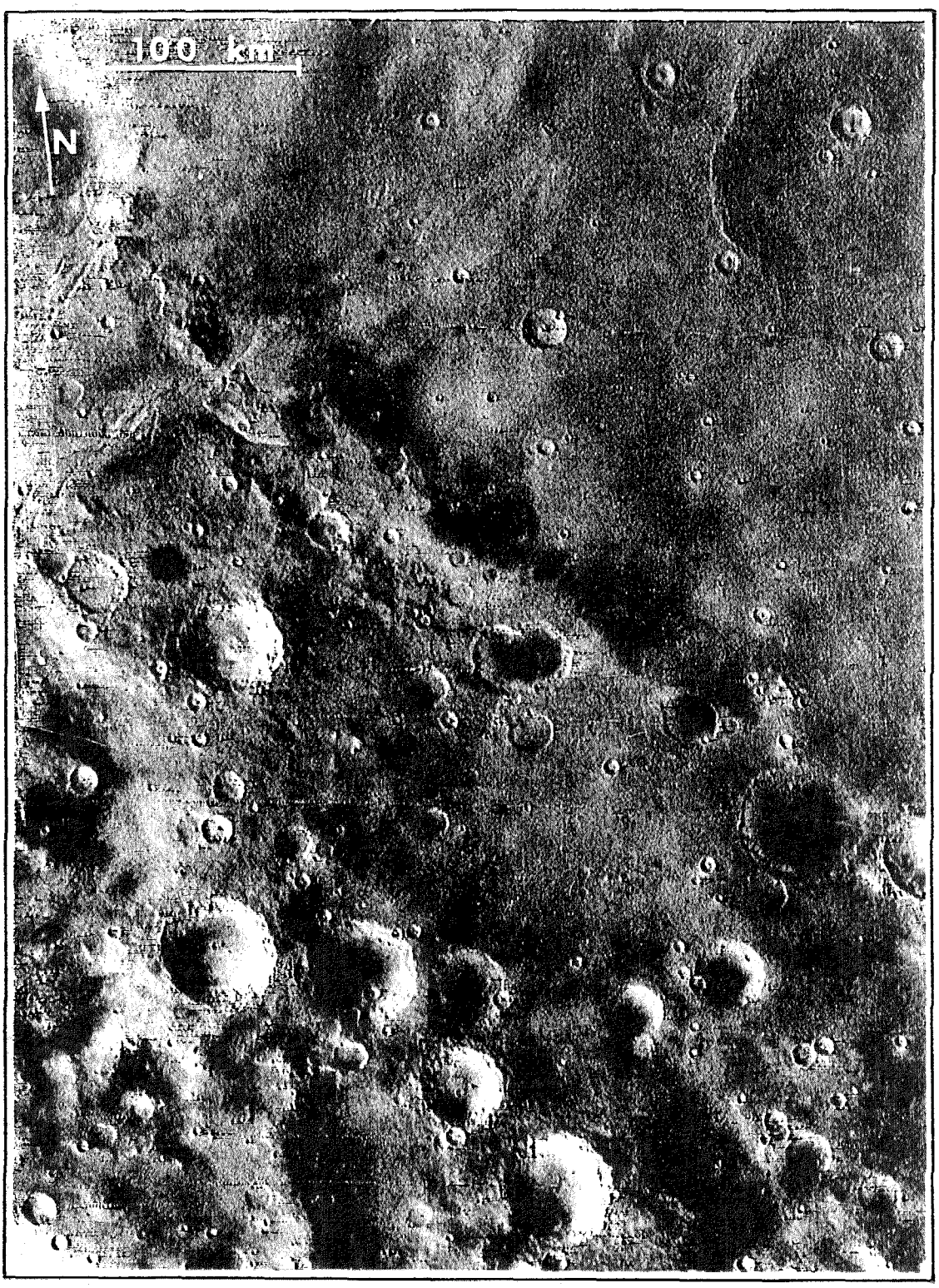

Figure 3A

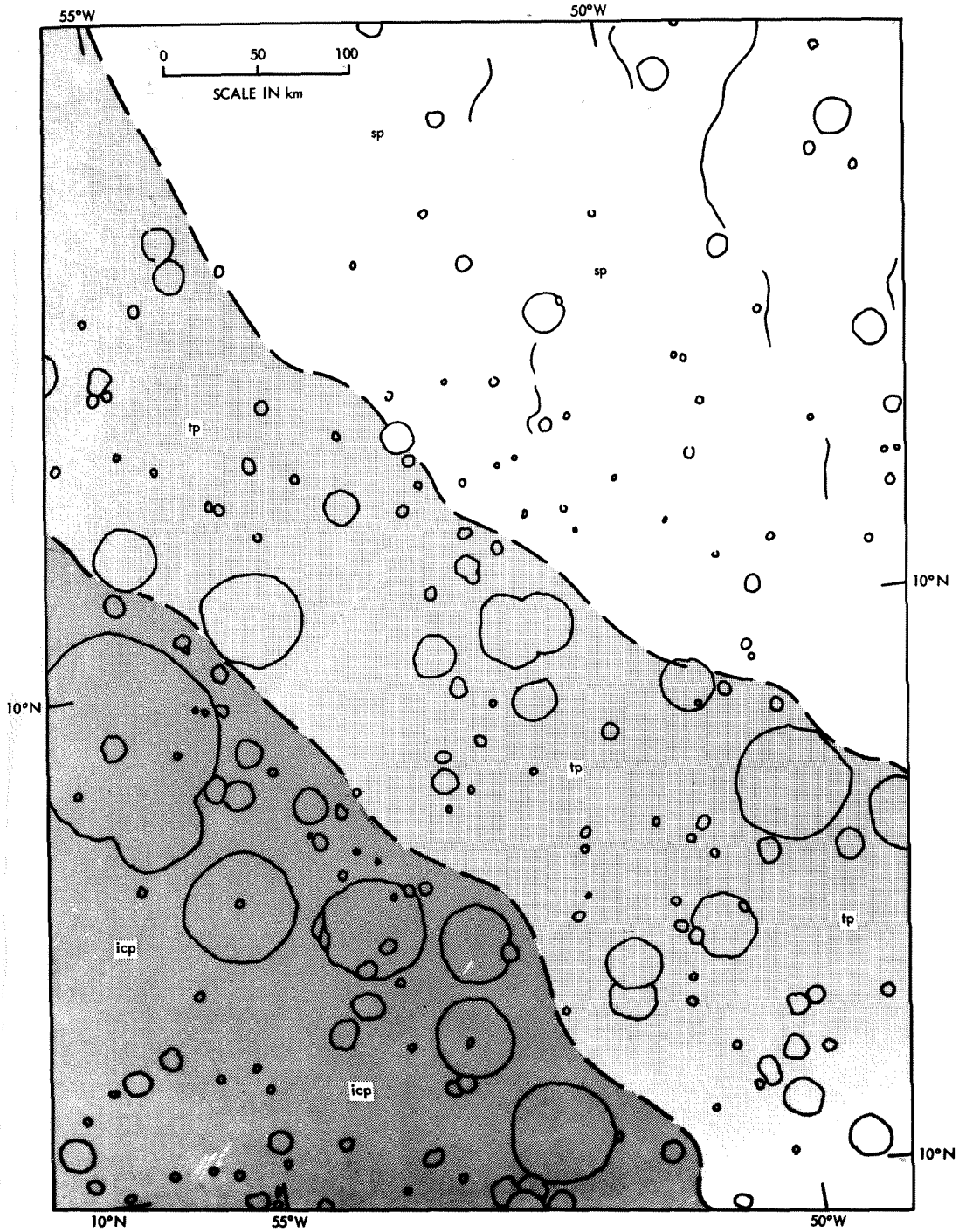
55°W
50°W
0
50
100
SCALE IN km
sp
sp
tp
10°N
10°N
tp
tp
icp
icp
10°N
10°N
55°W
50°W

Figure 3B

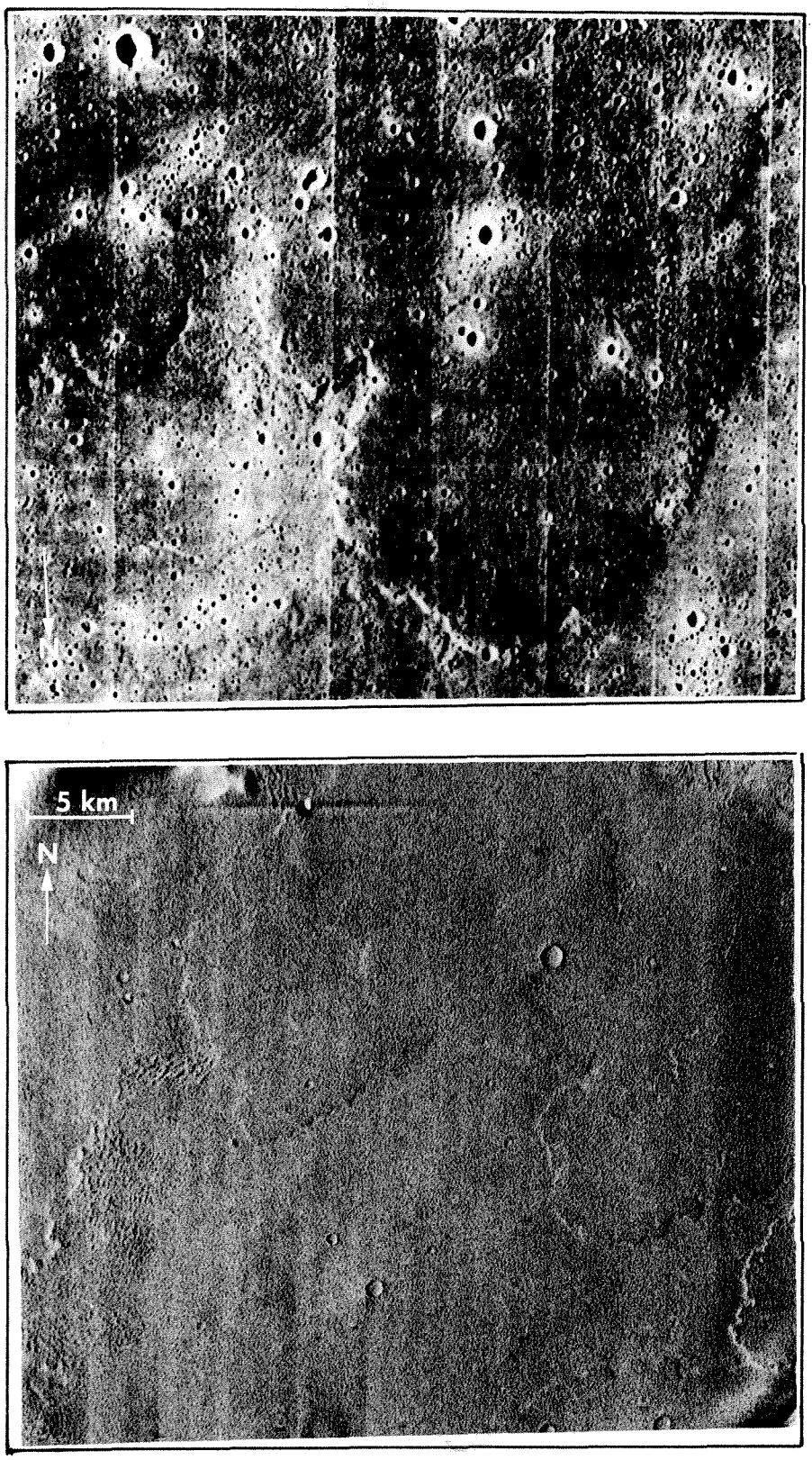

Figure 4

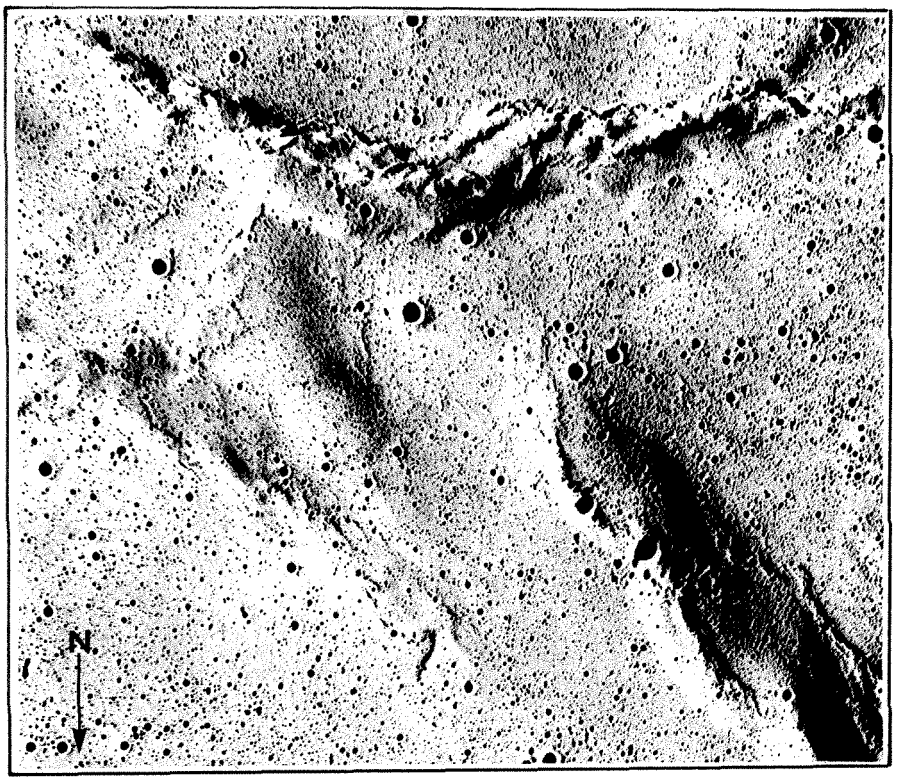

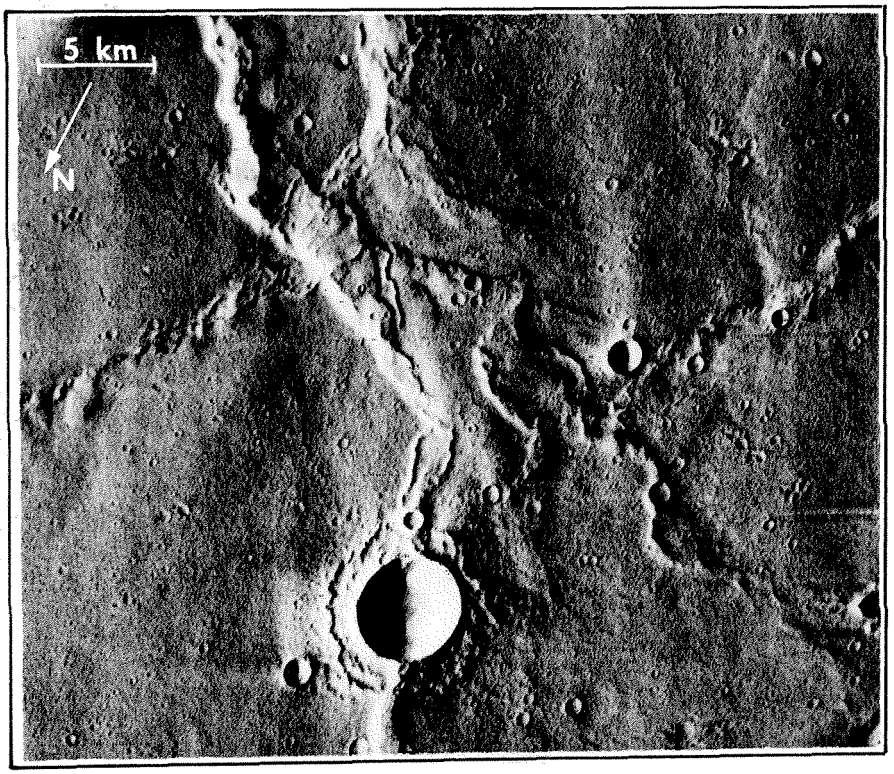

Figure 5(I)

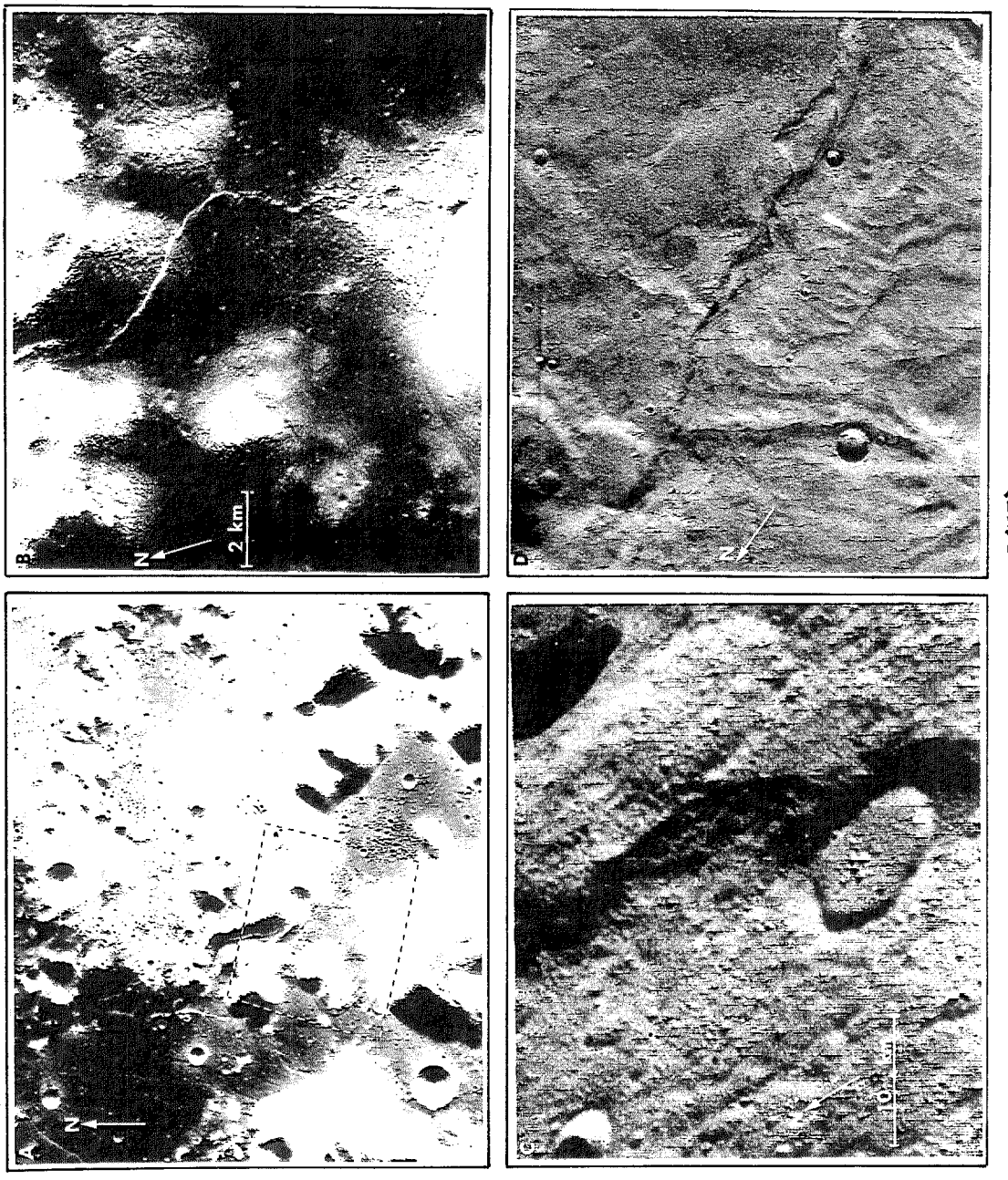

Figure 5(II)

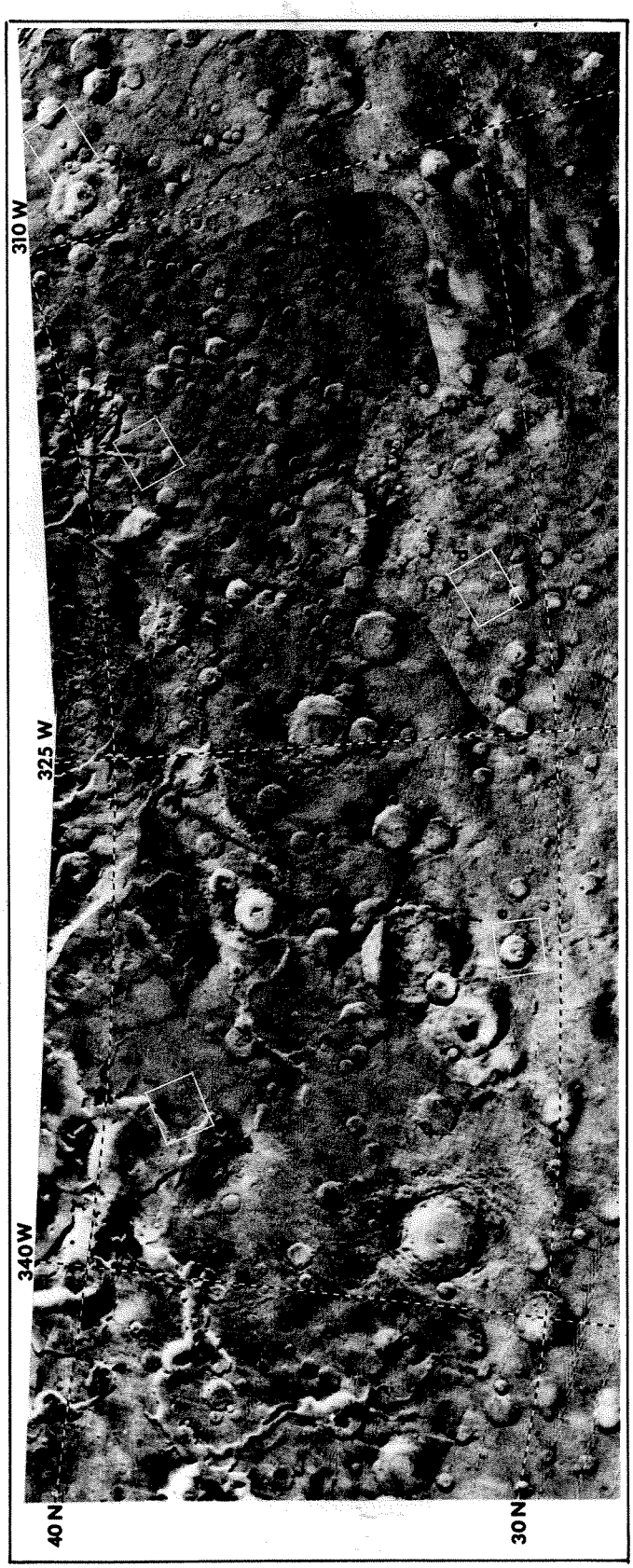

Figure 6A

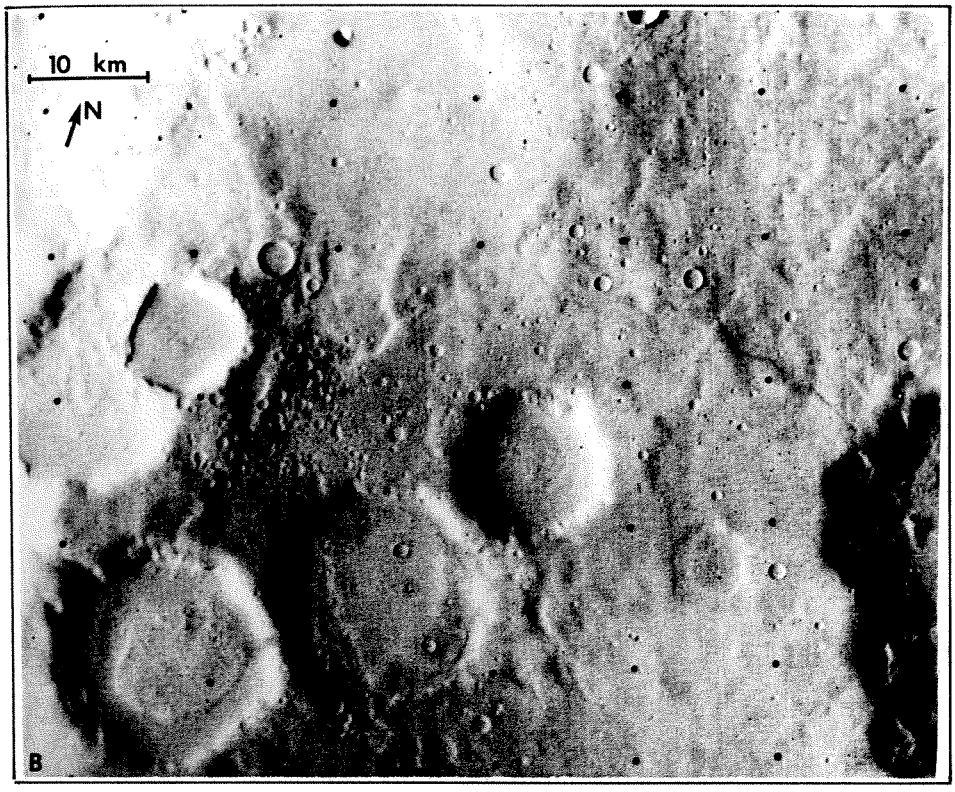

Figure 6B

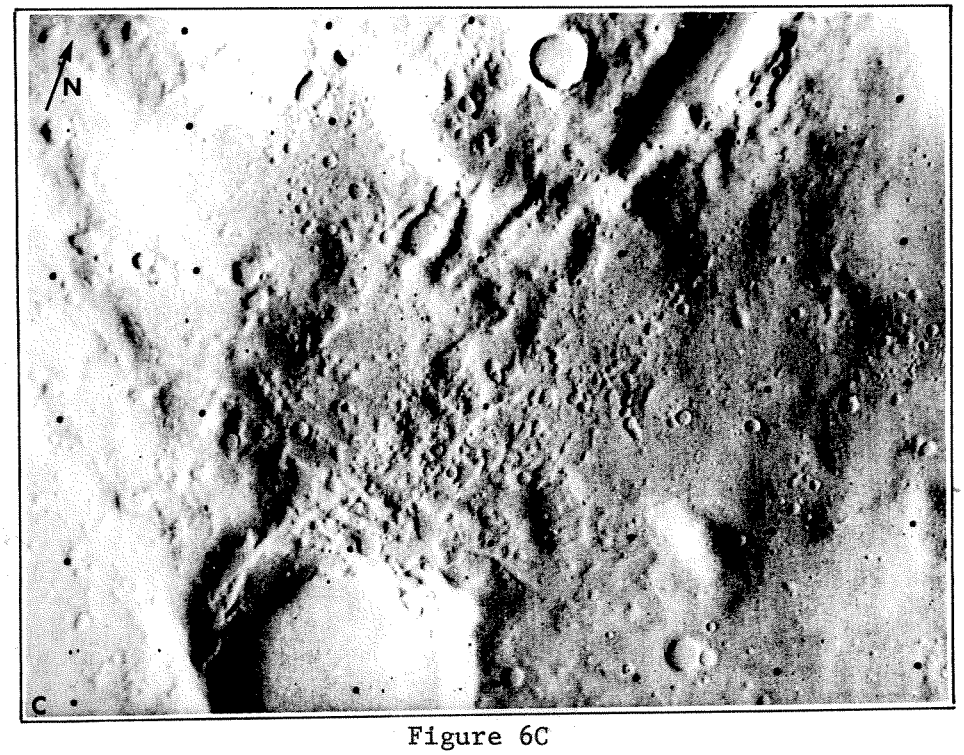

Figure 6C

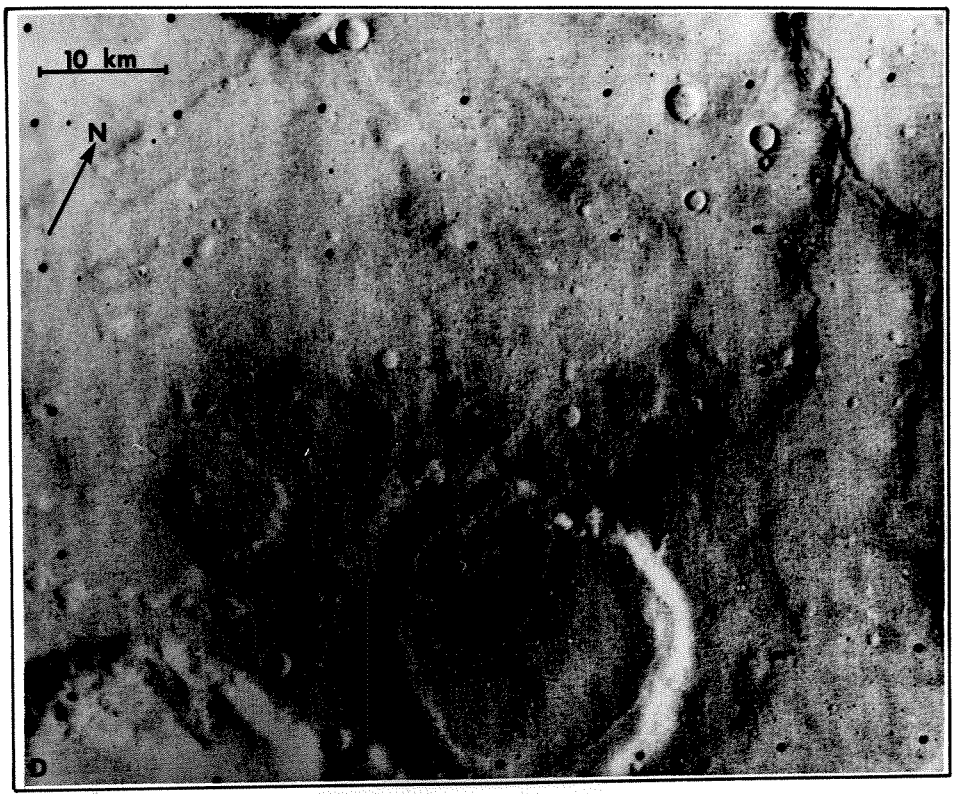

Figure 6D

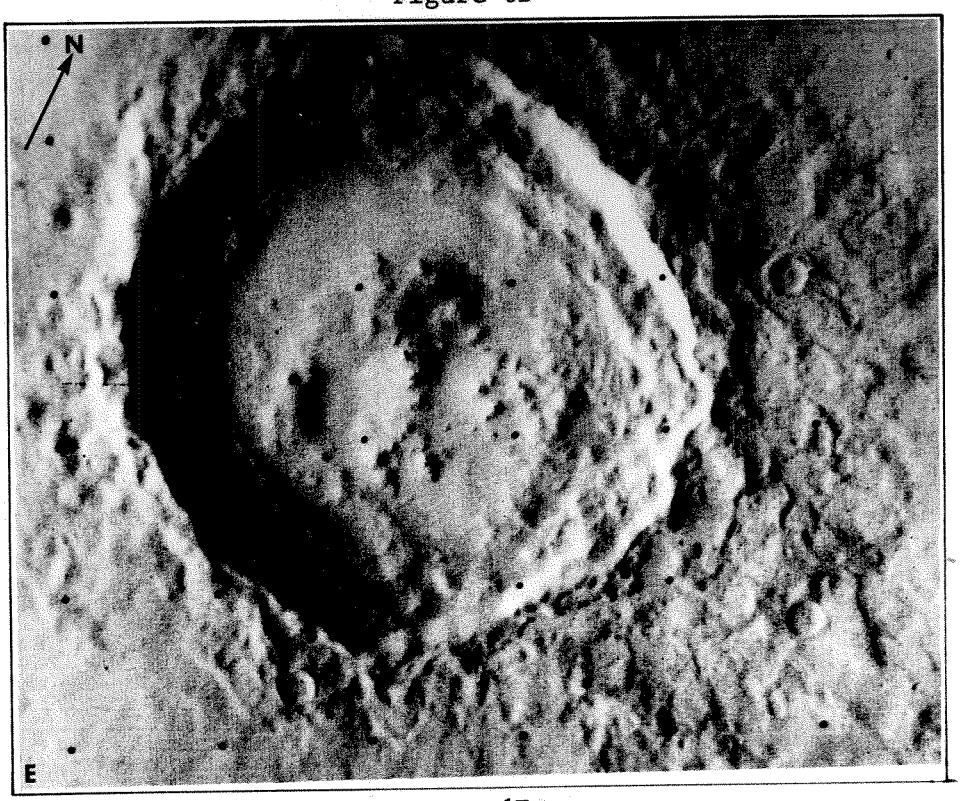

Figure 6E

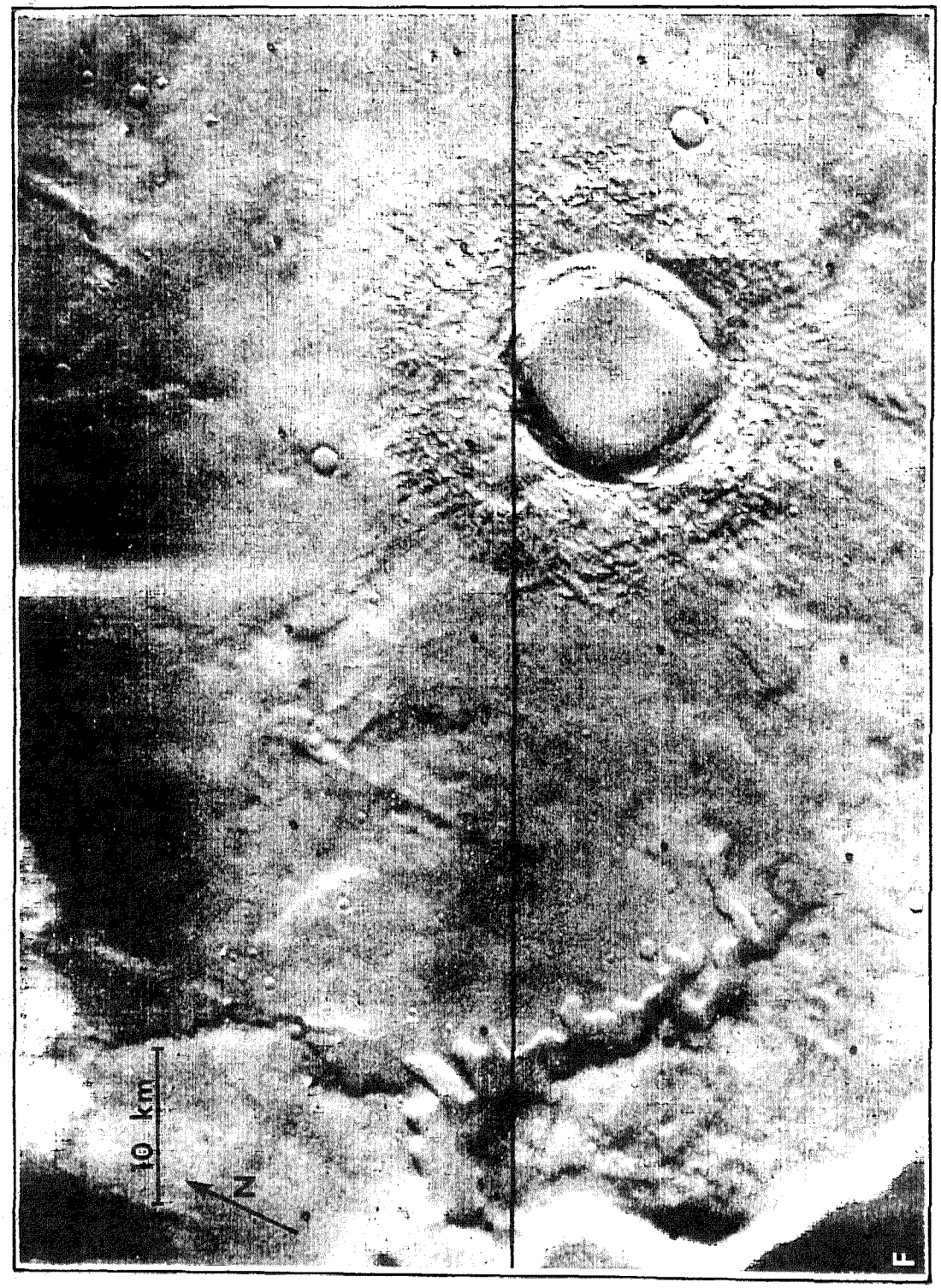

Figure 6F

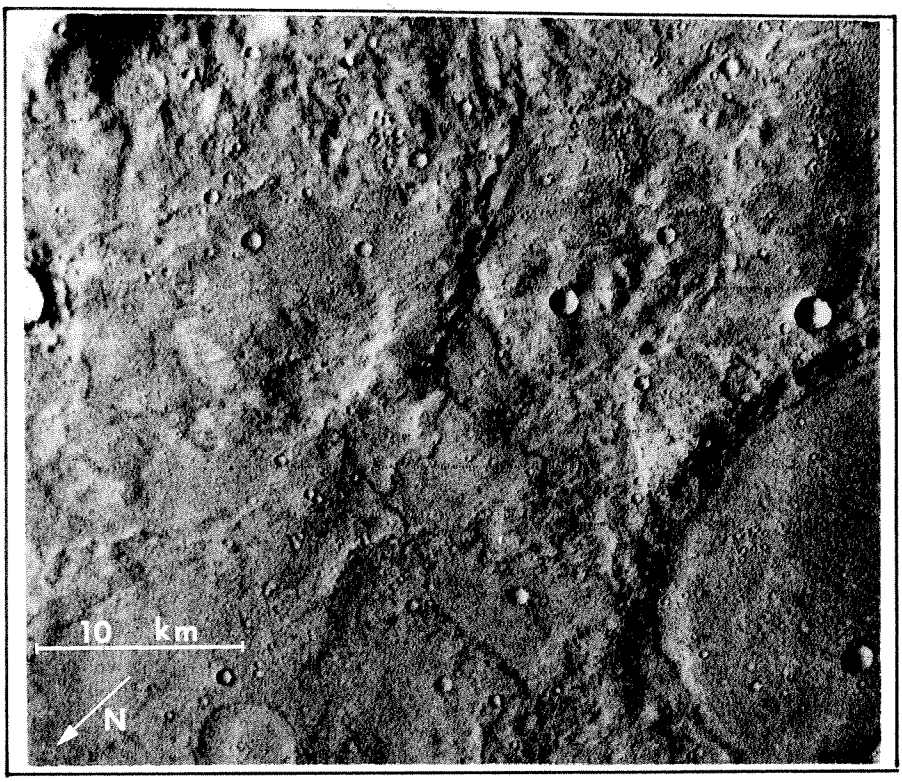

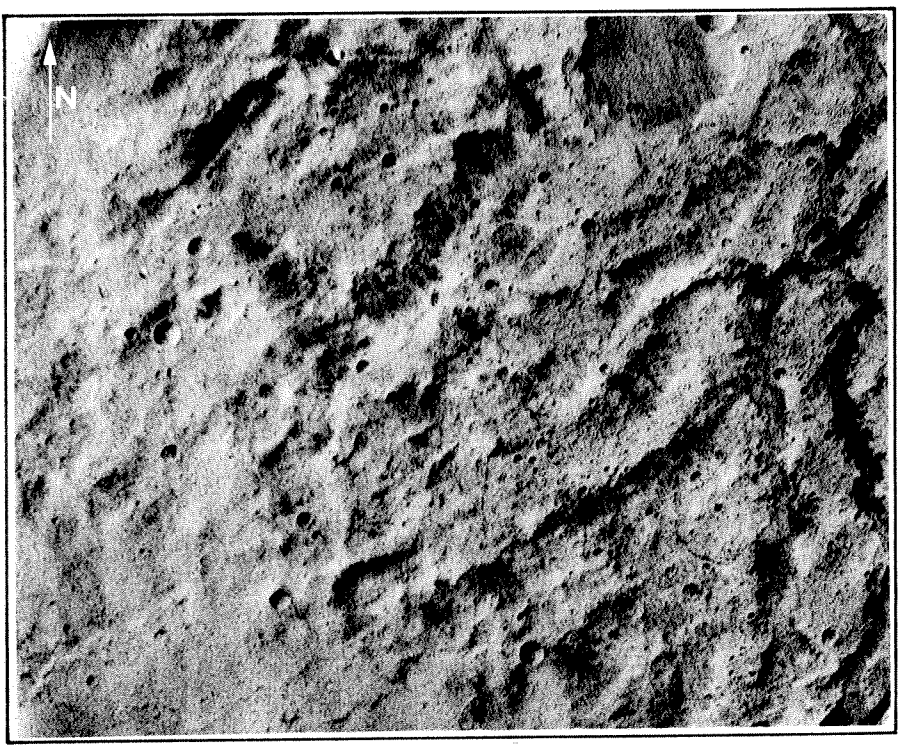

Figure 7

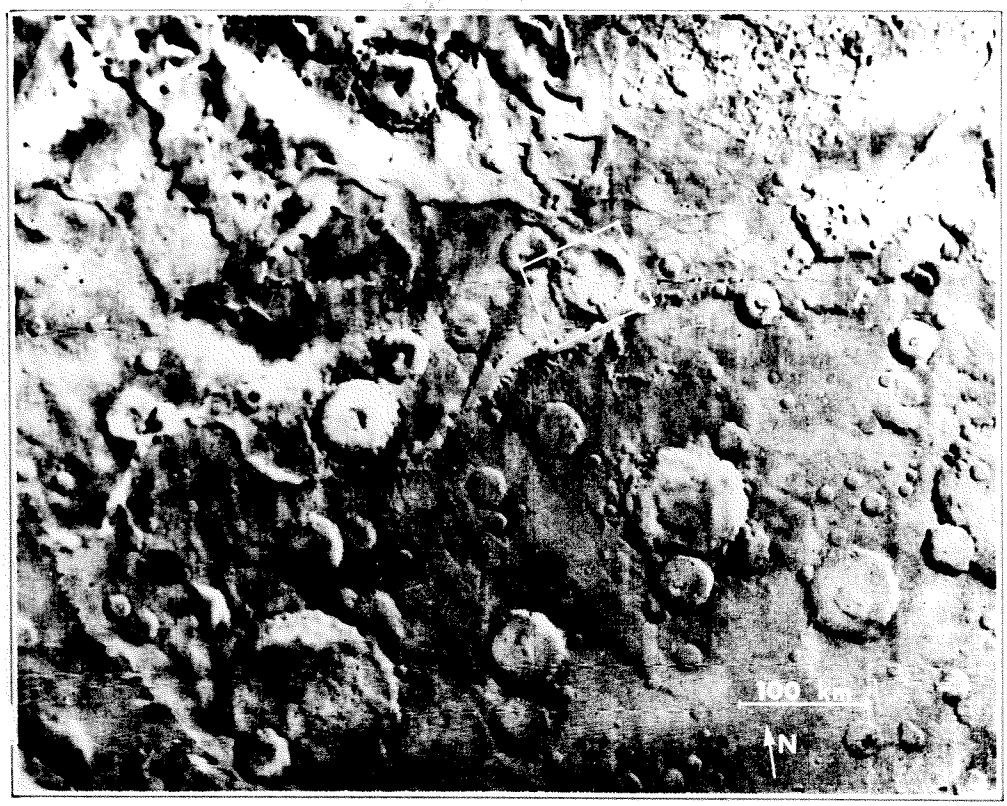

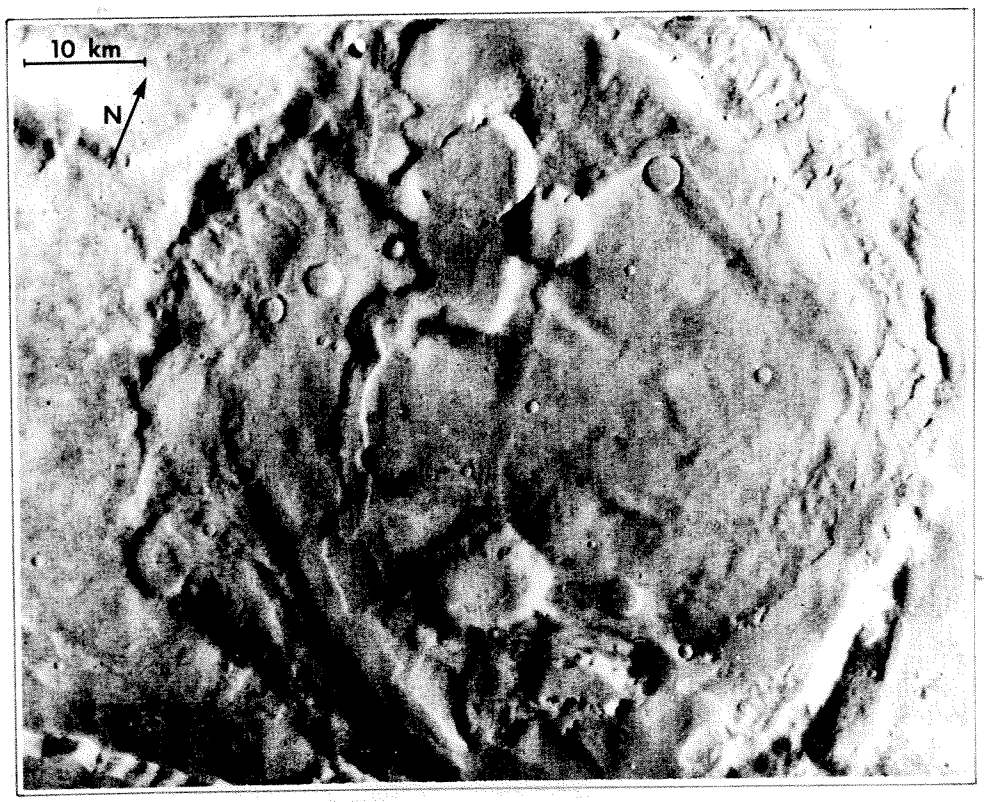

Figure 8

Figure 9A

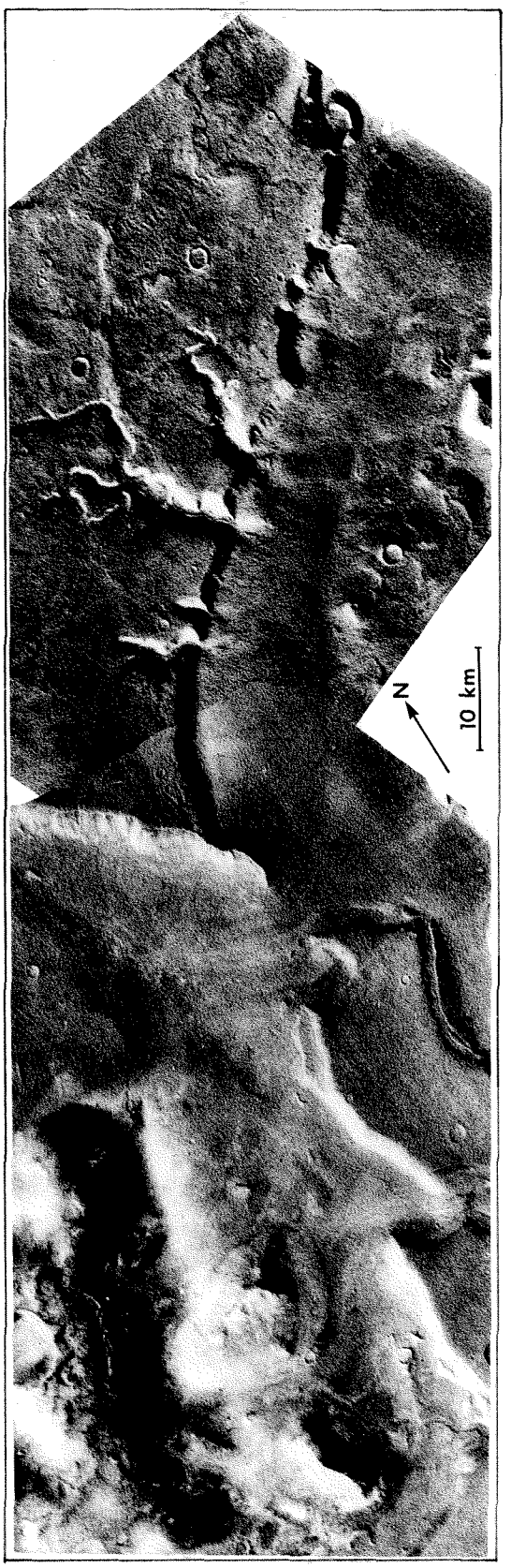

Figure 9B

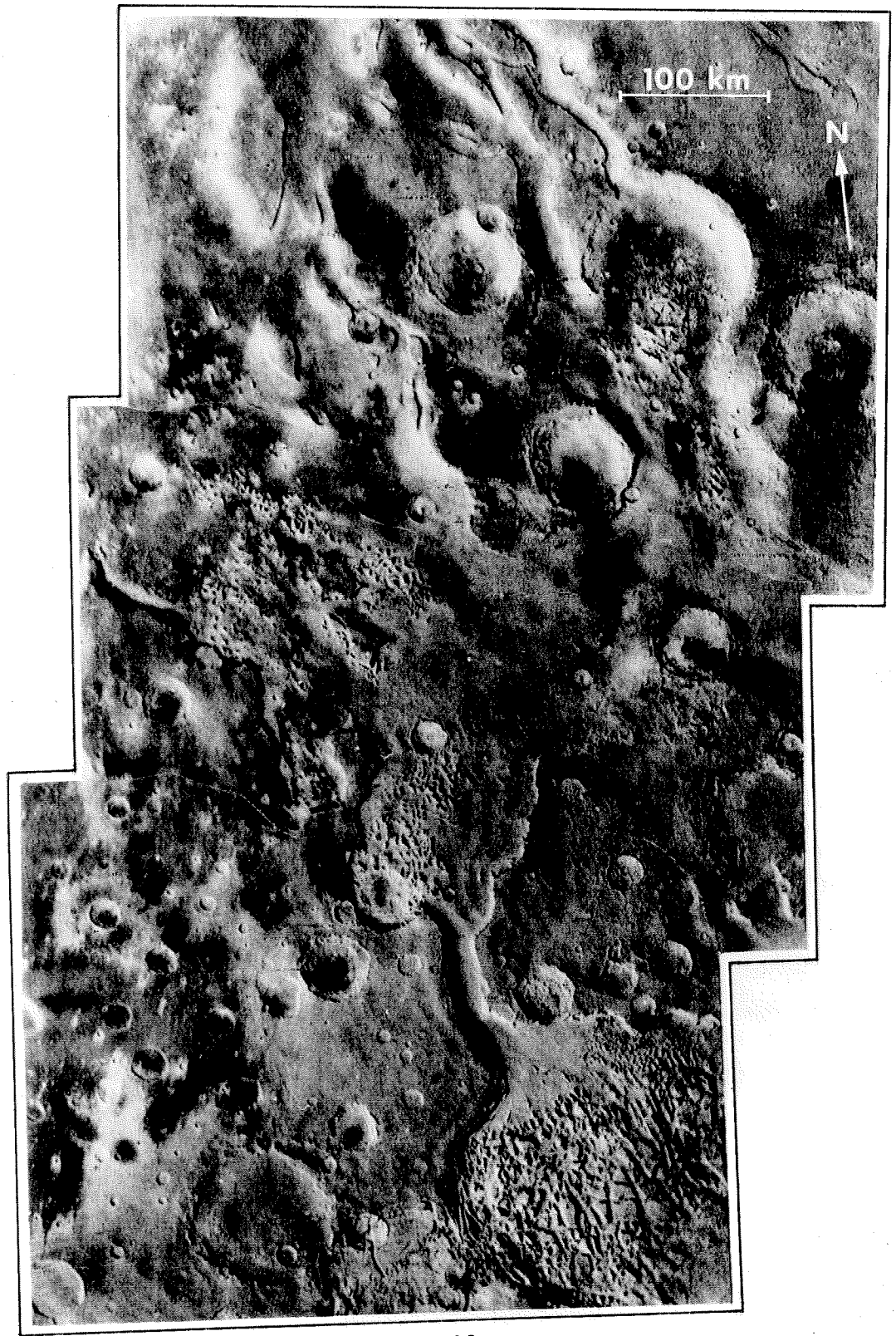

Figure 10

Figure 11A

Figure 11B

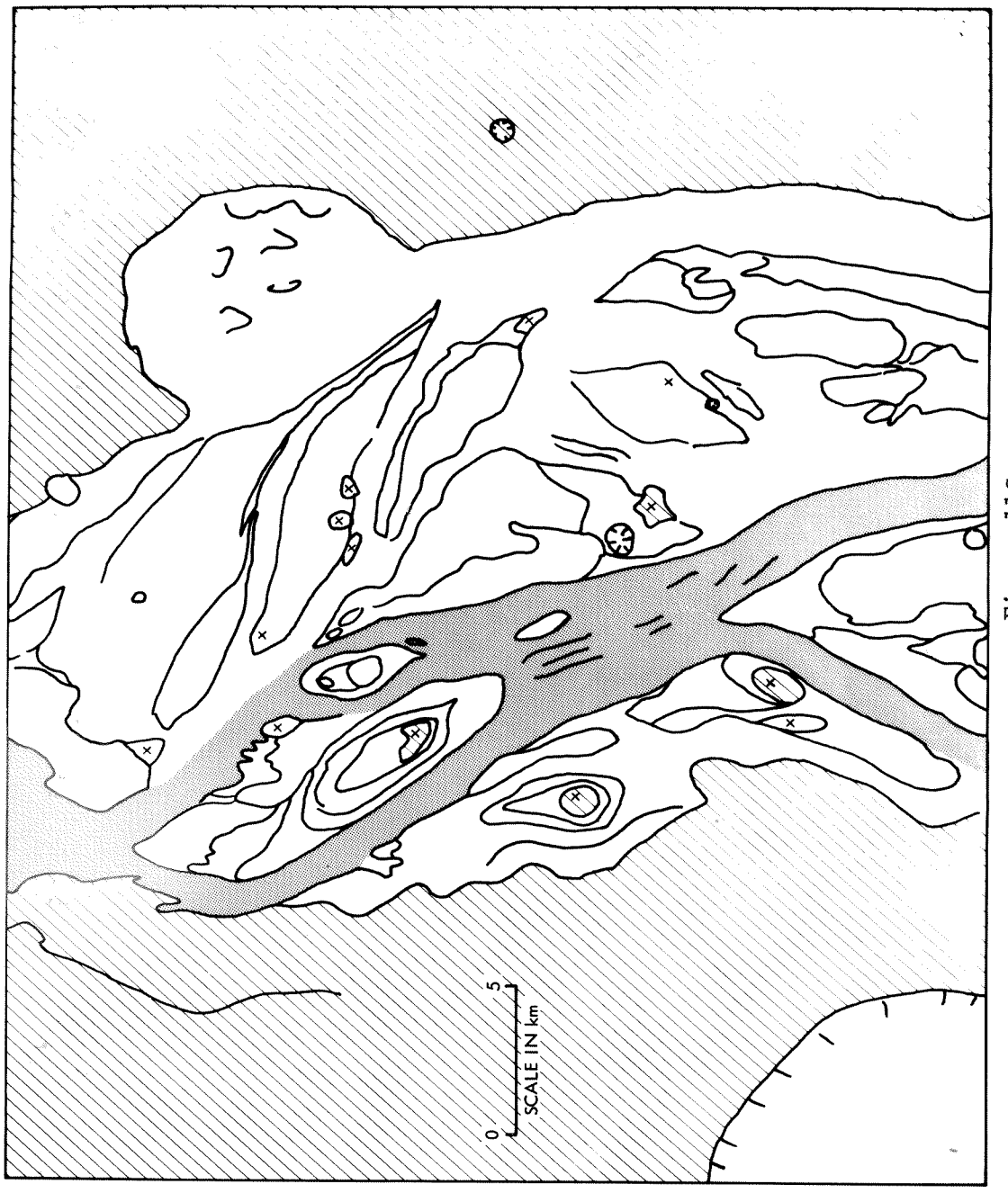

Figure 11C

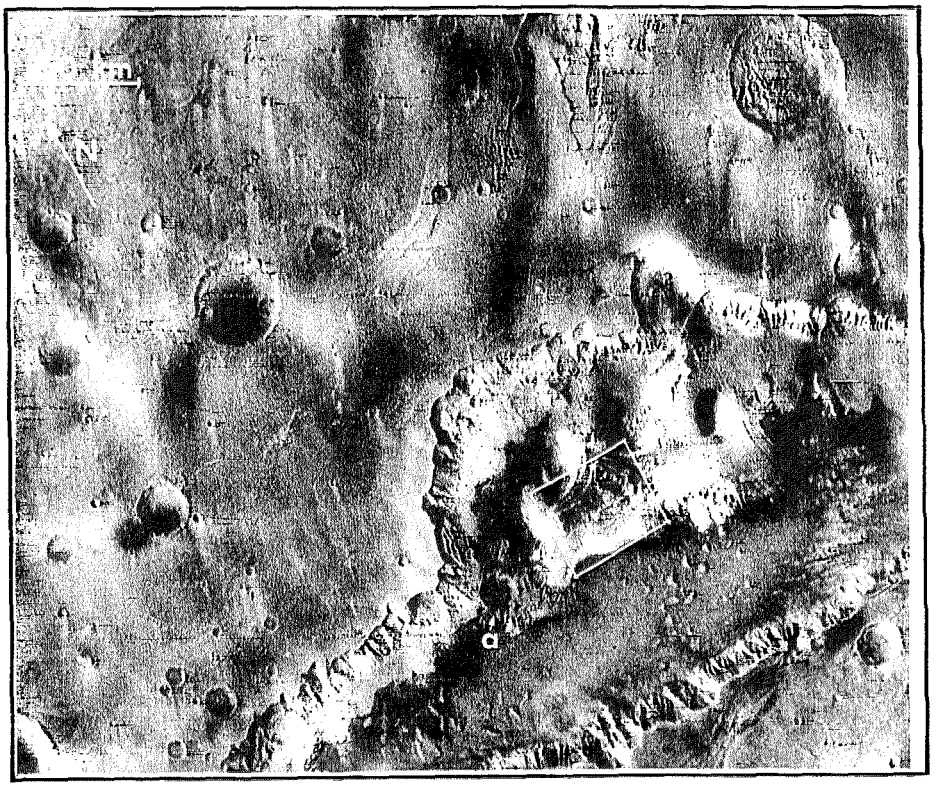

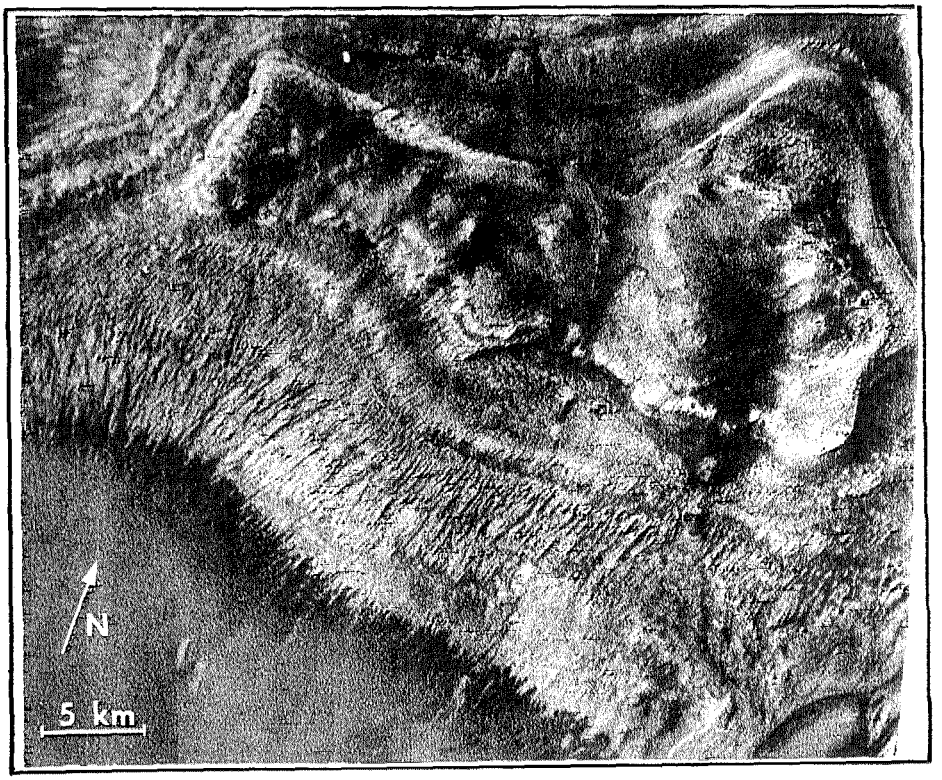

Figure 12

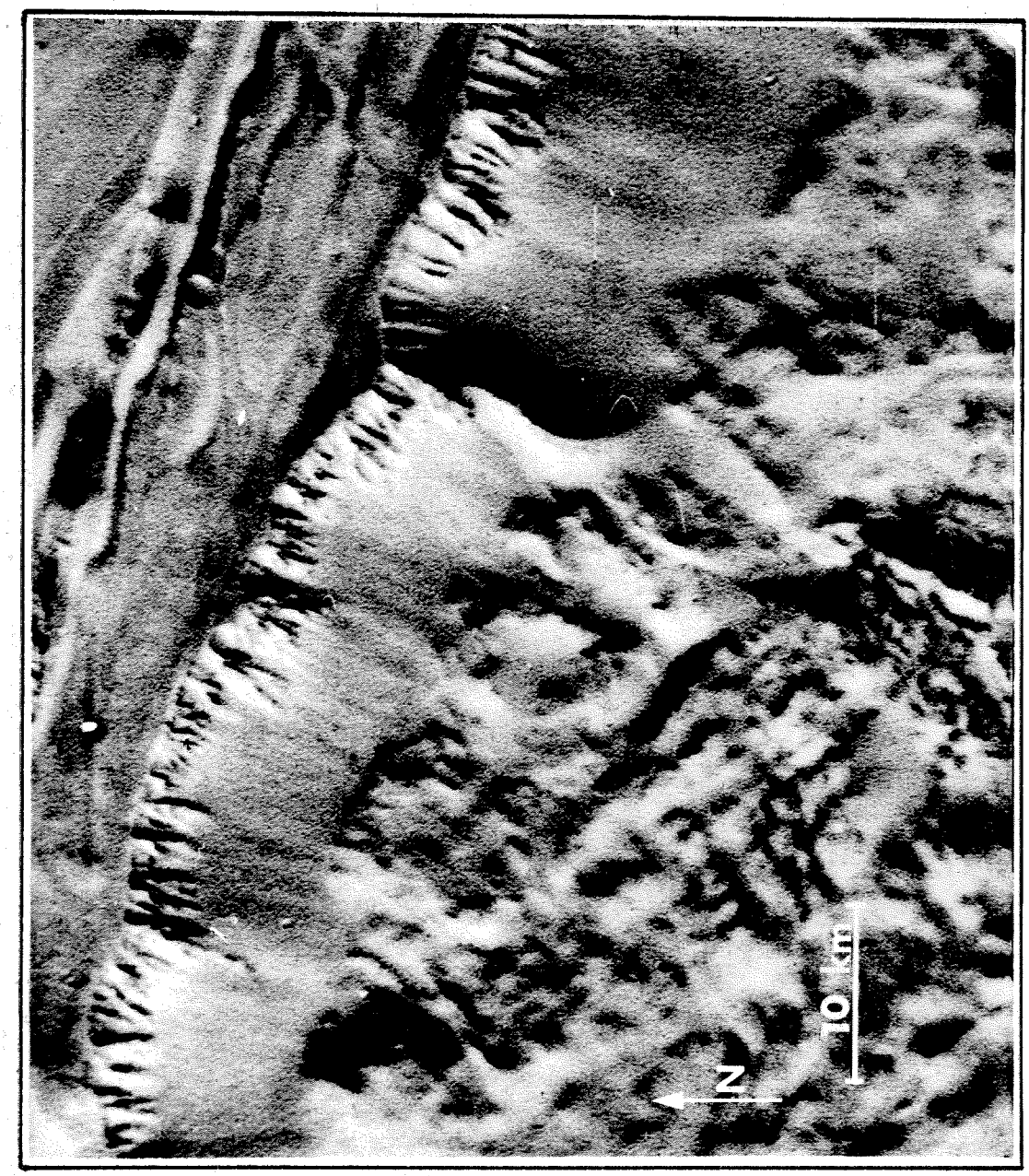

Figure 13A

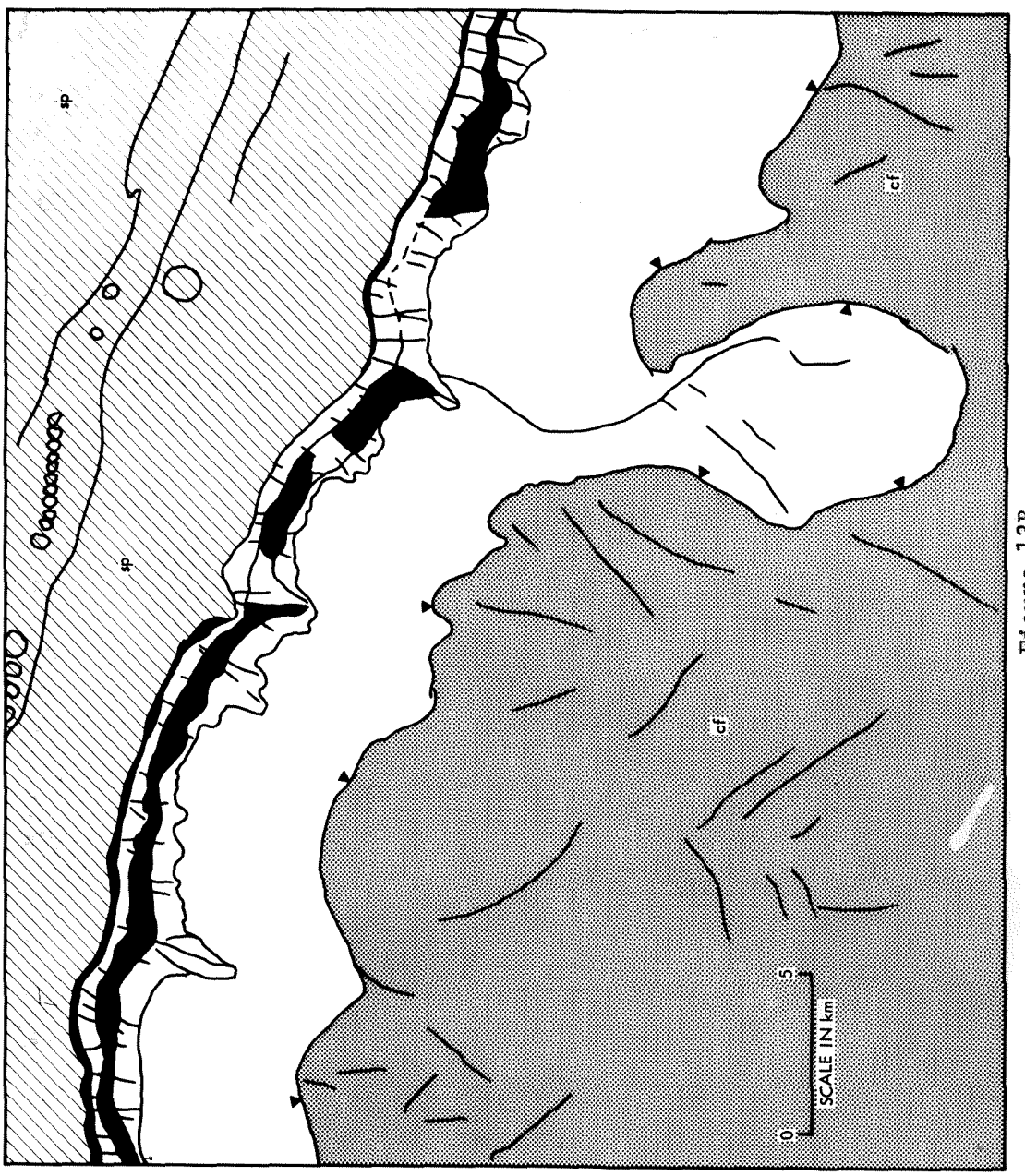

Figure 13B

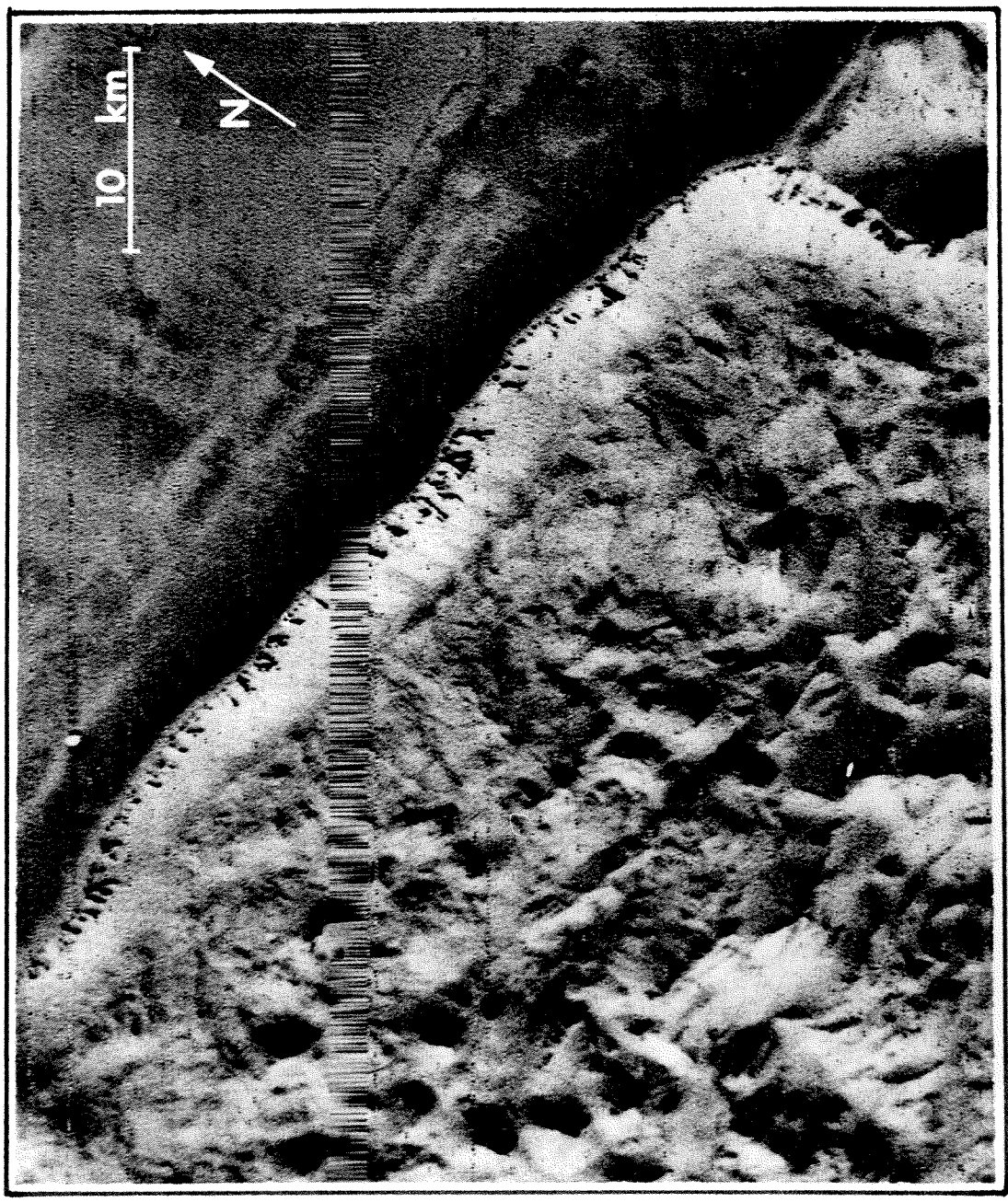

Figure 13C

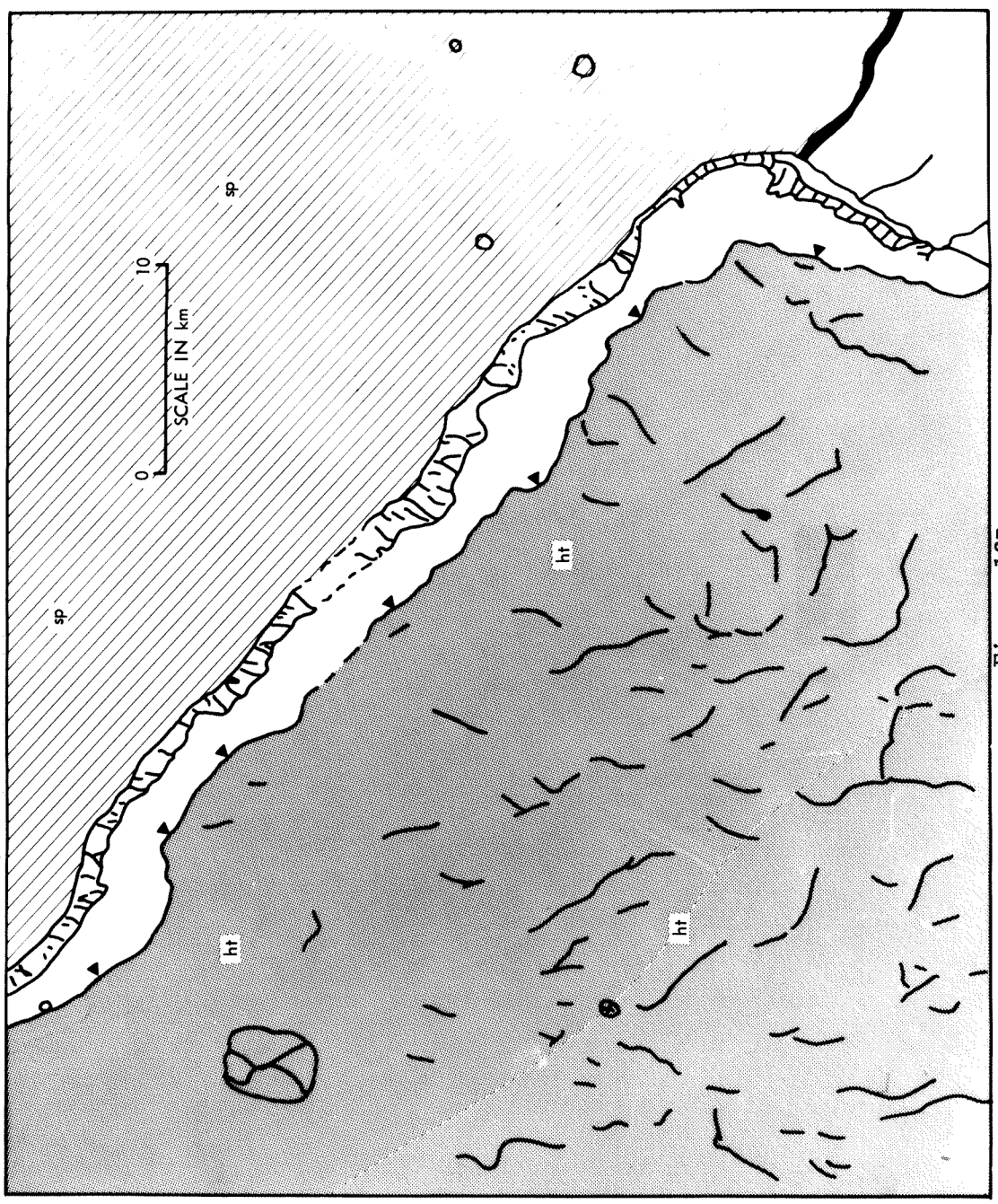

Figure 13D

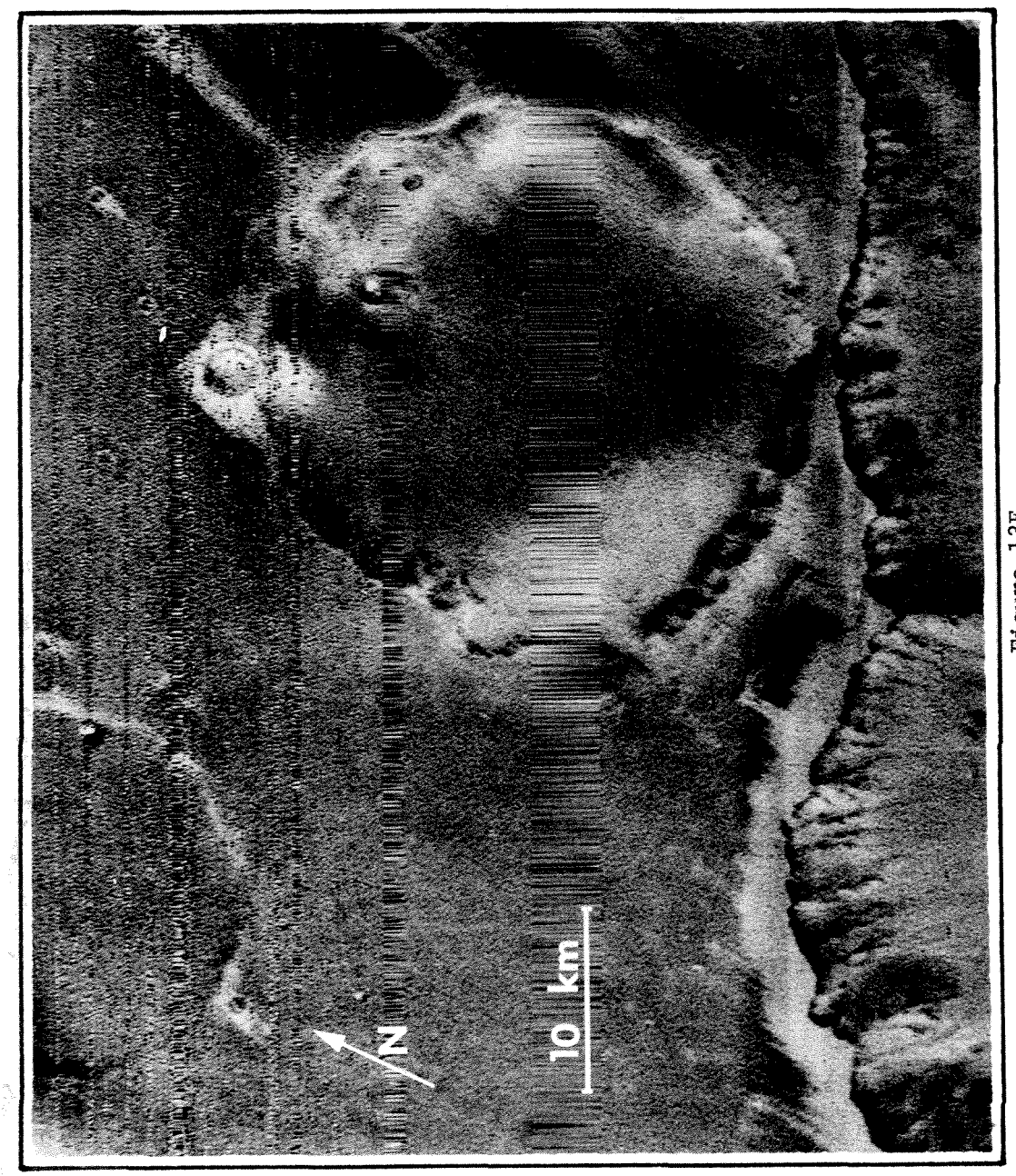

Figure 13E

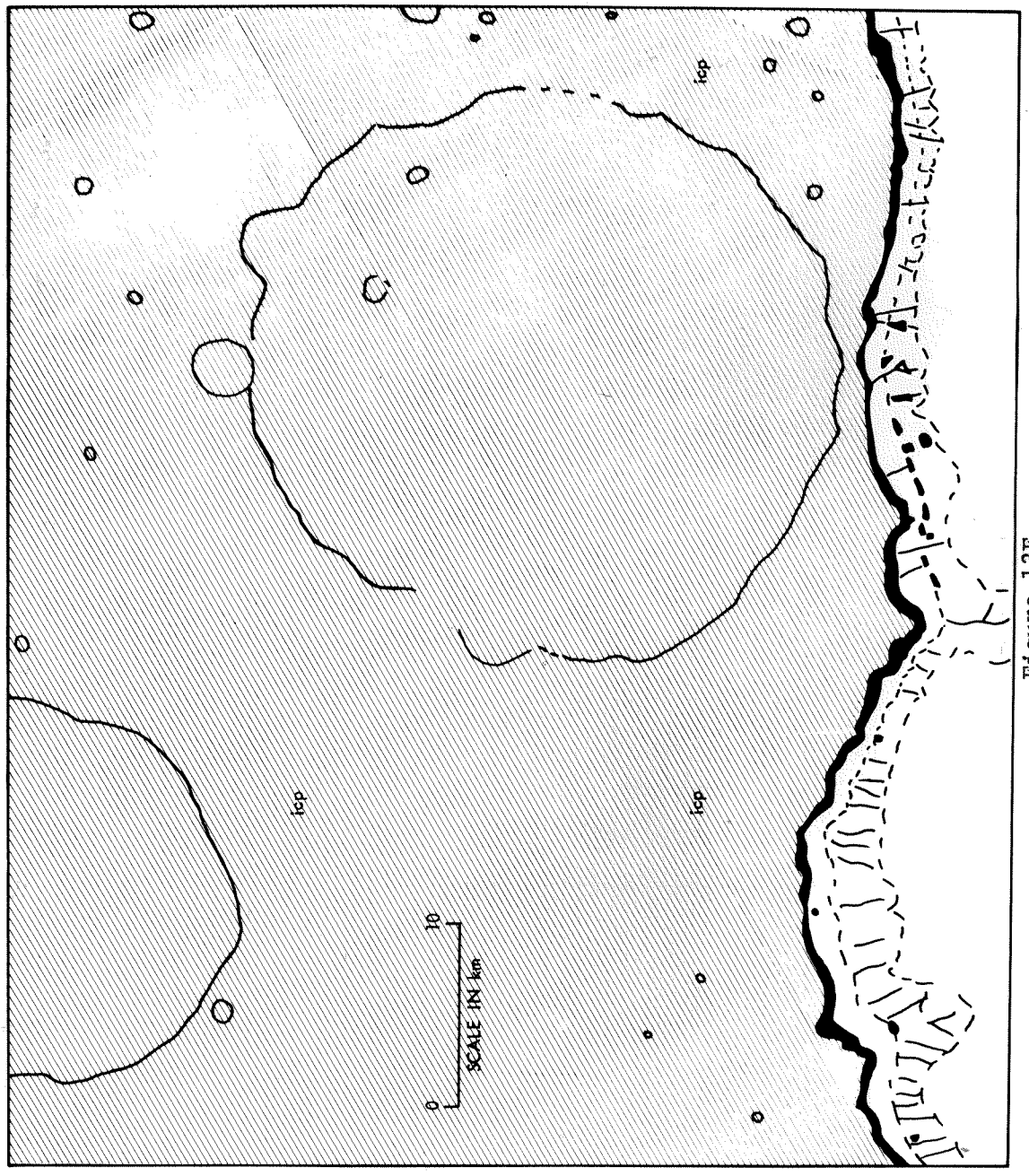

Figure 13F

Figure 13G

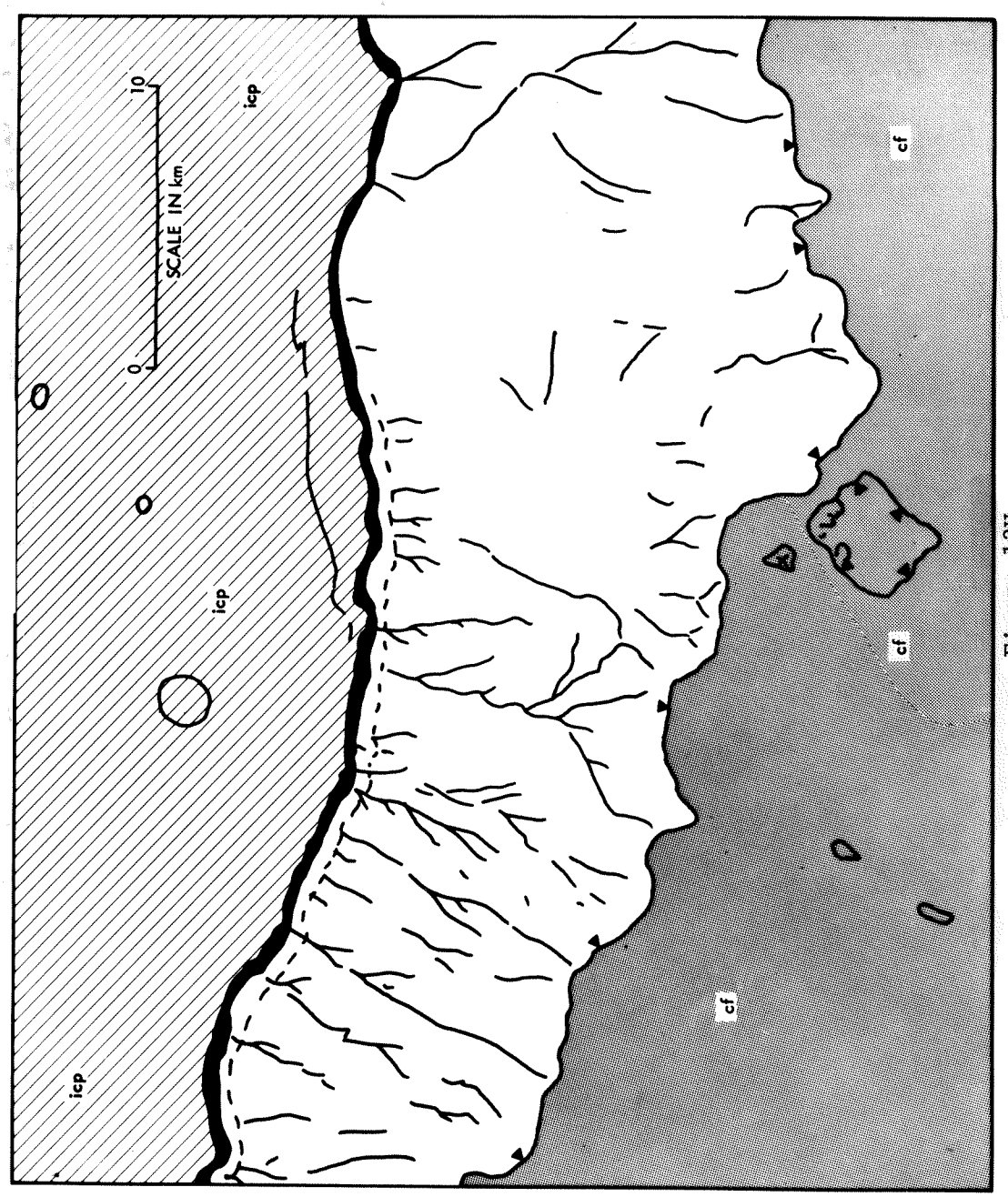

Figure 13H

Figure 13I

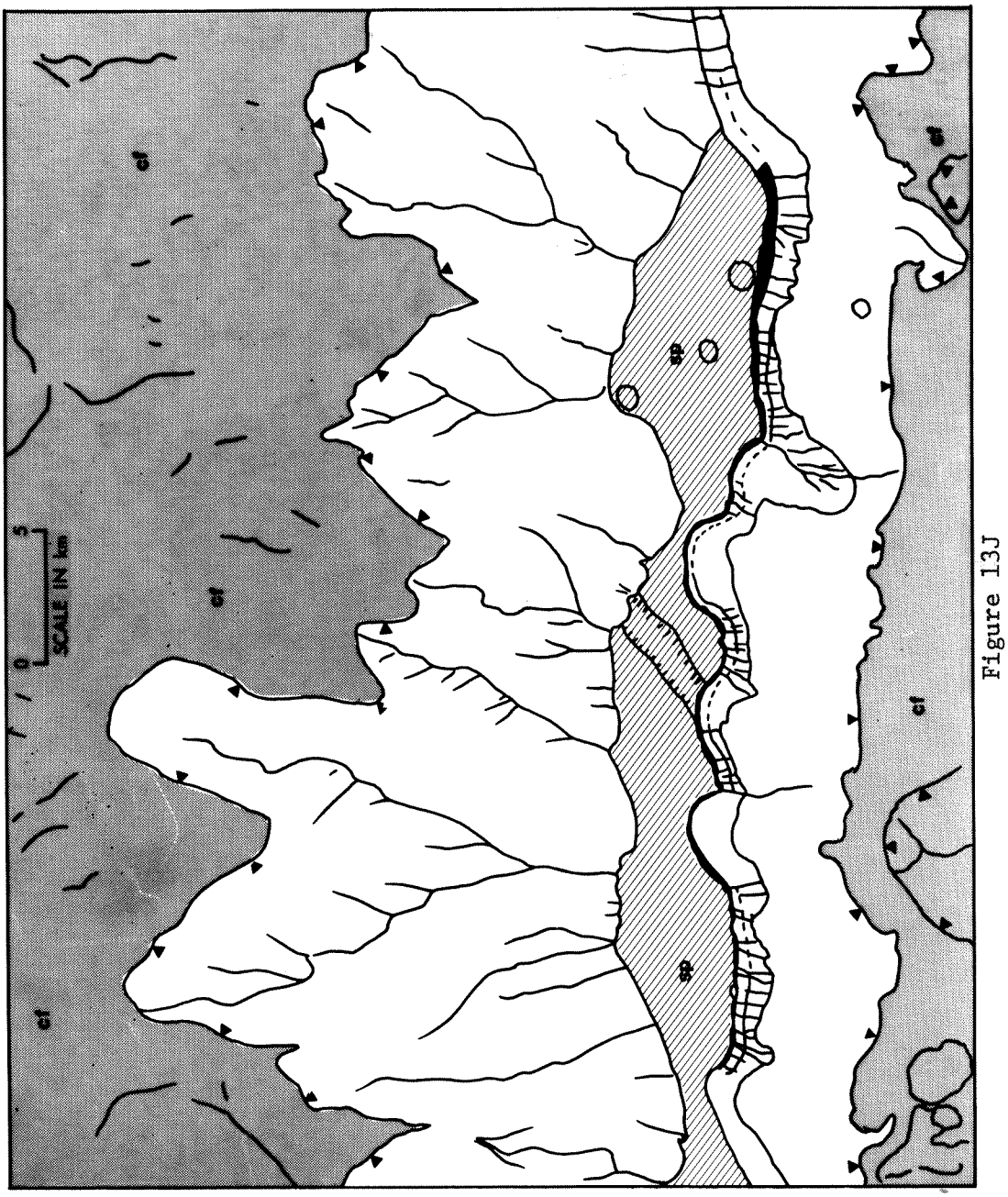

Figure 13J

Figure 13K

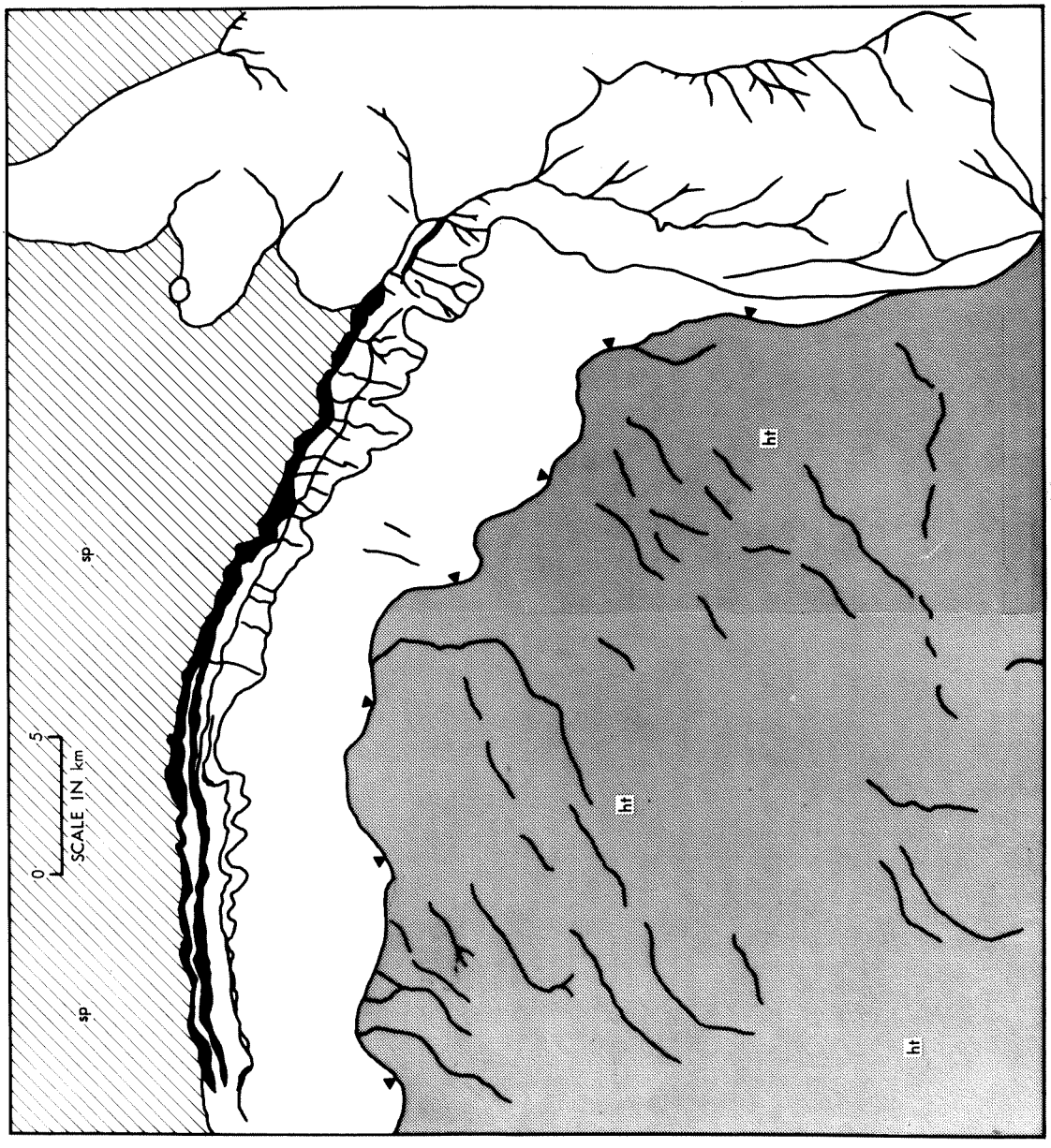

Figure 13L

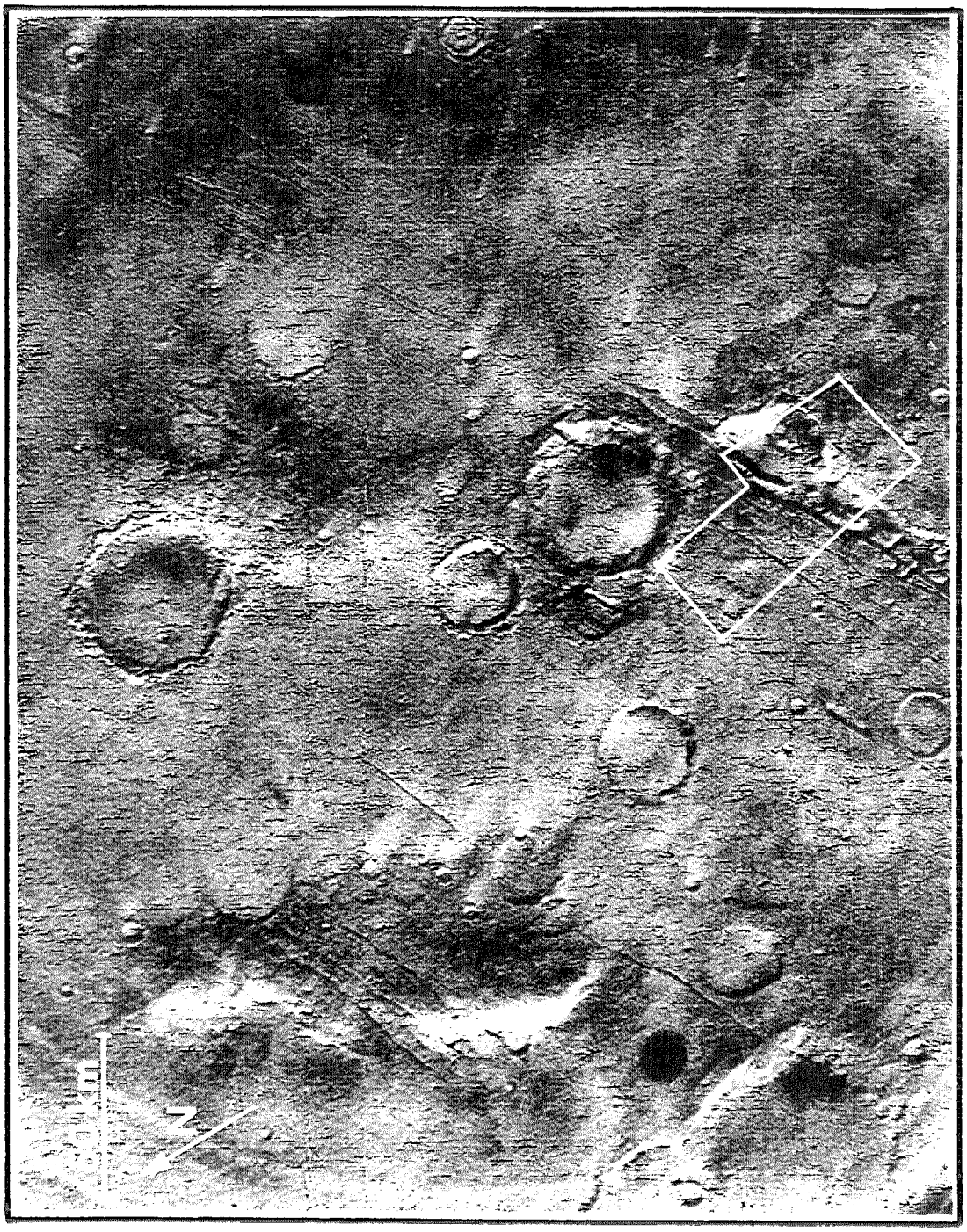

Figure 14A

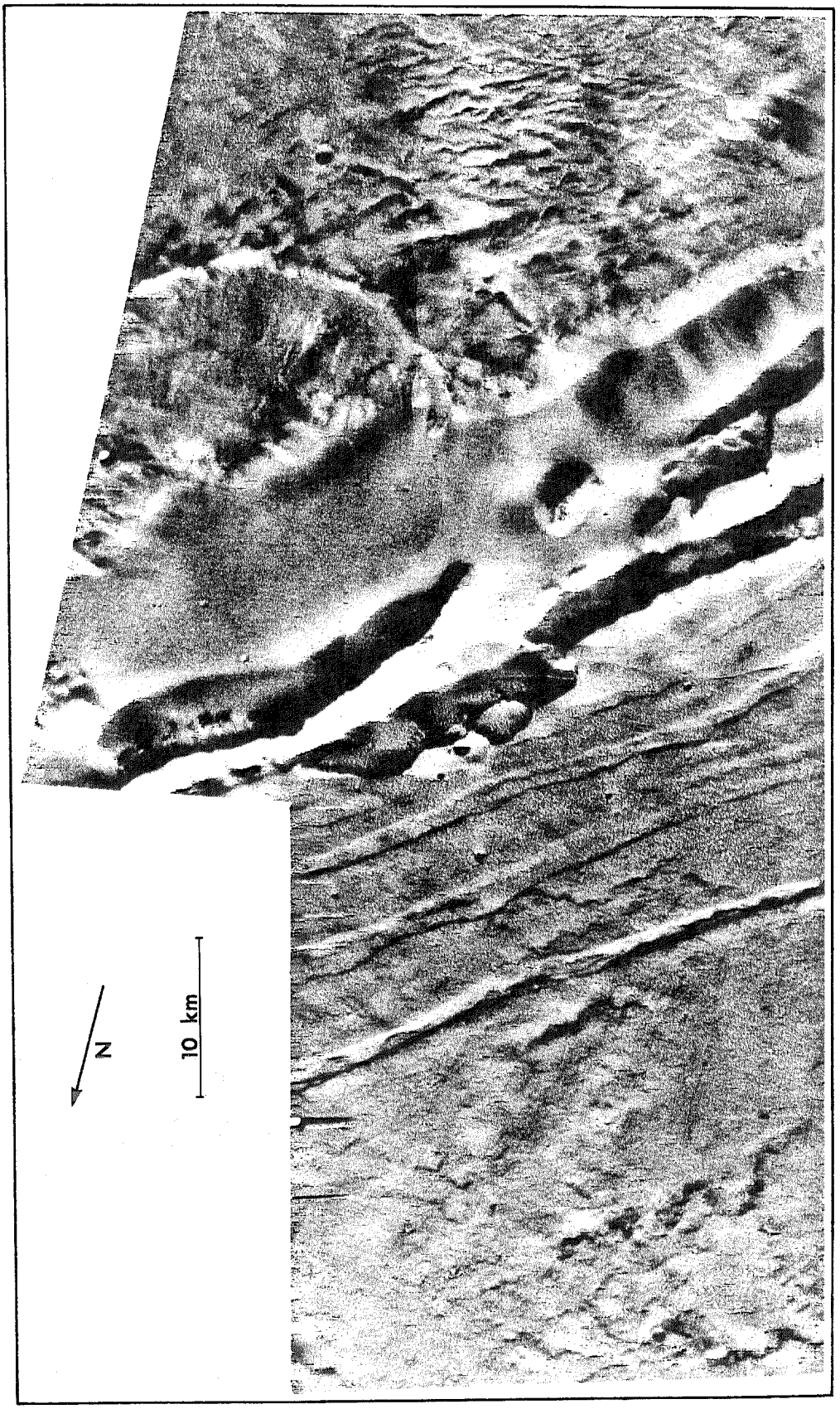

Figure 14B

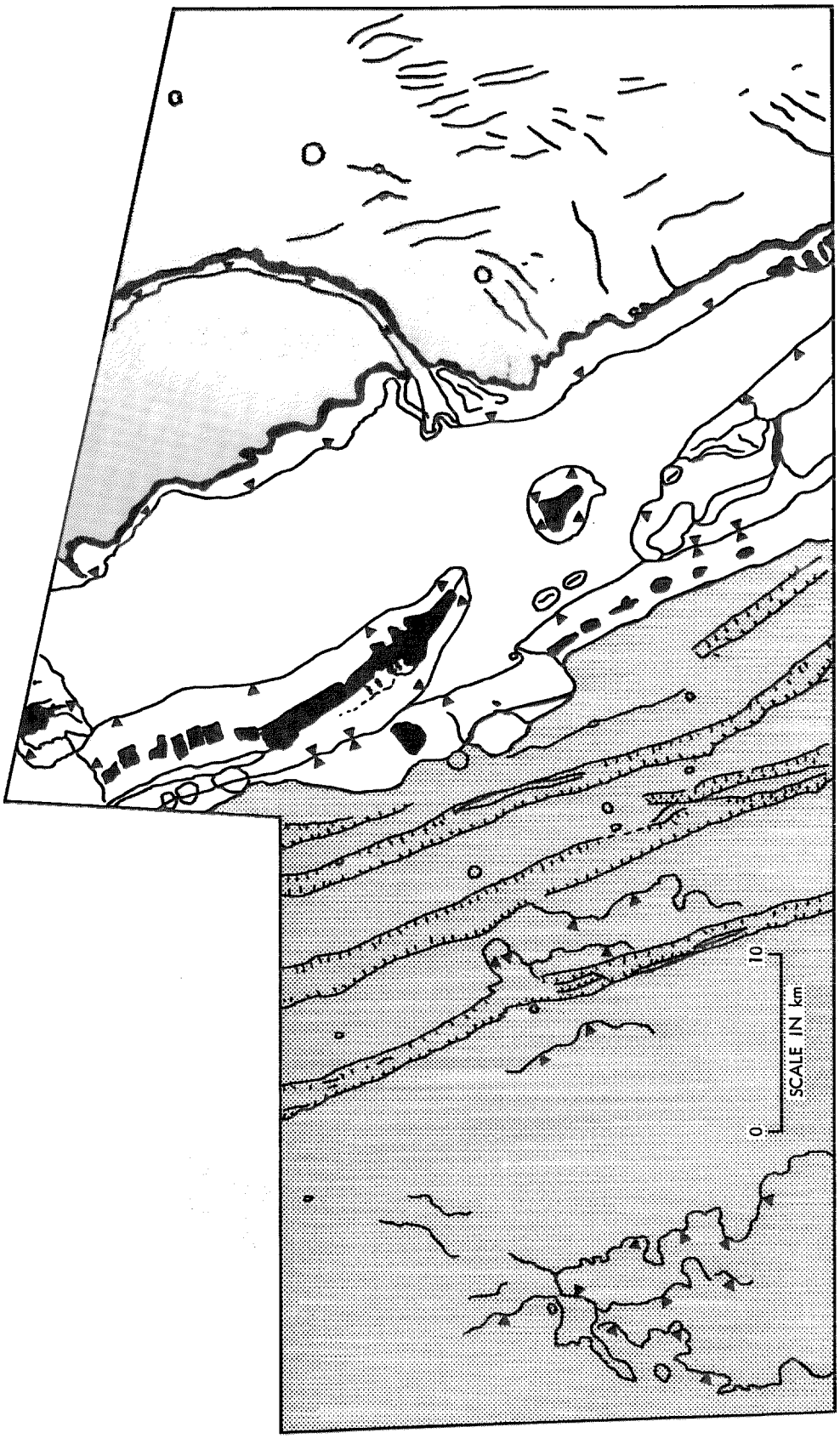

Figure 14C

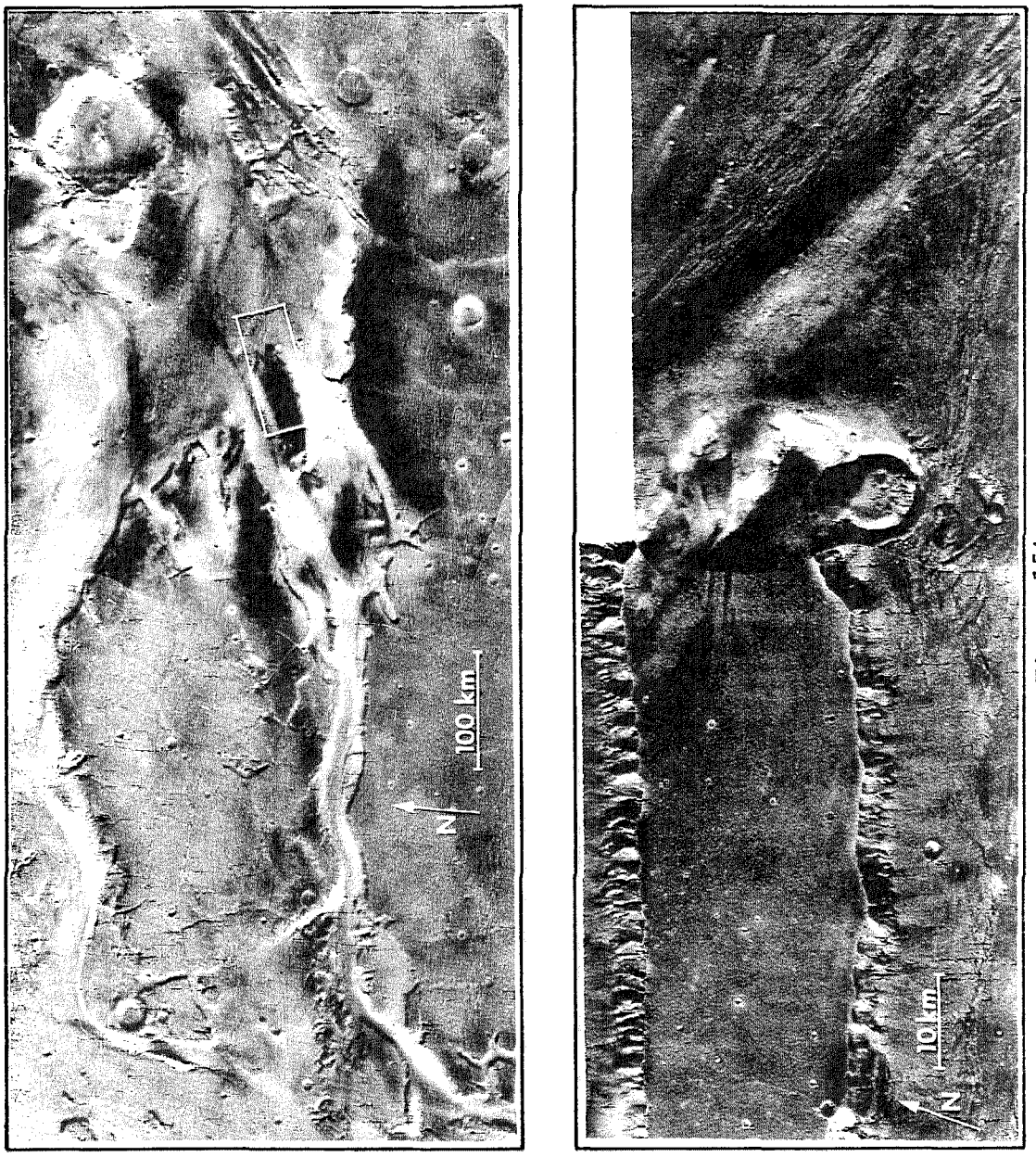

Figure 15A

Figure 15B

Figure 15C

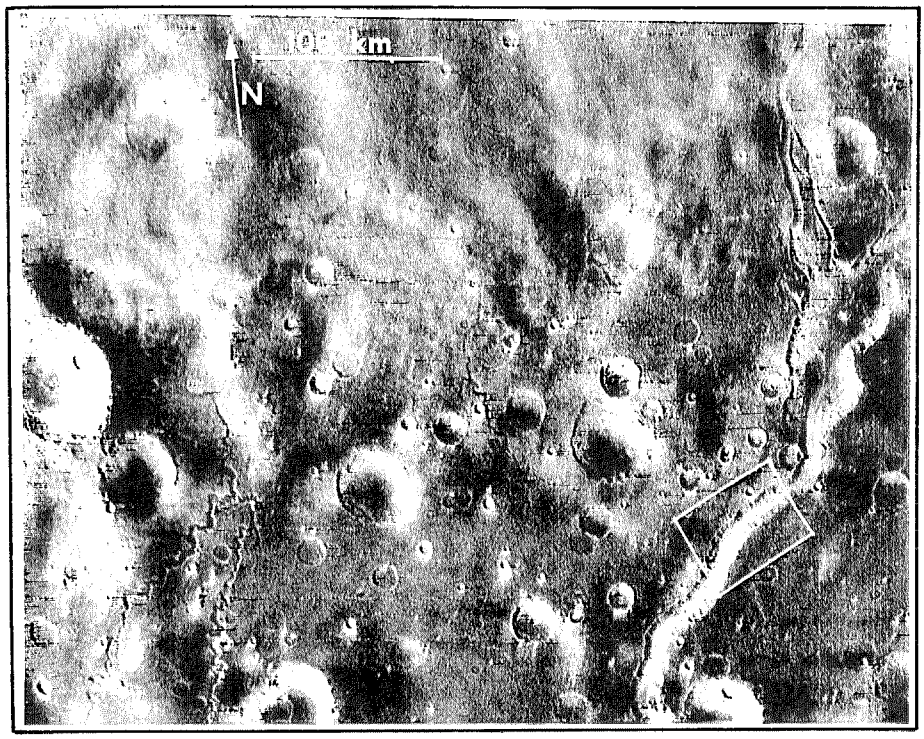

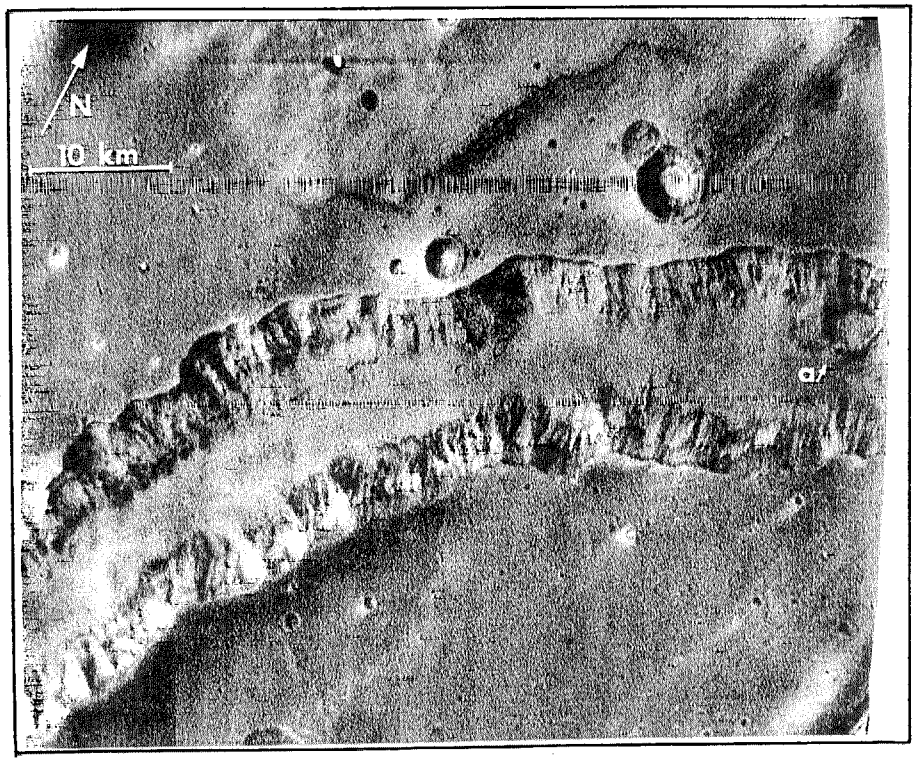

Figure 16

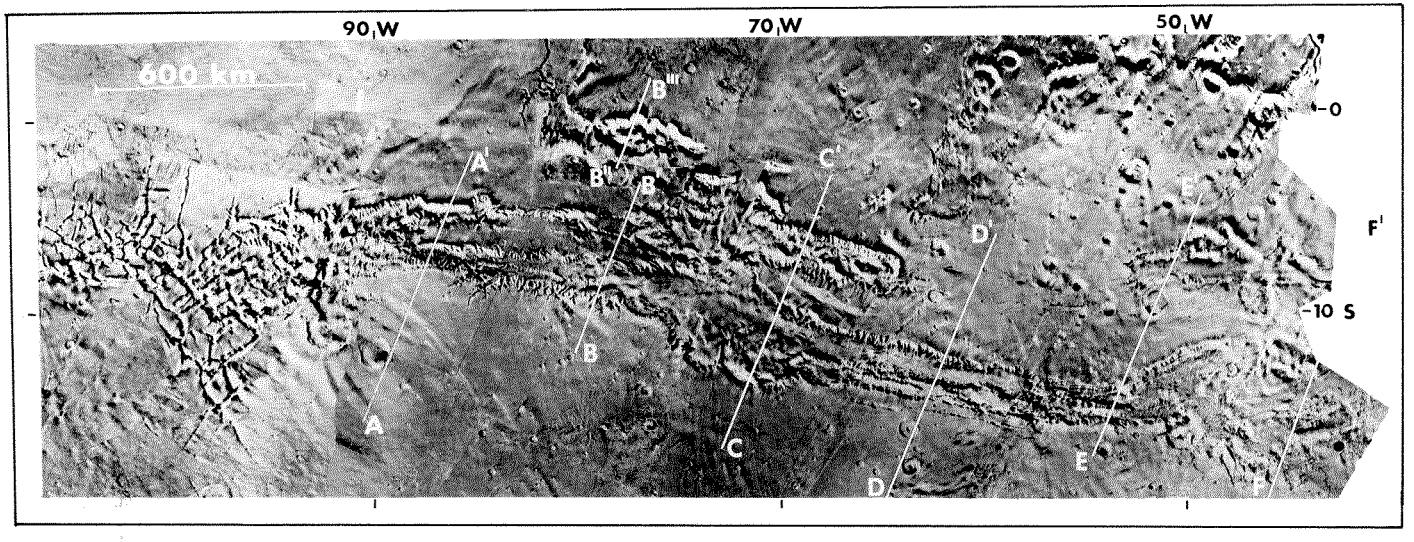
90°W
70°W
50°W
600 km
0
10 S
A
A'
B
B'
B''
B'''
C
C'
D
D'
E
E'
F
F'

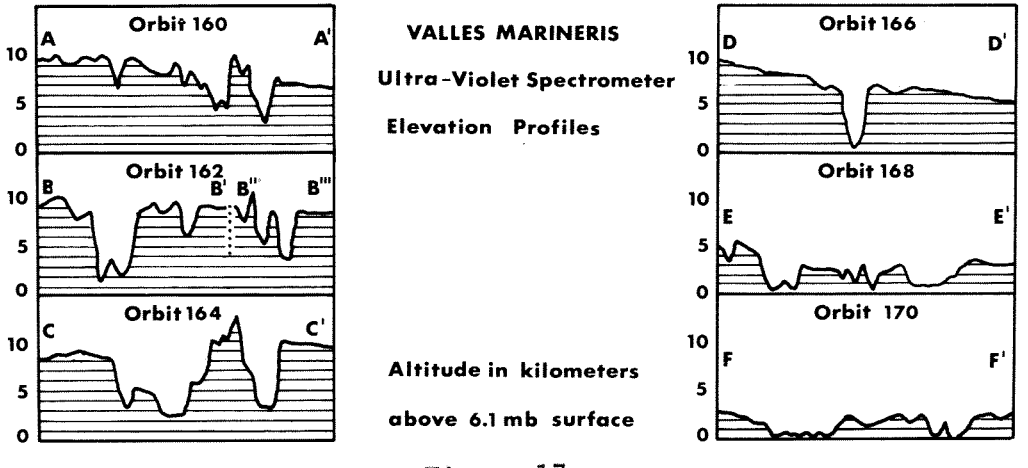
Orbit 160
A
A'
10
5
0
Orbit 162
B
B'
B''
B'''
Orbit 164
C
C'
VALLES MARINERIS
Ultra-Violet Spectrometer
Elevation Profiles
Altitude in kilometers
above 6.1 mb surface
Orbit 166
D
D'
Orbit 168
E
E'
Orbit 170
F
F'

Figure 17

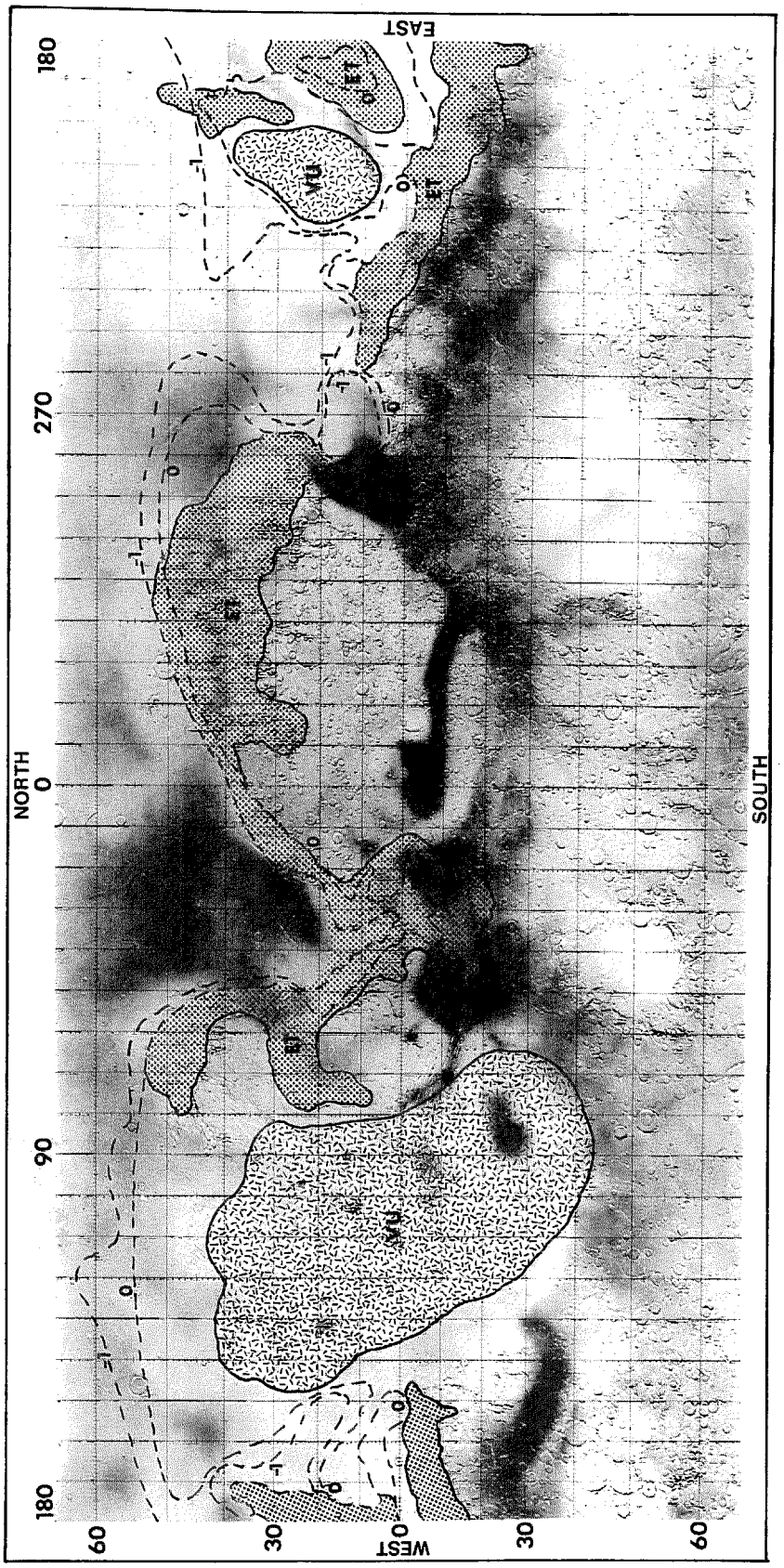

Figure 18